

Metallogels as Functional Catalysts: Bridging Soft Materials with Sustainable Transformations

Sumit Mondal,^[a] Joydeep Ray,^[a] and Debajit Sarma*^[a]

Supramolecular gels have become an intriguing medium for investigating the principles of dynamic assembly and creating systems with targeted applications in recent years. The integration of metals (including metal ions, metal nanoparticles, and metal-organic components) into a gel matrix forms soft polymeric structures, called metallogels. Metallogels represent a new category of functional soft materials, wherein the structural framework is constructed through metal–ligand coordination alongside other noncovalent interactions. Fascinating character-

istics, like sol–gel reversibility and facile tunability, distinguish them from other inorganic–organic hybrid materials. Herein, we have summarized the design principles of these soft hybrid materials and the exploration of their catalytic behavior as efficient heterogeneous catalysts (for organic transformation, electrocatalysis, and photocatalysis). This review lays the groundwork for the scientific community by providing an understanding of important concepts, methodology, and current advances in the area.

1. Introduction

Gels are prevalent and significant part of our daily lives. Despite their jelly-like appearance, gels are metastable soft materials that resemble solids but are predominantly liquid in nature.^[1] From the beginning of the day, starting with toothpaste and concluding with dessert at dinner, gels are integral to our daily routines. It exhibits viscoelastic properties, demonstrating characteristics of both solids and liquids in terms of mechanical strength.^[2] The term gel, derived from gelatin, was initially coined by the Scottish chemist Thomas Graham in 1861.^[3] Moreover, in 1926, Dorothy Jordon Lloyd articulated that “gel” is more readily identifiable than explicable.^[4] In 1974, Paul Flory characterized gel as a substance with a continuous microstructure that retains solid-like properties up to a specific strain threshold, despite exhibiting liquid-like behavior concurrently.^[5] Conversely, Almdal et al. characterized gels as a semisolid viscoelastic substance.^[6] In rheological behavior, the elastic region is represented by the storage modulus (G'), while the viscous liquid component is manifested by the loss modulus (G''). For a gel substance, the value of G' consistently exceeds that of G'' across the plateau region.^[6] As defined by the International Union of Pure and Applied Chemistry (IUPAC), gels are “non-fluid colloidal networks” permeated with fluid and distributed over their entire volume.^[7] Hence, gels comprise a substantial volume of solvents, entrapped inside a cross-linked solid matrix. Depending on entrapped solvents, gels are classified into three categories: organo, hydro, and xerogel. It can be made with water (hydrogels), organic solvents (organogels), or aqueous organic combinations.^[8] In contrast, aerogels or xerogels are the

terms for gels in which the solvents are not present. Chemical or polymer gels, such as silica gel, are formed when the gel network consists of covalent bonding. However, a supramolecular gel is created when such network formation is due to supramolecular interactions (noncovalent, like H bonding, hydrophobic, electrostatic, and π – π stacking interactions), which are known as a physical gel.^[2,9] These gels are typically synthesized using diverse low-molecular-weight gelators (LMWGs).^[10] Despite the intriguing features of supramolecular gels, their initial invention was a result of serendipity rather than intentional design. They were typically observed while doing recrystallization.^[9,11] Till the 1990s, multiple research groups had not endeavored to produce low molecular weight gelators utilizing organic compounds. Although organic gelators have been around for a while, investigations into metal complexes as supramolecular metallogelators have significantly intensified over the last decade.^[12] This category of gels is referred to as metallogels, in which metal constituents engage with organic gelators that are directly or indirectly implicated in the development of cross-linked gel networks. The integration of metallic components allows for the amalgamation of their distinctive properties (conductivity, magnetic, redox, and sensing) with those of organic gelators.^[13] Furthermore, metal components facilitate auxiliary interactions among the supramolecular network structure, which induces tunable morphology and rheological behaviors. Investigations into metallogels commenced in the late 20th century and proliferated significantly in the early 21st century. To date, numerous metallogels originating from organometallic complexes, metal-organic cages, metal nanoparticles, metal–ligand coordination complexes, and composite materials have been recognized for their applications in optics, biomedical, catalysis, rheology, redox activity, magnetism, and others.^[14]

Importantly, catalytic transformation denotes a chemical reaction process involving catalysts that diminish the activation energy required to cleave chemical bonds, which yields high selectivity with great atom economy toward desired prod-

[a] S. Mondal, J. Ray, D. Sarma
Department of Chemistry, Indian Institute of Technology Patna, Patna, Bihar
801106, India
E-mail: debajit@iitp.ac.in

uct formation.^[15] In this context, numerous innovative catalysts, especially metal complexes, have been developed and utilized to activate various chemical bonds (like C–C/C–H/C–N).^[16] Over the past decade, catalysis-mediated self-assembly has been extensively utilized in the design and fabrication of functional soft materials, especially as functional biomaterials.^[17] In recent times, metallogel materials have garnered significant interest due to their concurrent development with metal-organic framework (MOF) materials.^[18] The MOF, a category of porous crystalline substances composed of organic linkers and inorganic clusters, has garnered more use and recognition. However, the predominantly amorphous metallogel materials remain comparatively underexplored.^[9,19] These gels are formed by the self-assembly of low-molecular-weight gelators (LMWGs), which aggregate through reversible, weak, and cooperative supramolecular interactions such as hydrogen bonding, π – π stacking, and metal–ligand coordination to form a 3D fibrillar network that can entrap solvent molecules. The dynamic characteristics of the noncovalent interactions can modulate the structural integrity of this gel network. In contrast to other rigid supramolecular hosts, gels do not possess a pre-formed enclosed area; rather, they develop under appropriate experimental conditions.^[20] Furthermore, the hierarchical porous structure includes mesopores and macropores with accessible active centers of these materials also makes it easier for mass and charge transportation.^[21] It helps in improving reaction kinetics. For instance, Araujo and coworkers synthesized metallogels with L-valine-derived gelators that were functionalized with triazolyl groups and coordinated with Cu(I) ions in

methanol.^[22] These metallogels function as effective heterogeneous catalysts for the azide-alkyne cycloaddition reaction. In comparison to the homogeneous Cu(I) catalyst, the metallogel system demonstrated superior yields and conversions, owing to the stabilization of Cu(I) by triazole ligands and the spatial confinement of catalytic centers inside the gel matrix. Interestingly, wide-angle X-ray diffraction (WAXD) analysis revealed that gels with lower short-range order demonstrated better catalytic performance, possibly due to increased substrate accessibility. Metallogels can be hybridized with electroactive or photoactive substances to enhance their catalytic performances. The integration of conductive additives like graphene, carbon nanotubes (CNTs), or photosensitizing compounds into the gel matrix or solvent phase improves electronic conductivity and charge transfer capabilities.^[14e] In addition, metal-organic hydrogel shows good accessibility to aqueous electrolytes rendering them especially appealing for electrocatalytic applications. The excellent water retention capacity, adjustable porosity, and modular functionalization provide a solid foundation for the development of advanced catalytic soft materials.

The metallogels show widespread application in catalysis research where gelators play potential roles with distinct functionalities ($-\text{NH}_2$, $-\text{COOH}$, $-\text{OH}$, $-\text{SH}$, etc.). The catalytically active metal nanoparticles (MNPs) are decisively bound to these functionalities of gels via coordination or electrostatic interactions. It can easily modulate the surface charge, electronic property, and catalytic efficiency. Incorporating nanoparticles into a gel network restricts the migration and aggregation ability of the particles, which largely impacts particle size and surface



Debajit Sarma received his M.Sc. from the Indian Institute of Technology, Delhi, and Ph.D. from the Indian Institute of Science, Bangalore. He was a Postdoctoral Fellow at Northwestern University before joining the Department of Chemistry at the Indian Institute of Technology Patna (IIT Patna), in 2017. He is currently an Associate Professor at IIT Patna, and his current research interests include inorganic materials for sensing, catalysis, energy conversion, and environmental remediation.



Sumit Mondal received his BSc (Honours) degree in Chemistry from the University of Burdwan, India. His MSc degree was completed in organic chemistry from Bilaspur Vishwavidyalaya, Chhattisgarh, India. Recently, he has been working in the field of porous material synthesis and its application in catalysis and sensing with the solid-state and

inorganic chemistry group at the Indian Institute of Technology, Patna.



Joydeep Ray received his M.Sc. in organic chemistry from the National Institute of Technology Durgapur, West Bengal, India. He has recently been working on the synthesis of inorganic soft materials and metal clusters, focusing on their applications in sensing, catalysis, and data encryption, as a research fellow at the Indian Institute of Technology Patna.

accessibility. Nanoparticle-infused hydrogels and xerogels serve as robust, reusable, and highly effective heterogeneous catalytic systems. For example, Au or Pd nanoparticles were stabilized within peptide-based hydrogels and demonstrated superior catalytic efficacy for C–C coupling or reduction processes relative to their freely dispersed equivalents.^[23] Similarly, Pd-NP-loaded supramolecular gels have shown greater catalytic activity compared to colloidal Pd catalysts in C–C coupling reactions and also demonstrated enhanced reusability and superior control over nanoparticle size and distribution.^[24] Recently, researchers have been developing noble techniques to use soft materials in advanced catalysis applications.^[25] To this end, the integration of magnetic nanoparticles into the gel matrix facilitates enhanced separation and recycling operations for catalysis research.^[26] In addition, gel-nanocomposites with noble metal NPs (like Au, Ag, and Cu) mediated research may also be impactful for surface-enhanced Raman scattering and catalysis applications.^[27] Nanoparticle-incorporated hydrogels function as hybrid catalytic systems that combine the high surface reactivity of nanocatalysts with the structural integrity, modularity, and environmental responsiveness of soft materials, offering a versatile platform for sustainable and efficient catalysis.

Numerous review articles exist regarding MOF materials, focusing on designing principles, characteristics, and applications.^[28] In contrast, there exists a limited number of review articles on metallogels. Individual review, presenting a distinct perspective. However, in the area of metal-mediated soft gels, discussions and possibilities regarding catalytic applications are still in the early stages. A thorough discussion of utilizing soft metallogels in diverse catalytic transformations can address this gap. This review is to portray the state of the art in metallogel research and emphasize their notable accomplishments in catalysis (Figure 1). The discussion will initially focus on the rational approach to the design principles of metallogels. Second, the direct utilization of these soft materials as catalysts in different reactions. This detailed survey of these soft materials, both in organic transformation and as photo/electro-catalysts, provides additional insights into contemporary concerns. Finally, the latest researches are summarized in three unique tables illustrating the application of soft gels as diverse catalysts. This review article intends to elucidate recent progress in the catalytic applications of soft inorganic–organic hybrid gel materials.

2. Design Strategies for Metallogels:

2.1. Rational Approach to Design Low Molecular Weight Gelators

Low molecular weight gelators (LMWG) are small organic compounds (molecular mass ≤ 3000 Da) that may self-assemble under different conditions to create various structures and are capable of immobilizing the solvent. In general, it gives rise to fibers, niddle, tapes, tubes, and helical elongated 1D structures. When these definite branches further entangle, a network structure may be developed, which results in the formation

of 3D supramolecular gels. The controlled growth of these 3D network structures can be regulated by the width of fibers, cross-linking ability, and functionalities in the LMWGs entity.^[12a,29] A gel network that incorporates metal, either as a coordinated metal complex or as metal nanoparticles, is termed metallogels. The very first metallogel, lithium urate hydrogel was discovered in 1841 by Lipowitz et al.^[30] Projecting the gelation result from the interaction of a low molecular weight gelator (LMWG) with a metal ion remains highly critical, perhaps due to the sensitivity of the reaction circumstances (mainly solvents). The polarity, temperature, concentration, and LMWG conformation may result in significant variations in gelation capacity. However, choosing appropriate low molecular weight gelators (LMWGs) and metal ions may result in self-assembled gel nanostructures.^[31]

The successful synthesis of a metallogel primarily involves the systematic design of low molecular weight gelators (LMWGs). The LMWG must comprise metal binding groups, arranged to facilitate coordination-driven self-assembly into 1D, 2D, or 3D network structures. The coordinating groups include carboxylate, terpyridine, pyridine, and tetrazole manifest binding with distinct metal centers. Along with metal–ligand coordination, the ability to engage in noncovalent interactions is the primary requirement for a molecule or complex to demonstrate gelation behavior. Hence, definite groups that can take part in active gelation can be categorized into distinct categories (Figure 2). The LMWG may contain hydrophilic, hydrophobic, or amphiphilic functional groups.^[32] Functionalities like amide groups are a significant category of LMWGs due to their ability for noncovalent interactions via polar amide groups. It undergoes a self-assembly process through the formation of coordination bonds at terminal coordinating sites, such as carboxylate and nitrogen donor sites, as well as intermolecular hydrogen bonding interactions involving the amide C=O and N–H groups. Moreover, the inclination for cooperative intermolecular amide–amide hydrogen bonding promotes hydrophilic environments.^[33] As a hydrophobic entity, cholesterol-based steroidal derivatives are widely recognized for their tendency to form helical chains through aggregation. The architecture of the cholesterol molecule is captivating, including its aliphatic rings interconnected in a transform. The cyclohexane rings adopt a stable chair conformation, allowing the molecule to attain a rigid structure.^[34] On the other hand, amphiphilic LMWGs possess hydrophilic as well as hydrophobic moieties that facilitate self-assembly in aqueous and nonaqueous environments.^[35] Organic extended π -conjugated chromophores like porphyrins may induce π – π stacking and van der Waals forces, which help further in the self-assembly.^[36]

2.2. Interactions and Classification

Molecular assembly directed by metal–ligand coordination chemistry is a relatively recent area of study in materials science. The employment of metal–ligand interactions as a driving factor for constructing large-scale structures is attributed to their diversified and unidirectional features, which facilitate

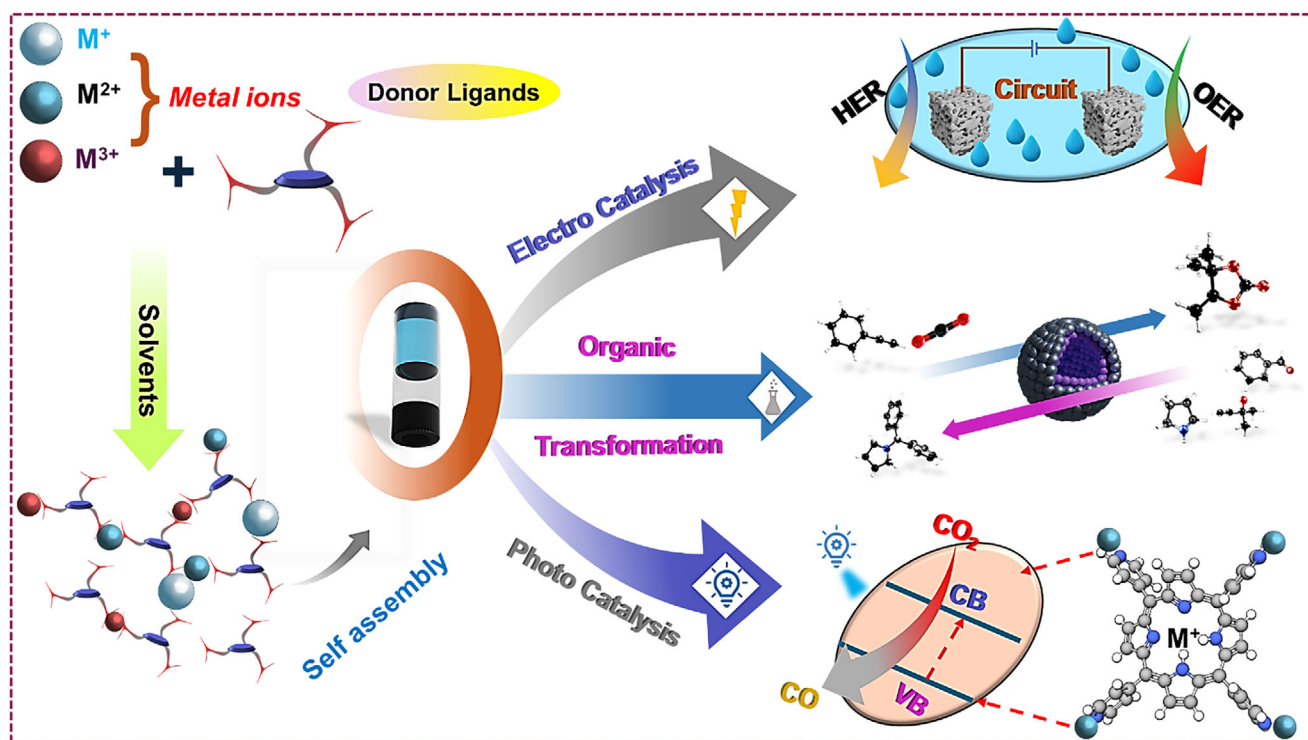


Figure 1. Schematic representation of the low molecular weight gelators with distinct functionalities.

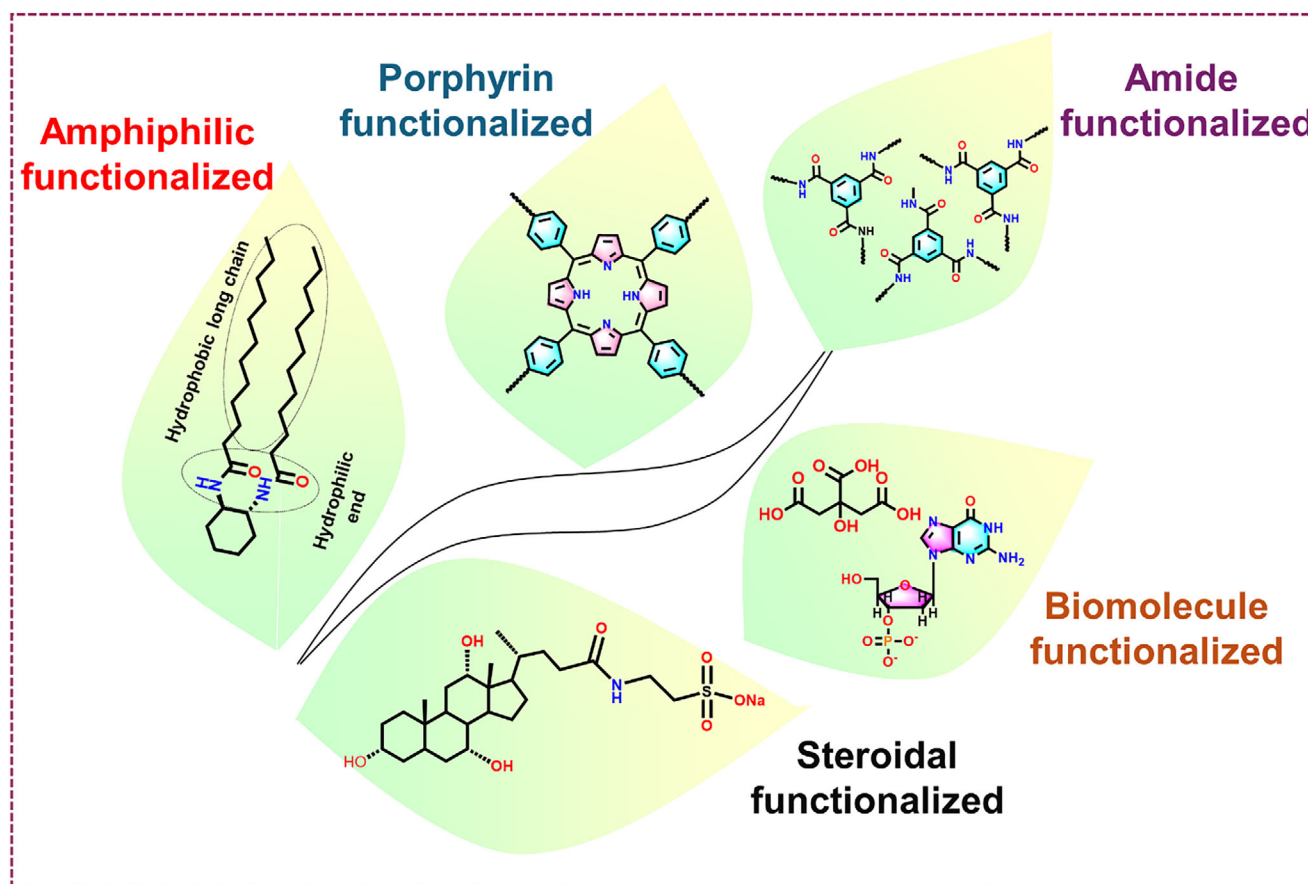


Figure 2. Functionalized low molecular weight gelators.

the construction of controllable and extended architectures. Apart from this, different noncovalent interactions play a definite role in forming metallogels.^[37] Hydrogen bonding is the most common interaction among these, which is a vital factor in the biophysical mechanism of molecular recognition, as it governs the structure of biomacromolecules such as DNA and proteins.^[38] Similar to the biophysical self-assembly process, hydrogen bonding is frequently utilized in supramolecular gel synthesis. On the other hand, distinct types of π interactions (such as cation $\cdots\pi$, anion $\cdots\pi$) can stabilize the supramolecular structures.^[39]

Gelators can be categorized mainly by their molecular structure and the types of interactions that promote gel formation. Discrete gelators and coordination polymer gelators represent two distinct categories, both physically and functionally. Discrete gelators are often low-molecular-weight substances that self-assemble through noncovalent interactions to form fibrous networks capable of immobilizing solvents. In contrast, coordination polymer gelators involve the formation of extensive metal–ligand networks, where coordination bonding plays a crucial role in the gelation process.^[10b]

(a) **Coordination polymer gels:** Coordination polymers are formed by extended metal–ligand interactions to build long-range ordered 1D/2D/3D structures.^[40] Alongside the progress of coordination polymers, analogous to CPs, recent years have seen substantial research on supramolecular gels, where metal–ligand interactions have played crucial roles in the self-assembly process. The integration of metal centers into supramolecular gels is anticipated to produce multifunctional metallogels. The metal–ligand interactions can link organic ligands to create extended multi-dimensional structures that facilitate gel formation. Importantly, this interaction can be very specific for their binding motif. For instance, adenosine monophosphate (AMP) /guanosine monophosphate (GMP) (nucleotide building unit) possesses strong coordinating affinity to distinct metal ions such as Ag^+ , Zn^{2+} , Mn^{2+} , Pt^{2+} , and Hg^{2+} .^[41] At neutral pH, guanosine can effectively bind with Ag^+ to form a supramolecular gel network via self-assembly.^[42] In general, hard–soft acid–base (HSAB) theory plays an impactful role in coordination chemistry.^[43] Like other coordination complexes, gelators with certain ligand field strengths generate metallogel complexes with hard or soft metal ions. For example, oxalate, with medium ligand field strength, can preferentially bind with hard to borderline metal ions Cu^{2+} to produce a persistent gel. Although gelation was not observed in the presence of other soft (Ag^+ , Cd^{2+}) and hard (Fe^{3+} , Mn^{2+}) metal ions.^[44] Similarly, the terpyridine moiety has a strong interaction with trivalent lanthanides, Fe^{3+} , Ni^{2+} , Zn^{2+} , and Ru^{3+} . Sutar and coworkers developed a series of metallogels where modified terpyridine gelators have been extensively utilized.^[45] In nature, binding selectivity for Fe^{3+} is exhibited by siderophores, which primarily serve to selectively extract iron from their surroundings.^[46] In this regard, Munjal and coworkers strategically designed a mixed gelator system that shows excellent specificity toward Fe^{3+} among other transition metal ions and demonstrates the biomimicking

activity of siderophores.^[47] Depending upon the coordination geometry and spatial arrangement of the LMWGs, metallogel shows diverse applicability ranging from tunable redox and spectroscopic properties to catalytic activity, which can barely be attainable with organic moieties. Kuroiwa and coworkers elucidated how coordination geometry may influence gelation and the optical properties of the material.^[48] The lipophilic Co(II) -triazole complex exhibits reversible heat-induced gelation. The alteration in color and phase of the material was predominantly contingent upon the coordination geometry surrounding Co(II) . A blue gel was produced at room temperature while Co(II) was in tetrahedral geometry, whereas a pink sol phase with octahedral geometry around Co(II) was created upon cooling to 0 °C (Figure 3a–d).

(b) **Discrete metallogels:** In comparison to recent developments in coordination polymer gels, discrete small molecule-based metallogels are less explored. Along with noncovalent interactions, unidirectional metal–metal interactions (d^8 - d^8/d^{10} - d^{10}) play a crucial role in forming self-assembled supramolecular gels.^[8] In coordination and organometallic chemistry, gold(I) complexes are gaining interest for their potential to generate Au–Au interactions (aurophilicity).^[49] Importantly, M^{n+} – M^{n+} interactions may induce metal-to-metal charge transfer absorption in the lower energy spectrum, which significantly alters the photophysical properties of the framework.^[50] The initial report was on Au(I) mediated pyrazole-based gel by Kishimura et al. The gel exhibits a strong red luminescence under a UV source ($\lambda_{\text{ex}} = 254 \text{ nm}$) (Figure 3e).^[51] Later, cyclometalated Au(III) complexes were utilized to develop supramolecular gels. Wong and coworkers developed alkynyl gold(III) gels, where π – π stacking as well as intermolecular hydrogen bonding play a crucial role in stabilizing the supramolecular network.^[52] Since the last two decades, platinum(II) based square planar complexes have been largely explored based on intriguing spectroscopic behaviors.^[53] The first example of Pt(II)-mediated metallogelator was reported by Shirakawa and coworkers.^[54] Hydrophobic interactions from the long-alkylated chain and π – π interaction from the 8-quinolinol group induce structural stability to form a supramolecular gel. Along with Au/Pt complexes, Fe-mediated discrete metal complex also forms gels. In this context, Roubeau et al. developed a Fe-triazole-based thermoreversible gel, which further exhibited strong spin-cross-over behavior with switchable optical transformation.^[55] Likewise, the Pd(II)-mediated discrete metal complex exhibits effective gelation. Tu et al. developed a pyridine-based pincer Pd(II)-complex, that shows gel formation ability in the presence of a variety of organic solvents (protic/aprotic).^[56] Diverse noncovalent interactions, including π – π interactions of aromatic rings, van der Waals interactions among alkyl chains, and M^{n+} – M^{n+} interactions may be crucial for self-assembly.

The preceding explanation suggests that the creation of metallogels is an intricate phenomenon potentially influenced by metal–ligand coordination and several types of supramolecular interactions (Figure 4).

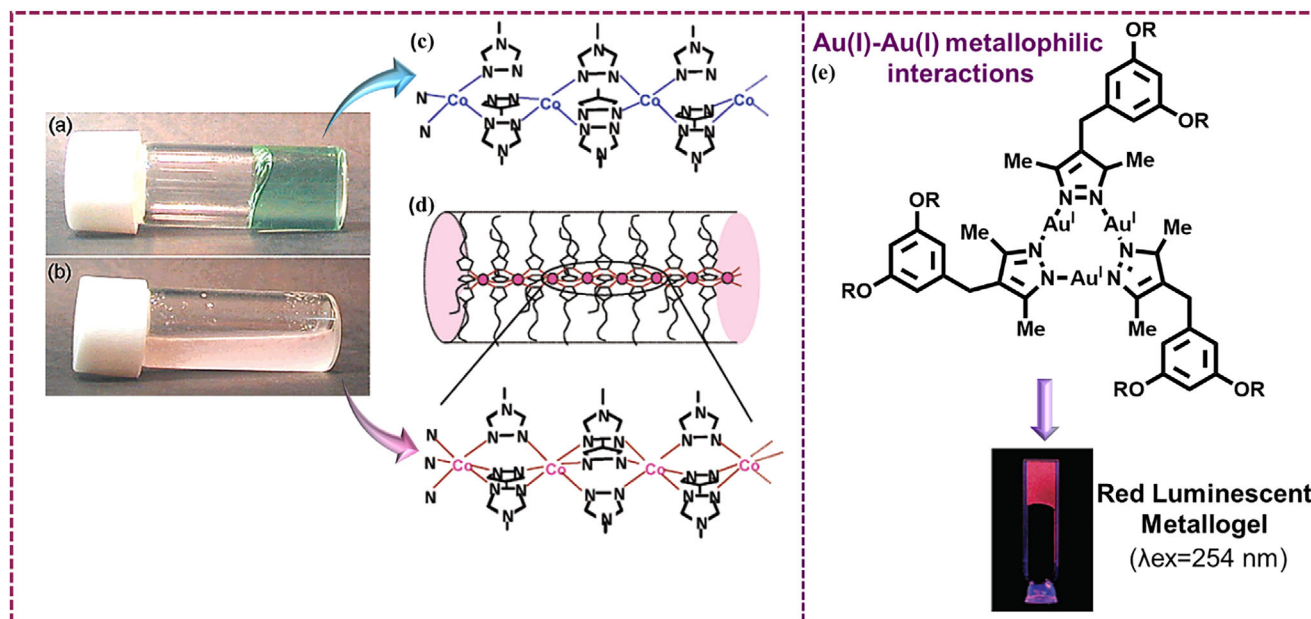


Figure 3. (a) Blue-like gel of Co(II)-Td complex, (b) pale-pink sol of Co(II)-Oh complex, (c) schematic representation of the Co(II)-Td polymeric structure, and (d) schematic representation of the Co(II)-Oh polymeric structure. Partly adapted figure and structure from Ref. [48]. Copyright (2004), with permission from the American Chemical Society. (e) Metallogel formation with Au(I)-pyrazole mediated discrete gelator. Partly adapted figure from Ref. [51]. Copyright (2005), with permission from the American Chemical Society.

2.3. Bridging Between Soft and Crystalline Architectures; From Molecular Assembly to Functional Properties

In contrast to crystalline MOFs, metallogels possess identical components and can be transformed into their MOF equivalents through suitable stimuli or inducing factors. Considering the intrinsic relationship between MOFs and metallogels, which possess analogous bonding connections yet exhibit varying structural regularity, specific techniques can be employed for the selective synthesis of these functional materials.^[10b]

(a) **Nucleation process-gel/crystal transition:** Gelators are entrapped in a substantial amount of solvents to develop 3D network architectures. Gelators must be solubilized to create a supersaturated solution, after which additional stimuli (such as heating, sonication, and cooling) initiate the aggregation process. Subsequently, the aggregation commences the initialization of self-association, wherein chemical or physical interactions may play a crucial role. The self-association process can be categorized into three subclasses based on aggregation modes – (1) random aggregation without any short-range or long-range order form amorphous precipitation; (2) meanwhile, the crystallization process includes self-assembly in a highly ordered way; (3) ultimately, the gelation is observed in an ordered way through entrapment of the solvents (Figure 5).^[10b,57] Importantly, interparticle aggregation serves as the principal force for gelation, which is necessary for the meticulous regulation of the classical crystallization process. In a recent study, Fu and coworkers explored gel-crystal evolution utilizing UiO-66(Zr).^[58] Nonclassical gel-crystal transformation of MOF gel and sol-gel self-assembly are

investigated. Zirconium oligomer formation was crucial to make the differences between the gelation and conventional crystallization-precipitation.

- (b) **Hybrid gel formation from MOF nanoparticles:** Gelation can occur by the aggregation of nanoparticles (NPs). This method enables the formation of gel networks by the mismatched growth of MOF nanoparticles.^[59] The combination of metal components and gelators in solution facilitates the formation of MOF nuclei. Subsequently, MOF nuclei transform into MOF nanoparticles. Directional growth can yield metal-organic frameworks (MOFs), while mismatched growth of MOF nanoparticles under appropriate conditions results in the development of metallogels. In this context, Li and coworkers developed Al(III)-mediated MOF nanoparticles using the benzene dicarboxylic acid (H_2BDC) gelator, which further induces gelation due to perturbation via other competing interactions.^[60] Later, Jayaramulu and coworkers reported a facile synthetic approach to develop a gel system from Al(III) and benzene tri-carboxylic acid (H_3BTC) gelator.^[61] Fluorinated graphene oxide (FGO) was introduced into the solution to the Al(III)-MOF-based gel. FGO acts as a structure-directing agent. The different oxygen-mediated functionalities (carboxylates, epoxy) of FGO facilitate gel formation from MOF nanoparticles via coordination-perturbed self-assembly (Figure 6). Furthermore, Chakraborty et al. utilized ZIF-8 (zeolitic imidazolate framework-8) nanoparticles to form a hybrid gel composite through charge-assisted self-assembly.^[62] Negatively charged laponite (LP) clay was introduced to interact with ZIF-8 (having a surface positive charge) to form a ZIF-8/LP-mediated hydrogel nanocomposite.

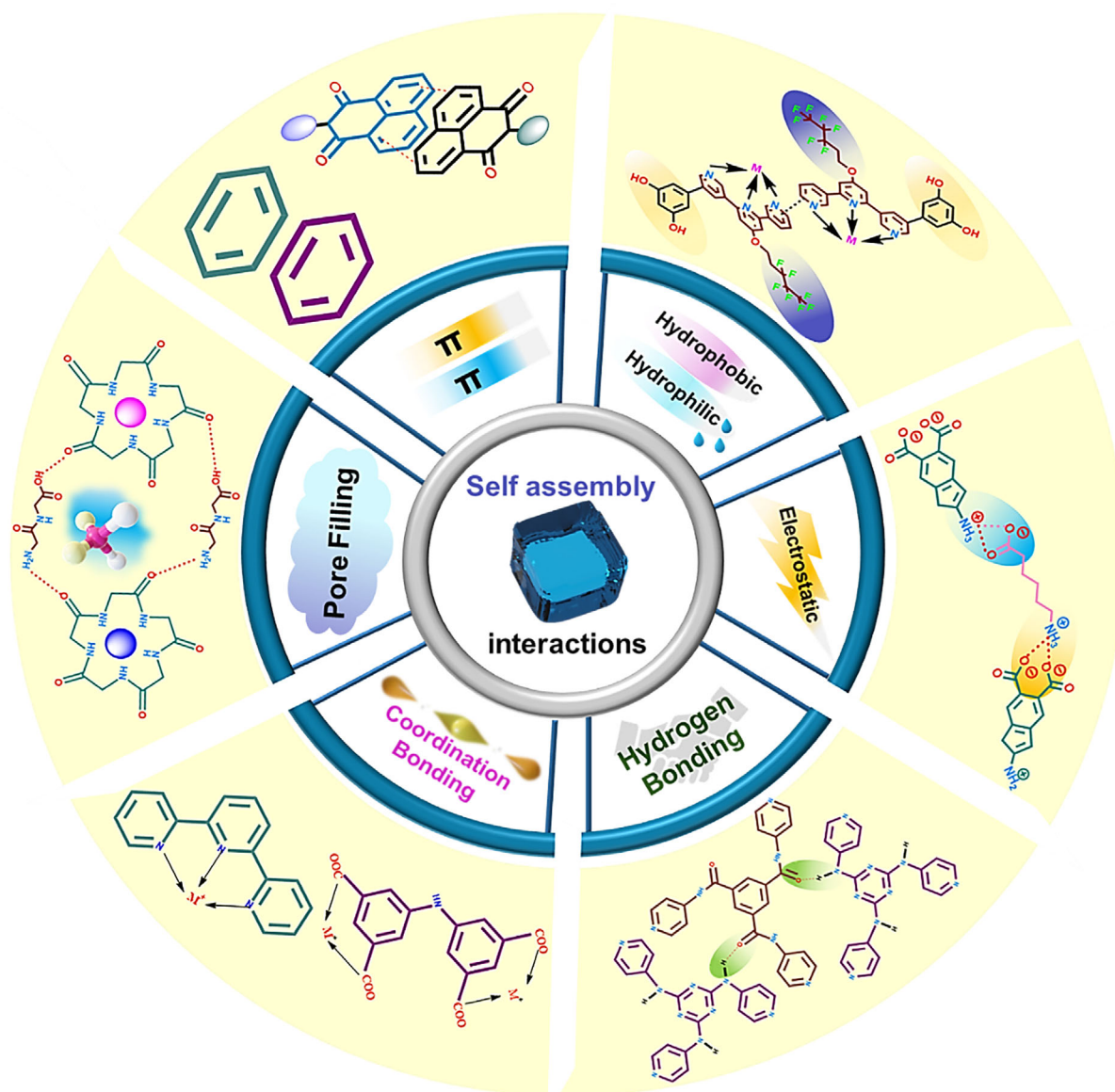


Figure 4. Types of interactions are responsible for the self-assembly process.

(c) **Variations in reaction conditions:**

Concentration: The aggregation, precipitation, and gelation are significantly influenced by variations in reactant concentrations. High reactant concentrations are notably more favorable for gel formation in solution-phase reactions. For example, Bueken et al. have shown the generation of gel and MOF crystal by simply varying reactant concentration.^[63] A high reactant concentration gives rise to “nonflowing” gel, while reduction of reactant concentration leads to UiO-66 crystals. An increasing reactant concentration might facilitate the nucleation of UiO-66 crystals while hindering their subsequent growth, which results in the aggregation of UiO-66 particles to form gels.

Metal/ligand ratio: The metal/ligand ratio significantly impacts the generation of MOFs or metallogels. The selection of the metal–ligand ratio is crucial for determining the critical gelation point, a fundamental parameter in the syn-

thesis of supramolecular gels. Zhao and co-workers reported a cadmium-based metallogel with a low metal-to-ligand ratio varying from 0.4:1 to 1.6:1, but a cadmium(II)-MOF was synthesized at a slightly higher metal-to-ligand ratio of 2.1:1.^[64] Alterations in reaction conditions induce morphological differences in supramolecular frameworks. A nanofibrous structure was generated in the xerogel system, while microcrystals of 10 μm in size were produced for the MOF particles. In another study, Liao et al. demonstrate a variation in the metal/ligand ratio associated with morphological and rheological alterations.^[65] Compared to fibrous CuBTC-0.5:1, granular CuBTC-1.2:1 gel showed improved gas absorption performance due to its increased permanent porosity. Interestingly, interwoven fibers of CuBTC-0.5:1 induce more rigidity than CuBTC-1.2:1, which was reflected in the high storage modulus of the former.

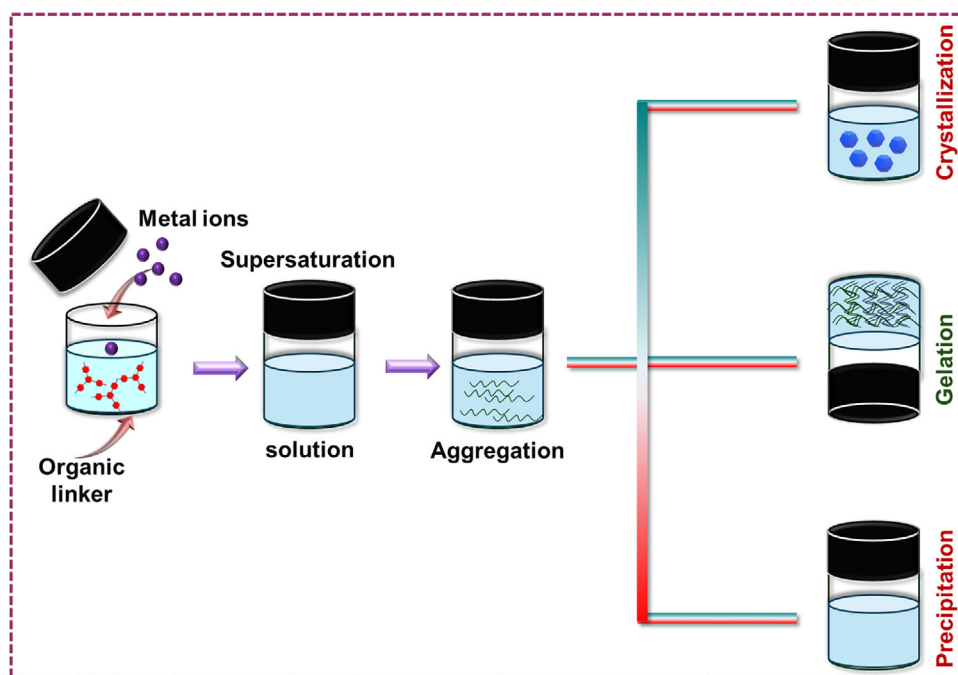


Figure 5. Schematic representation of self-assembly processes: crystallization, gelation, and precipitation.

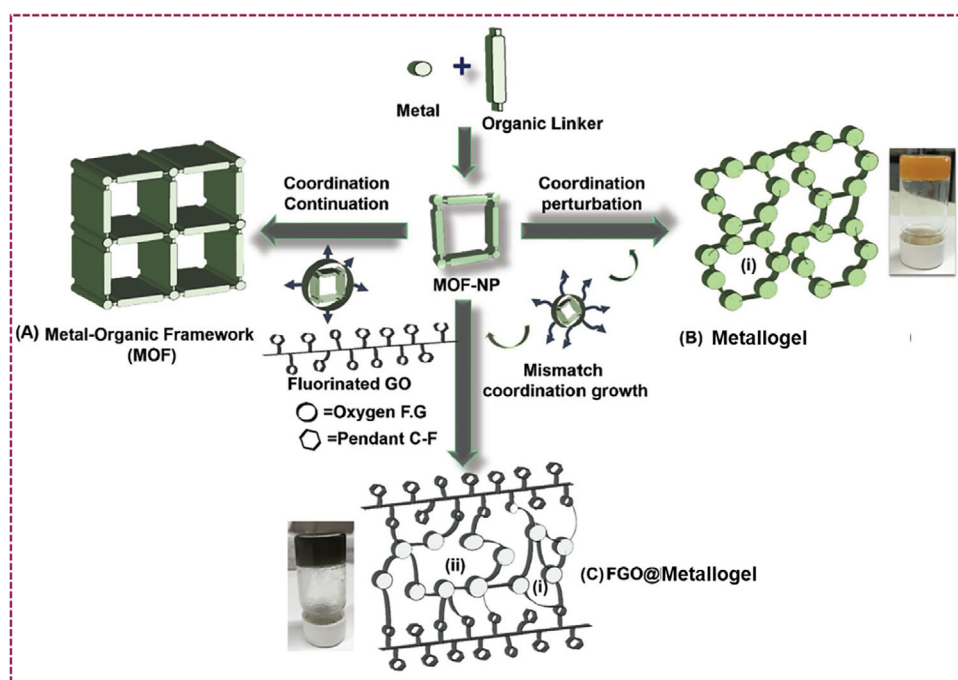


Figure 6. Formation of MOF and metallogel using a similar metal-linker approach from MOF-nanoparticles (mismatch coordination growth). Reprinted from Ref. [61].

Other conditions: Along with the above two important factors, several other reaction conditions play an active role in MOF/metallogel tailoring. Bueken et al. reported a Zr-MOF/metallogel system, where the metal source plays a definite role in the synthesis of the supramolecular framework.^[63] $\text{ZrOCl}_2 \cdot 8\text{H}_2\text{O}$ was more prone to form gel, whereas the use of ZrCl_4 led to form a microcrystalline precipitate. Similarly, the solvent medium also plays

a crucial role in determining the gel-crystal transition. Mallick et al. reported a Ca-mediated gel that exhibited gelation under different solvents, such as dimethyl sulfoxide (DMSO), *N,N*-dimethylformamide (DMF), quinoline, *N,N*-dimethylacetamide (DMA), and *N,N*-diethylformamide (DEF).^[19b] Although crystal of Ca-MOF was obtained in mixed solvent conditions (DMF/water = 1:1, v/v). The supramolecular frameworks exhibit varying properties in response to

structural modifications. The gel component shows solvent removal within a broader temperature range in the TGA curve in comparison to its MOF equivalent. The xerogel shows 20% more CO₂ uptake capacity than the MOF analogous. In a distinct study, Preet et al., developed a separate gel/crystal system with a similar metal/linker approach.^[66] The variation in solvent conditions facilitates gelation or crystallization. In presence of methanol (MeOH), zinc ions give rise to form Zn-gel, while DMF/water combination manifests crystallization (coordination polymer; Zn-CP). The structural analysis of Zn-gel indicates an entangled spongy-like fibrous network, composed of microfibers within the supramolecular metallogel matrix. In contrast, the structural analysis of Zn-CP demonstrates the formation of a 2D sheet-like structure. Zn-gel demonstrates notable stimuli-responsive behavior in response to temperature and mechanical force. However, the Zn-CP shows superior catalytic activity compared to Zn-gel for the conversion of CO₂ to cyclic carbonate from various epoxides. In another study, Nandi et al. reported different supramolecular assemblies (gel-crystal) from a similar metal-linkers approach by varying solvent conditions.^[67] Lanthanoids were used to synthesize MOFs and gels with 3,5-pyridinedicarboxylate and 5-bromonicotinic acid. Gels were synthesized in the presence of DMA. Although MOFs were created in the presence of DMF. Both solvents (DMF and DMA) yield analogous coordination polymeric networks, including hexagonal channels with solvent-accessible pyridyl sites. The increased size of the DMA results in the immobilization of solvents within the channels, which facilitates the development of metallogels transforming MOFs into gel materials offers numerous advantages. For example, the transformation of MOFs into metallogels enhances the chemical homogeneity of this metal-organic multicomponent system, which can further tune the sorption ability and catalytic properties.^[10b,68] Furthermore, sol-gel like smart preparatory method and the high flexibility of gel materials induce distinct shapes, including tubular, network, and fiber. For instance, Jayaramulu et al. reported Al(III)-MOF-based gel, synthesized through mismatch growth of MOF nanoparticles.^[61] The synthesized composite gel material exhibits a deviation in morphological behavior compared to the pristine MOF nanoparticles. On the other hand, gels use the microporosity of their MOF framework to create supplementary pores in the composite material and manifest hierarchical pore architectures.^[69] Many times, activated metallogel-based aerogels are produced during supercritical drying or controlled thermal decomposition, creating extensive voids of meso- and macropores, together with significant structural stability.^[57] Importantly, mechanical stability is a crucial attribute of porous materials for their practical uses. Conventional MOF synthesis yields powders, which may lead to complications such as clogging in practical applications. Metallogels are far easier to synthesize than pristine MOFs or MOF-based monoliths, and they may be molded into specific forms without compromising their properties or structural integrity.

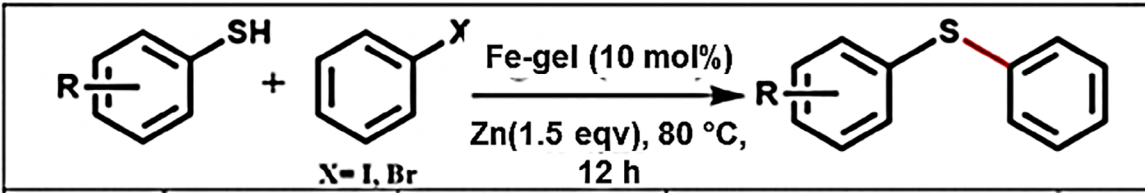
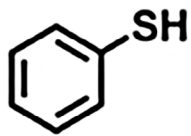
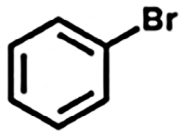
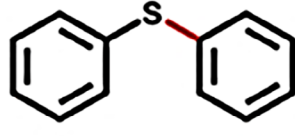
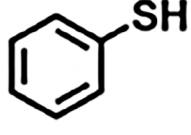
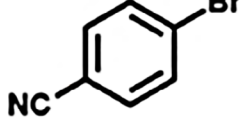
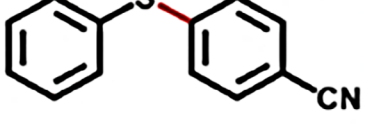
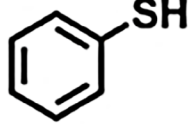
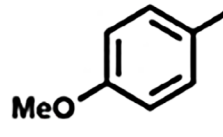
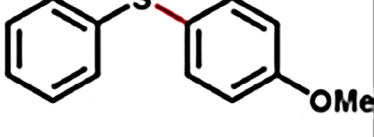
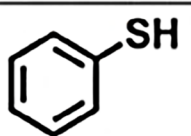
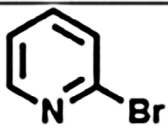
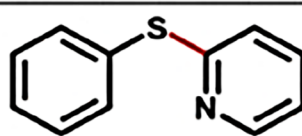
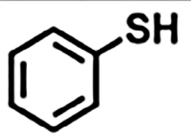
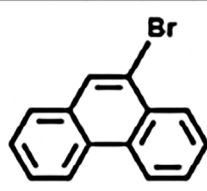
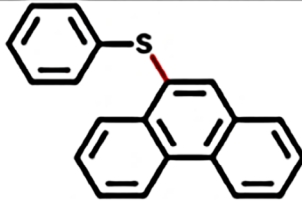
3. Metallogels in Catalysis

Metal complexes are recognized for their crucial roles in a variety of catalytic transformations, and numerous highly active metal catalysts have been developed.^[70] Over the last two decades, catalysts derived from metal-organic frameworks (MOFs) have garnered significant attention, and several methodologies have been explored in the literature to utilize MOFs as active agents in diverse reaction types. The challenge of processing MOFs without compromising their structural integrity confines their usefulness in this field.^[71] To this end, metallogels derived from identical building components as their progenitor MOFs are emerging as next-generation catalytic systems. The incorporation of metal centers into gelator molecules may confer onto metallogels potential applications as innovative supramolecular catalysts in diverse catalytic transformations.^[68] The high catalytic competence of metallogels for a variety of organic transformation reactions/electrocatalytic oxidation-reduction/photocatalytic/bio-mimicking transformations are elaborately described in Tables 2–5.

3.1. Organic Transformation

Besides the conventional requirement for efficient and selective catalytic processes that convert raw materials into valuable fine chemicals, catalytic-driven sustainable chemistry also aims for waste minimization, atom efficiency, and high catalyst recovery rates.^[72] MOFs have gained significant prominence in the field of functional materials. In one of the initial proof-of-concept investigations in the domain of MOF catalysis, a Cd-4,4'-bipyridyl coordination polymer was utilized by Fujita et al., which facilitated the cyanosilylation of carbonyl compounds.^[73] In these preliminary investigations, catalysis was not an objective in itself; instead, the emphasis was devoted to investigating the accessibility of active sites and their distribution within the framework. The integration of metal ions as pincers into metal-organic frameworks (MOFs) and their catalytic function in various organic processes has increased over the last decade.^[74] In comparison to MOFs, metallogels represent a novel and intriguing category of soft materials within the domain of heterogeneous catalysis. The first report was documented by Xing and co-workers, where metallogel was utilized as a catalyst.^[75] They developed a Pd(II)-mediated metallogel system for the oxidation of benzyl alcohol. Since then, a steep rise has been observed in metallogel-mediated catalytic transformations. Distinct metal centers are essential in many catalytic transformations. Palladium-mediated soft gel matrices and copper-based gels, similar to metal-organic frameworks (MOFs), enable coupling and azide-alkyne cycloadditions (Figure 7a).^[68] On the other hand, active catalytic centers can be produced through either the direct incorporation of metal centers or postsynthetic modification. Metal-mediated nanoparticles can create additional active centers, thereby enhancing their utility in selective catalytic transformations. The in-situ insertion of metal nanoparticles within metallogel templates generates additional

Table 1. Conversion of substrate scopes for Aryl-S coupling reaction. Reprinted table from Ref. [88]. Copyright (2020), with permission from the American Chemical Society.

				
entry	thiol	aryl halide	aryl sulfide	yield (%)
1.				88
2.				89
3.				87
4.				88
5.				90

active sites (Figure 7b).^[76] The interactions of metal nanoparticles with definite functionalities of substrates enable suitable mass transfer and enhance catalytic efficiency. Like metal-mediated catalytic centers, the use of functionalities in organic linkers may also impact organic transformations. For instance, hydrogen bond donating (HBD) functionalities in Friedel–Crafts alkylation reactions are a recognized area of catalytic research within MOF chemistry.^[77] Hence, there is a great opportunity to utilize these soft gel materials in effective organic transformations (Figure 7c). The enantioselective transformations utilizing a soft gel matrix are also in the early stages of development. The incorporation of specific linkers can adjust the available centers for active

transformations (Figure 7d).^[78] Soft materials can serve as chiral catalytic scaffolds, especially when they incorporate chiral ligands or metal centers that induce stereoselectivity. The 3D fibrous network of metallogels provides a confined microenvironment that facilitates selective interactions between the substrate and the chiral catalytic sites. This confinement can improve reaction rates and enantioselectivity, resembling enzyme-like behavior.

(a) **Coupling reaction and C–C bond formation.** Numerous important compounds (pharmaceutical, biological, optoelectronic, etc.) that are either commercially available or still in the development stage have aromatic carbon–

Table 2. Metallogels act as catalysts for diverse organic transformation reactions.

Entry No.	Metallogel System	Active Site	Reaction	Reference
1.	Pd-mediated discrete gel	Pd(II)	Double Michael addition	[56]
2.	Pd-metallogel	Pd(II)	Oxidation of benzyl alcohol	[75]
3.	Pd(II) Metallogel	Pd(II)	Suzuki–Miyaura cross-coupling	[82]
4.	Iron/Palladium-based mixed gel	Pd(II)	Suzuki cross-coupling	[83]
5.	L6–Pd (Pd incorporated iron-based metallogel)	Palladium(II)	Suzuki–Miyaura cross-coupling	[84]
6.	Cu-based coordination polymer gel	Copper(I)	1,3-dipolar Huisgen cycloaddition reaction	[95]
7.	Fe ₃ O ₄ @Pd-gel	Pd(II)	Suzuki–Miyaura coupling	[26]
8.	Calcium based gel	Ca(II)	Hydrosilylation reaction between benzaldehyde/diphenylsilane	[19b]
9.	Iron-based gel	Fe(III)	Benzyl alcohol conversion (using 10% H ₂ O ₂)	[121]
10.	Ag ⁺ -tetrazole-based metallogel	Silver ion	4-nitrophenol reduction	[111]
11.	Silver-based gel	AgNPs	4-nitrophenol reduction	[112]
12.	Au@L16-gel	AuNPs	4-nitrophenol reduction	[119]
13.	Silver metallogel	AgNPs	Reduction of 4-nitrophenolate	[114]
14.	Phosphine-Pd gel	Pd(II)	Suzuki–Miyaura coupling	[85]
15.	Rh-based gel	Rh(II)	CO ₂ cycloaddition	[103]
16.	Copper(I) metallogel	Copper(I)	Click reaction	[22]
17.	Zr-mediated gel	Zr cluster	CO ₂ cycloaddition	[104]
18.	L25-Pd ₃ L (Palladium-based metallogel)	Pd(II)	Suzuki–Miyaura coupling	[86]
19.	Silver nanoparticles incorporated Fe(III) metallogel	AgNPs	4-nitrophenol reduction	[116]
20.	Copper(II) metallogel	Copper(II)	Azide–alkyne cycloaddition and CO ₂ fixation	[96]
21.	Silver-based hydrogel	AgNPs	Reduction of 4-nitrophenol/methylene blue/Cr(VI)	[113]
22.	Rh(II) metallogel	Rh(II)	Hydrosilylation (reduction of aldehyde and ketones)	[122]
23.	Coporphyrin gel	Co(II)	Acyl transfer and Diels–Alder reaction	[123]
24.	Cu-metal-organic gel (MOG)	Copper	Conversion of SO ₂ and CO ₂ to corresponding cyclic carbonates	[105]
25.	Fe(III) Metallogel	Iron (III)	Aryl–S coupling	[88]
26.	Silver incorporated iron based gel	Iron(III) and silver(0)	Reduction of nitroaromatics	[117]
27.	Copper metallogel	Copper(II)	Click reaction	[97]
28.	Cu-glycoclusters gel	Cu(I)	Click reaction	[98]
29.	Silver mediated gel matrix	AgNPs	Multicomponent A ³ coupling	[91]

Table 2. (Continued)

Entry No.	Metallogel System	Active Site	Reaction	Reference
30.	Nickel(II)-Xerogel	Nickel(II)	CO ₂ fixation and Knoevenagel condensation	[106]
31.	Zn-CP1	Zinc ion	CO ₂ fixation	[66]
32.	M ^I G7TA _g	Iron(III) and AgNPs	Nitro group reduction	[118]
33.	Fe-metallogel	Fe ³⁺	Nitroarene reduction	[120]
34.	Ag@Fe_MG	AgNPs and Fe(III)	CO ₂ fixation and A ³ coupling	[76]
35.	Silver-based gel	AgNPs and —OH/—NH functionality	CO ₂ fixation	[107]

Table 3. Tabulation of Metallogel as photocatalysts for various transformations.

Entry No.	Metallogel System	Active Site	Reaction	Reference
1.	Cr(III)-mediated gel	Hydroxyl radical generation on the metallogel surface	Dye (MO, MB, RhB) degradation	[126]
2.	Zn(II)-based gel	The nanofibrous structure of xerogel helps in the entrapping and separation of charges at the surface	Dye (MO, MB) degradation	[127]
3.	Ag and Au-based gel	Ag/Au nanoparticle formation upon gel matrix	Photocatalytic reduction of 4-nitrophenol	[128]
4.	Pd-metallogel	Pt-nanoparticles, Pd center, and porphyrin-mediated photoactive moiety	Photocatalytic hydrogen production	[133]
5.	Zn(II) mediated gel	Terpyridine-anthracene-based extended conjugated linker acts as a light-harvesting agent, and zinc acts as the active site	Photocatalytic H ₂ production	[125]
6.	Pt-loaded zinc-mediated gel	Pt nanoparticles and Zn centers synergistically play as the active center and intermolecular charge delocalization in the L47 linker	Photocatalytic CO ₂ reduction and H ₂ production	[134]
7.	Ru-mediated gel	Porphyrin-terpyridine mediated extended conjugated linkers for intermolecular charge delocalization and Ru as the active center	Photocatalytic CO ₂ reduction	[135]
8.	Co-mediated gel	Hydrophobic microenvironment within gel matrix and active metal centers	Photocatalytic CO ₂ reduction	[136]
9.	Nd mediated nitrogen-doped carbon quasiaerogel	Highly porous quasiaerogel and active Nd center	Photocatalytic CO ₂ reduction	[137]
10.	Fe ₃ O ₄ /metallogels/SA	Fe ₃ O ₄ nanoparticles and active metal centers of metallogels	Removal of chlortetracycline hydrochloride	[138]
11.	Silver-based gel	Cooperation between plasmonic silver nanoparticles and strong CO ₂ adsorption efficiency	Photocatalytic CO ₂ reduction	[107]
12.	Co-mediated gel	Photoactive organic moiety and active Co ²⁺ center	Photocatalytic CO ₂ reduction	[139]

carbon and aromatic carbon–nitrogen bonds.^[79] In the presence of a base, a potent and versatile technique for the production of carbon–carbon bonds can be achieved through the palladium-catalyzed cross-coupling reaction involving organoboron compounds and a variety of organic electrophiles.^[80] By seeing the impact on organic synthesis, in 2010, the Nobel Prize in Chemistry was awarded to Heck, Negishi, and Suzuki for discovering Pd-mediated catalysis for C–C bond formation.^[81] Palladium can be immobilized on diverse solid substrates, including polymeric structures, activated carbon, and porous frameworks to

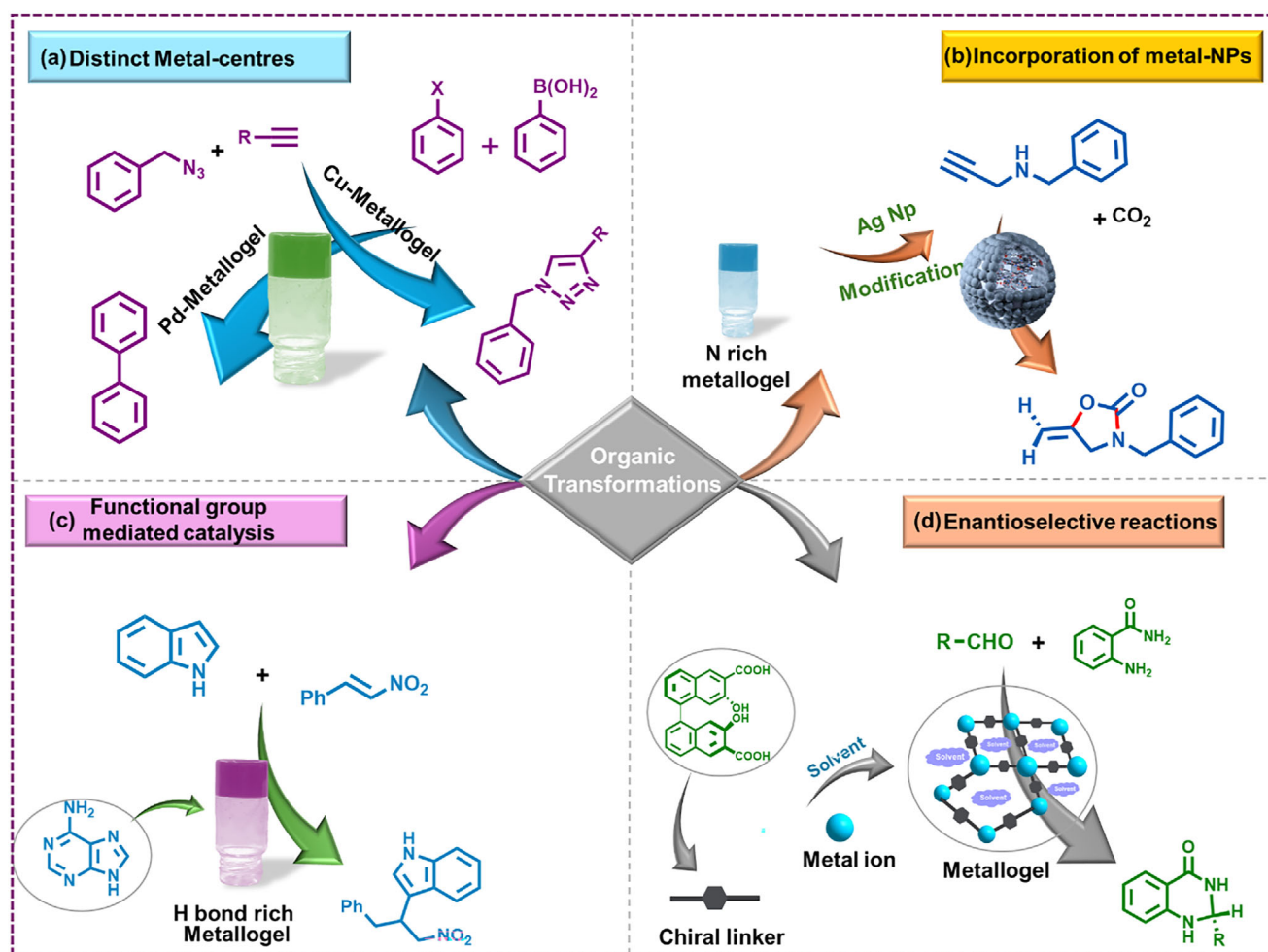
increase the catalytic activity. In this context, the application of supramolecular gels as support for Pd incorporation has opened a significant pathway to constructing an efficient catalyst for C–C bond formation. For instance, Tu et al. developed the first air-stable Pd-mediated organometallic LMWG, which was able to form a gel in the presence of diverse organic solvents and exhibited efficient catalytic activity for C–C bond formation.^[56] L1 (Figure 8) linker with a shorter alkyl arm shows poor solubility in organic solvents, whereas long C₁₆ alkyl chains enhance solubility in organic solvents. This induces aggregation through van der Waals

Table 4. Tabulation of metallogels as electrocatalysts.

Entry No.	Metallogel System	Active Site	Reaction	Reference
1.	Fe ₃ O ₄ /N-doped graphene aerogels	Fe ₃ O ₄ nanocrystals anchored on 3D graphene networks	ORR	[143]
2.	Fe-L55 gel/Al-L55 gel	Active iron center	OER	[144]
3.	Co ₂ P@CoNPG-900	Co nanocrystals and Co-Nx/P-doped carbon matrix	OER/ORR	[145]
4.	Fe-metallogel/ NCNTs-hybrid composite	Core-shell Fe-Fe ₂ O ₃ nanoparticles anchored onto NCNTs	ORR	[146]
5.	Co-Gel	Co(II) center and Co ₃ O ₄ nanoparticles	OER	[147]
6.	Co-Gel	Co(0) nanoparticles embedded with heteroatom-doped carbon structure	OER	[148]
7.	CoNC-MOG-9	Co nanoparticles and nitrogen-doped porous carbon structure	ORR/OER	[149]
8.	Ni-based gel	N/O-doped graphitic carbon structure and nickel clusters	HER/OER	[150]
9.	Ni-mediated gel	Active Ni-centers	OER	[151]
10.	AgNP-Gel	Peptide containing a conjugated linker and silver nanoparticles in zero oxidation state	HER	[152]
11.	Fe-metallogel with nitrogen-doped carbonized material	Highly porous Fe-N doped interpenetrating polymer networks based graphitic carbon structures	ORR	[154]
12.	Co-Fe-Ni-based mixed metallogel	Spinel-type mixed metal oxide	OER	[155]
13.	Nitrogen/Phosphorus dual-doped carbon quas aerogels	CoP, FeP, and Ni ₂ P nanocrystals embedded in 3D conductive frameworks	ORR/HER	[156]
14.	Pd/Co-bimetallic gel	Pd-NPs and Co-centers	HER	[21]
15.	Zn/Co-mediated gel	Cobalt/nitrogen dual-doped porous carbon nanosheets	ORR	[157]
16.	Ni/Fe-mediated gel	Active Ni/Fe centers	OER	[158]
17.	Fe/Co/Ni-based gel	Multimetallic active centers and redox interplay between Fe ³⁺ /Fe ²⁺ and Ni ³⁺ /Ni ²⁺ states	OER	[159]
18.	Ni _{n-6} Fe _{n-4} -metallogel	Active Ni/Fe centers	HER/OER	[160]
19.	Fe/Co-mediated gel	Mixed valence states Fe(II)/Fe(III) and Co(III)/Co(II)	OER	[161]
20.	Fe/Cr/Ni-mediated gel	Active Fe/Cr/Ni centers	HER/OER	[162]
21.	Fe _{n-1} Co _{n-9} -metallogel	Active Fe/Co-centers and oxygen/nitrogen-rich gelator	ORR	[163]
22.	Al/Ni/Cu-mediated trimetallic gel	Distinct electronic configuration of nickel modulated by copper in Al/Ni/Cu-mediated gel network	Methanol electrooxidation	[167]
23.	Iron-porphyrin-graphene hydrogel	Redox-active porphyrin complex	Electrochemical reduction of CO ₂	[170]
24.	Porphyrin-ferrocene-based imine mediated metallogels (Ni ²⁺ , Co ²⁺ , Pd ²⁺ and Zn ²⁺)	Active center as metal ions and porphyrin ring for active proton adsorption/desorption	HER/OER/ORR	[171]
25.	Co-terpyridine-based gel	Active tpy-Co ²⁺ (3N-Co) configuration	OER	[173]
26.	Co-terpyridine-mediated gel	Cobalt-mediated rigid terpyridine-based polymeric unit	OER	[174]
27.	UiO-67-mediated gel	UiO-67 nanoparticles	Photoelectrocatalytic H ₂ production	[176]
28.	Zn-mediated gel	Nanoporous carbonized composite material with active cobalt/zinc centers from ZIF-67/Zn gel	ORR	[177]

Table 5. Tabulation of metallogels as biomimicking catalysts.

Entry No.	Metallogel System	Active Site	Catalytic Activity	Reference
1.	Cu ²⁺ -hydrogel	[(L + D)-L72-Cu ³⁺ -O ₂ ⁻] species	One-electron O ₂ reduction (artificial enzyme)	[180]
2.	Cu ²⁺ -gel	Cu ²⁺ -center	Catechol oxidation	[181]
3.	Dicopper-mediated gel	Cu ²⁺ -center	Catechol oxidation	[182]
4.	Ru-metallogel	Ru ³⁺ -centers and 3D fibrous porous structure of Ru-metallogel	Intrinsic horseradish and NADH-peroxidase biomimicking	[183]
5.	VO ₂ -L77 metallogel	Supramolecular gel network promotes easy diffusion of substrates	Bromo peroxidase mimicking activity	[184]
6.	Cu-based gel	Cu ²⁺ and nanodimension gel network structures	Phenoxazinone Synthase-like Activity	[185]
7.	Co-mediated gel	Co ²⁺ -center	Peroxidase-like activity and Phenoxazinone Synthase-mimicking	[41a]
8.	Fe(III)-metallogel	Fe ³⁺ -active center	Siderophore mimicking activity	[47]

**Figure 7.** Schematic representation of different organic transformations such as (a) distinct metal-center mediated, (b) metal nanoparticle-mediated, (c) functional group induced, and (d) enantioselective reactions utilizing metallogel as heterogeneous catalysts.

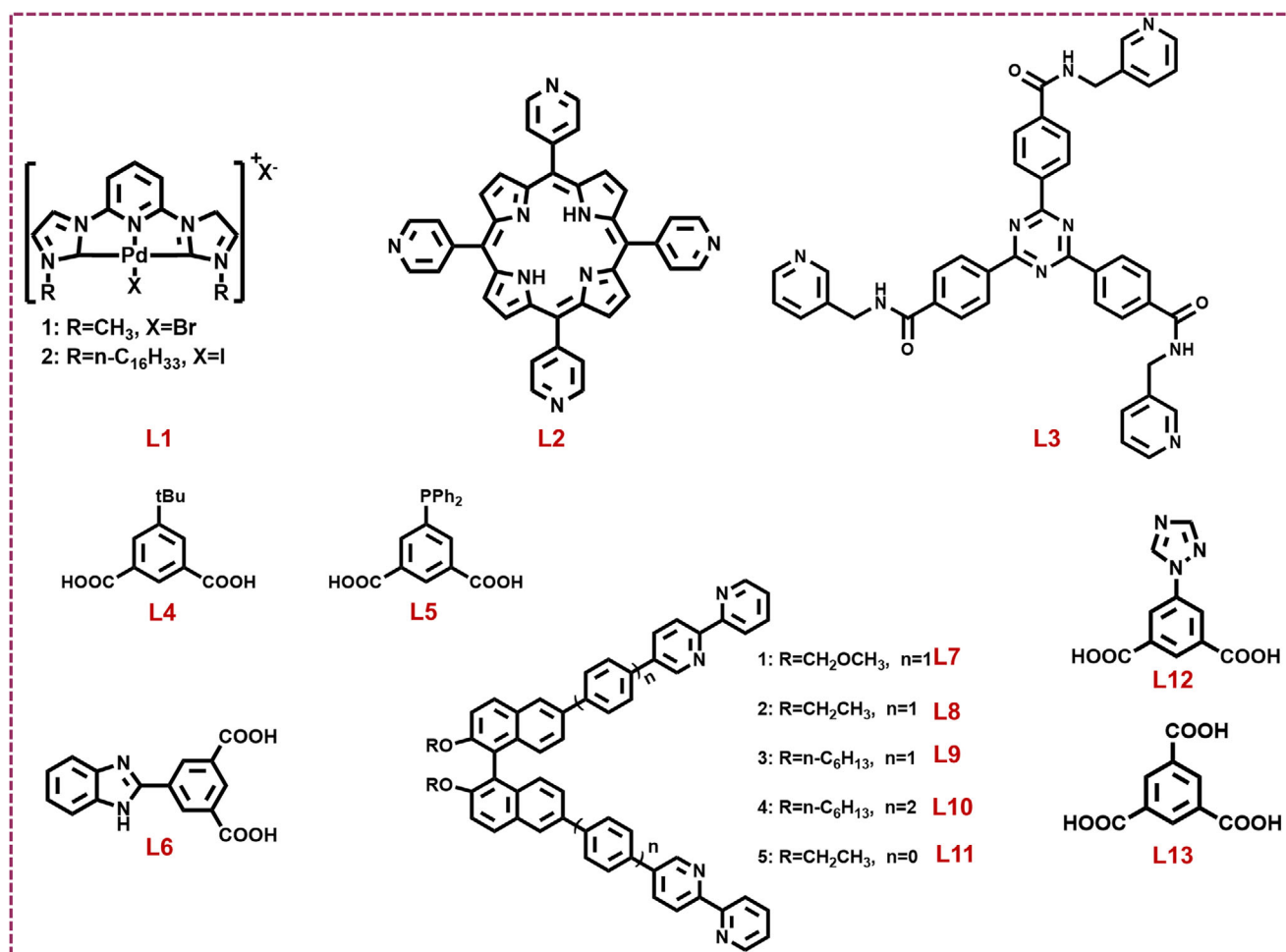


Figure 8. Gelators from L1–L13 were used to synthesize metallogels for diverse organic transformation reactions.

interaction and forms stable, transparent, and thermoreversible gels. Apart from this, π – π stacking and Pd–Pd interactions also favor the aggregation process to form 3D fibrillar gel networks. Furthermore, it was successfully used in C–C bond-forming via double Michael additions. The ability to carry out catalysis within the gel matrix, without gel degradation, suggests new paradigms in gel-phase catalysis. Liu et al. developed a Pd(II)-based metallogel,^[82] which was synthesized by combining a tripodal ligand (L3; Figure 8) and Pd(COD)(NO₃)₂ (COD = cycloocta-1,5-diene) in a CH₃OH–CHCl₃ solvent mixture. The gel formation was facilitated by Pd(II)–pyridine coordination, hydrogen bonding, and π – π interactions, which facilitated a fibrous network structure with a high surface area. The distinctive combination of noncovalent interactions and structural integrity renders the Pd(II)-metallogel an effective, reusable, and sustainable catalyst for Suzuki–Miyaura cross-coupling reactions. Zhang et al. immobilized the Pd center using Pd(COD)Cl₂ into iron-mediated gel matrix.^[83] The linkers L4 and L5 (Figure 8) were used as LMWGs. The gel network promotes effective mass transport of reactants to the catalytic sites and inhibits the agglomeration of Pd species. Later, Huang and coworkers also developed a Fe(III)/Pd(II)-mediated bimetallic soft gel

system using L6 (Figure 8) as a gelator.^[84] The gel network was formed by the strong coordination of Fe(III) to the carboxylate groups, and the imidazole nitrogen was coordinated to Pd(II) through a reversible coordination bond exchange. This dynamic immobilization improves the stability of Pd(II) and the catalytic effectiveness of the cross-coupling reaction. The coupling of iodobenzene with phenylboronic acid yielded >99% product in methanol at 60 °C within 30 min. In another study, Liao et al. designed a Pd(II)-based magnetite nanoparticle-supported metallogel (Fe₃O₄ @Pd-gel).^[26] The gel system was developed through the self-assembly of the L3 (Figure 8) ligand with Pd(COD)(NO₃)₂ in a CHCl₃–MeOH solvent system, which was further incorporated with superparamagnetic Fe₃O₄ nanoparticles. The Pd(II) ions coordinate with the pyridine donor sites of the ligand and exhibit a fibrous nanostructured network (Figure 9a–c). This Pd(II) xerogel serves as a heterogeneous catalyst in the Suzuki–Miyaura cross-coupling process. Interestingly, the superparamagnetic properties of Fe₃O₄ nanoparticles make easy recovery of the catalyst using a magnetic rod, avoiding the filtration or centrifugation process. The catalyst exhibited remarkable reusability, sustaining high yields (92%–99%) across four reaction cycles without considerable loss of activ-

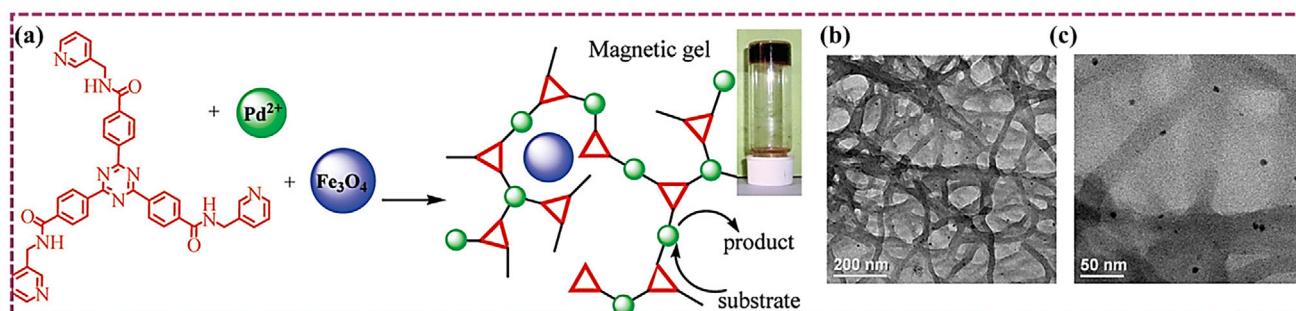


Figure 9. (a) Schematic representation of the formation of magnetic gel and nanostructure morphology, (b) field emission scanning electron microscopy (FESEM), and (c) transmission electron microscopy (TEM) of Fe_3O_4 @Pd-gel. Partly adapted structure and figures from Ref. [26]. Copyright (2010), with permission from the American Chemical Society.

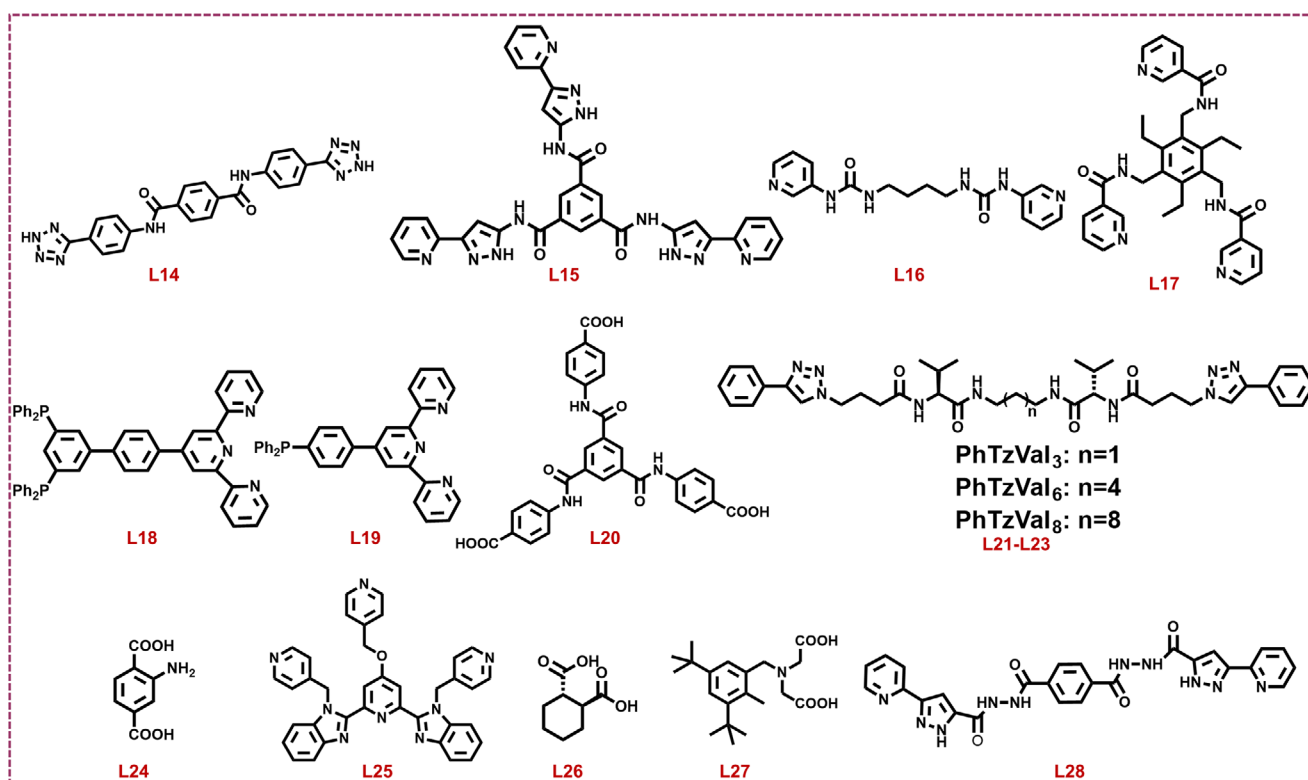


Figure 10. Gelators from L29–L40 were used to synthesize metallogels for diverse organic transformation reactions.

ity. Furthermore, this group also utilized phosphine-based gelators (**L18–L19**; Figure 10) to develop a Pd(II) metallogel and employed it for the Suzuki–Miyaura cross-coupling reaction.^[85] In a distinct study, Ye et. al. utilized a hexadentate linker **L25** (Figure 10) to form a Pd-based metallogel.^[86] This Pd(II) metallogel serves as a heterogeneous catalyst for the cross-coupling reaction, which manifests the coupling of aryl bromides with phenylboronic acid in the presence of potassium carbonate (K_2CO_3) as a base. Polar protic solvents were used to accomplish the reaction under mild conditions (70 °C, ambient atmosphere). This catalytic system offers exceptional efficiency (up to 99% yield) with minimal catalyst loading (0.001 mol%), which makes it an eco-friendly and scalable method for the Suzuki–Miyaura coupling reaction.

Because of the widespread use of carbon–sulfur (C–S) coupled products in pharmaceuticals and biology, transition-metal-catalyzed aryl–S cross-coupling reactions are of importance.^[87] In a recent study, Dhibar and coworkers developed a metallogel catalyst using iron as the metal source and **L31** (Figure 11) as a gelator to form metallogel, which was further utilized in the synthesis of aryl thioethers via a C–S coupling reaction.^[88] The catalyst reacts with aryl halides (bromo-/iodo-derivatives) with thiophenols. Such reactions have been the focus of medicinal chemistry and molecular biology, and their derivatives. The diphenylsulfide derivatives were obtained with a high yield (~90%), showing the efficiency of the metallogel as a catalyst (Table 1).

Multicomponent reactions (MCRs) are very efficient synthetic methodologies that produce important scaffolds (C–

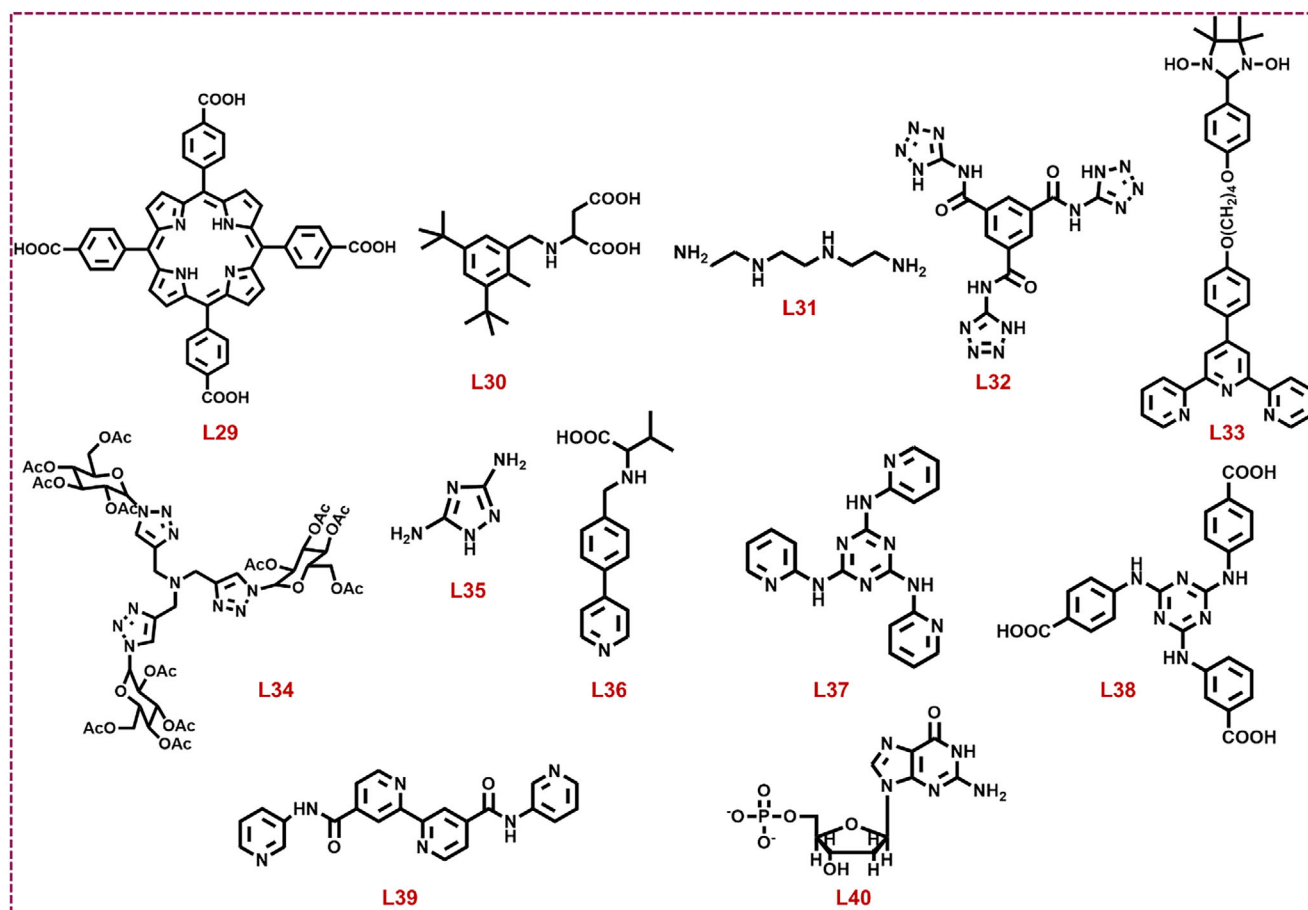


Figure 11. Gelators from L29–L40 were used to synthesize metallogels for diverse organic transformation reactions.

heteroatoms) from easily available precursor components.^[89] In the context of MCRs, A^3 coupling is known as one of the fundamental reactions. It is a transition-metal catalyzed three-component (aldehydes, amines, and terminal alkynes) reaction that forms propargyl amine derivatives as a product.^[90] Saha and coworkers recently designed a series of metallogels using Ag(I) precursors and an amine-functionalized gelator (L35; Figure 11).^[91] Gel 1 and Gel 2 were synthesized using AgOTf as a metal source in presence of water–methanol and water–THF solvent combinations, respectively. Whereas Gel 3 was synthesized using AgNO₃ as precursor metal salt and water–DMF combination as solvent medium. All silver-mediated gels show rod-belt-like morphology (Figure 12). These gels function as efficient catalysts for a three-component coupling process that includes benzaldehyde, morpholine, and phenylacetylene, which results in the formation of propargylamine derivatives. The triflate counter anion in Gel 1 and/or Gel 2 has poor hydrogen bonding compared to the nitrate counter anion in Gel 3, which manifests the lower yield and selectivity of propargylamine. In a separate study, Mondal and coworkers developed a strategy to build a bimetallic effective heterogeneous catalyst for the multicomponent A^3 coupling reaction.^[76] Silver nanoparticles were stabilized within Fe(III) gel matrix. Tripodal linker L38 (Figure 11) was used to synthesize a stable gel network structure.

(b) Click reaction. In 1960, Rolf Huisgen introduced the idea of 1,3-dipolar cycloadditions, which involve adding 1,3-dipoles to multiple-bond systems and became one of the most useful synthetic procedures in heterocyclic chemistry.^[92] Similar to the Diels–Alder reaction, a 1,3-dipole functions as a 4π system reacts with a dipolarophile as 2π electrons, which results in the formation of a five-membered product via $[3 + 2]$ cycloaddition. Before the revolutionary idea of click chemistry, the Huisgen reaction was a well-established method for producing heterocyclic molecules. In general, azide–alkyne cycloadditions give rise to form combinations of regioisomers under thermal conditions. In 2001, Devaraj et al. defined the criteria for an “ideal reaction,” termed a click reaction.^[93] In this scenario, the Cu(I)-catalyzed processes yield exclusively 1,4-disubstituted 1,2,3-triazole compounds under mild conditions. Copper(II)/copper(I) salts (CuSO₄, CuI, CuBr, etc) are used in azide–alkyne cycloadditions, where sodium ascorbate is used as a reducing agent for the reduction of Cu(II) to Cu(I). Along with this, organic polymer, MOFs, covalent organic frameworks (COFs), and silica-supported copper(I) substrates are extensively studied.^[94] In contrast, the utilization of metallogels for the Huisgen 1,3-dipolar cycloaddition of alkynes and azides is still in its nascent phase. He et. al. synthesized a series of chiral copper(I) metallogels using binaphthyl-based bisbipyridine ligands (L7–L11; Figure 8).^[95] Cu(CH₃CN)₄BF₄ was

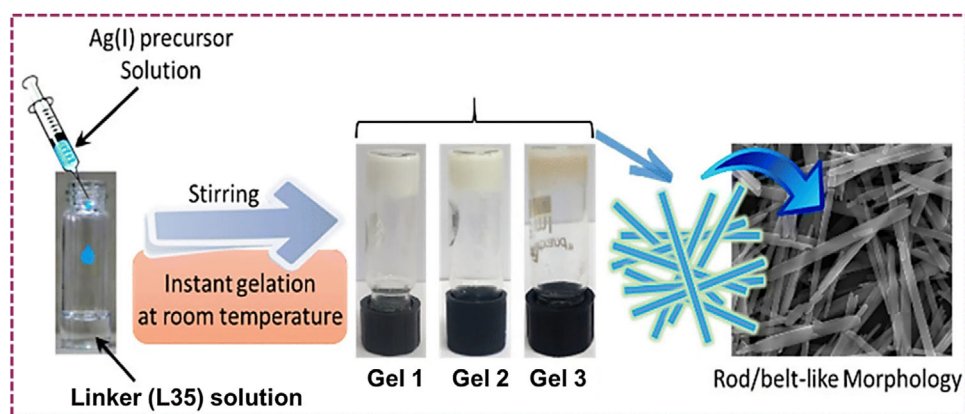


Figure 12. Schematic representation of silver-mediated gel synthesis using L35 linker and morphological analysis (FESEM image). Reprinted scheme from Ref. [91]. Copyright (2023), with permission from the Royal Society of Chemistry.

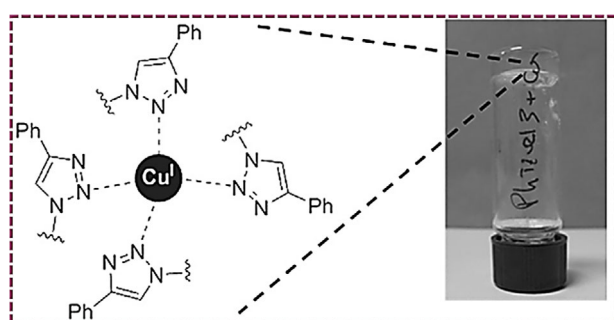


Figure 13. Probable interaction pathways of the tetrazole group with Cu(I) center. Reproduced from Ref. [22]. Copyright (2023), with permission from the Royal Society of Chemistry.

used as Cu(I) precursor with **L7**, **L8**, and **L9** gelators to form ordered fibrous gel networks in presence of acetonitrile (ACN)/dichloromethane (DCM) (V/V = 1:1). Interestingly, incorporation of hydrophilic moiety instead of hydrophobic component leads to better gel formation. Gelation was hardly observed in case of the **L9** linker, and no gelation was observed for the **L10** linker due to the increase in spacer size. **L7**-mediated Cu(I) gel shows multistimuli responsive behavior (e.g., temperature, ultrasonication, changes in redox behavior). These metallo-gels were used in Huisgen 1,3-dipolar cycloaddition. Among all, **L9**-mediated Cu(I) gel had the highest catalytic activity in water at ambient temperature. The long lipophilic carbon chain manifests a definite organic microenvironment in the aqueous medium, which accelerates the reaction process. In a distinct study, Araujo and coworkers synthesized low-molecular-weight gelators (**L21–L23**; Figure 10).^[22] The gelators were developed from L-valine and functionalized with triazole units. The triazole functionality efficiently coordinates with copper(I) ions to form metallo-gels (Figure 13). These metallo-gels function as heterogeneous catalysts for the Huisgen 1,3-dipolar cycloaddition, which entails the coupling of phenylacetylene and benzylazide. **L22** and **L23** (Figure 10) mediated Cu(I) gels show higher efficiency in catalytic conversion than **L21**, due to an increase in carbon chain length. In another study, Karan et. al. developed a copper(II) metallo-gel by combining CuCl₂ with **L27** (Figure 10) gelator in water.^[96] This metallo-gel serves as a multifunctional

precatalyst for Huisgen 1,3-dipolar cycloaddition reaction. Cu(II) was reduced to Cu(I) through electron transfer with the ligand, which subsequently activated the terminal alkynes for nucleophilic attack by azides. It produces regioselective 1,4-disubstituted triazoles with high efficiency (91% yield at 50 °C within 6 h). In a recent study, Zhao and coworkers synthesized a copper-mediated metallo-gel, where **L33** (Figure 11) was utilized as a gelator and CuSO₄·5H₂O was used as Cu(II) precursor.^[97] It was utilized as a heterogeneous catalyst for the copper-catalyzed azide-alkyne cycloaddition (CuAAC). Sodium ascorbate was used for in-situ reduction of Cu(II) to active Cu(I) species that coordinate with the azide group. Terminal alkyne was then activated by π -coordination. It increases the nucleophilicity that promotes regioselective attack by the azide. In a recent study, Bietsch and co-workers explored a new class of trimeric branched glycoconjugates as supramolecular gelators.^[98] **L34** (Figure 11) gelator demonstrated a remarkable ability to self-assemble in a range of solvents. Upon the addition of CuSO₄, these gels transform into metallo-gels that retain mechanical integrity and become catalytically active. The copper-metallo-gels catalyze the azide-alkyne cycloaddition reactions efficiently and achieve 100% conversion of reactants to triazole products in less than 2 h at room temperature. Interestingly, a smart column-mediated catalytic process was developed to enhance real-world applicability. The study illustrates the powerful combination of molecular self-assembly and catalysis, which offers a green, reusable, and versatile platform for promoting bioorthogonal chemistry and potentially extending to catalytic transformations.

(c) **CO₂ and SO₂ fixation.** The worldwide trend of environmental deterioration threatens the globe, epitomized by rising carbon dioxide (CO₂) emissions and growing ecological footprints, causing global warming.^[99] The increasing levels of carbon dioxide emissions lead to ecological disruptions, impacting human well-being and biodiversity, intensifying climate change, and other interconnected concerns. These concerns have sparked interest in employing natural materials to make green products and reduce anthropogenic carbon dioxide emissions in all feasible ways.^[100] In contrast to carbon capture and storage, the conversion of CO₂ into valuable

chemicals and fuels is a more viable approach for reducing carbon emissions.^[101] MOFs, COFs, ZIF, and porous organic polymer (POP) related porous frameworks have been extensively used in CO₂ fixation studies.^[102] Recent research on metallogels has identified them as viable catalysts for the utilization of CO₂ and their conversion into value-added products. In this context, Zhu et al. developed a rhodium-based metal-organic aerogel, which was further used as an efficient catalyst for CO₂ cycloaddition.^[103] Rh₂(OAc)₄ and the linker **L20** (Figure 10) were mixed with a solvent combination of DMF/water (20:1, v/v) to form a yellow-colored gel via the "heat-set" method (85 °C, for 50 h). Highly porous aerogel was obtained by drying with subcritical CO₂, which was composed of dinuclear rhodium paddle-wheel units. Concurrently, Liu and coworkers developed a Zr-based metallogel synthesized from ZrCl₄ and **L24** linker (Figure 10) in ethanol/DMF at 80 °C for 4.5 h.^[104] The gel was composed of UiO-66-NH₂ nanoparticles and combined the advantages of metal-organic frameworks (MOFs) with gel materials, offering a high surface area (up to 1040 m²/g), permanent porosity, and defect sites that enhance catalytic performance. It serves as a heterogeneous catalyst for the cycloaddition of CO₂ to form cyclic carbonates at atmospheric pressure and 100 °C, with tetrabutylammonium bromide (TBAB) as a cocatalyst. The catalytic mechanism entails the simultaneous activation of the epoxide and CO₂ by the acidic and basic sites within the material. The porous structure promotes efficient diffusion of reactants and products, which results in high catalytic turnover with yields surpassing 90%. In a separate study, Karan and coworkers synthesized a Cu-mediated metallogel utilizing **L27** as a linker and employed it to convert different epoxide substrates into cyclic carbonates through CO₂ fixation.^[96] Later Karan and coworkers introduced another copper-mediated metallogel for CO₂ fixation. A dark green-coloured copper(II) metallogel was synthesized by combining CuCl₂ and the disodium salt of **L30** (Figure 11) in water. It forms a stable fibrillar network via noncovalent interaction.^[105] In a distinct study, Saha and coworkers synthesized a nickel(II)-mediated gel.^[106] A nitrogen-rich amine functionalized **L35** (Figure 11) ligand and nickel(II) acetate were used to form a self-assembled structure. Micrographical analysis exhibits hexagonal sheet-like morphology (Figure 14a). The gel system possesses a high concentration of Lewis acidic Ni(II) sites and pendant Lewis basic primary amines (-NH₂), which establishes a bifunctional catalytic system. Ni(II) sites and amine groups synergistically capture and activate CO₂ molecules, which further facilitate their interaction with epoxides under mild circumstances in presence of a tetrabutylammonium bromide (TBABr) cocatalyst. The reaction occurs by the ring-opening of epoxide through bromide ions, followed by CO₂ insertion and subsequent ring closure to yield cyclic carbonates (Figure 14b). The porous network of the xerogel improves mass transfer, which reflects high catalytic efficiency with minimum catalyst loading (0.59 mol %) and remarkable recyclability. In a recent study, Preet and coworkers used **L36** (Figure 11) gelator and zinc acetate to create a gel and coordination polymer.^[66] Both the gel and coordination polymer were used as catalysts for CO₂ fixation via cycloaddition of epoxide derivatives.

Because of its lower metal concentration and distinct structural motifs, the gel has lesser catalytic activity than that of coordination polymer. This shows the importance of material architecture and composition in catalytic performance. In another study, Alam and coworkers developed silver-mediated gel with a guanosine-based linker (**L40**; Figure 11). The -OH/-NH functionalities of the linker induce a strong affinity toward CO₂ adsorption, which makes it an effective catalyst for CO₂ cycloaddition reaction.^[107]

Using propargyl alcohols to synthesize α -alkylidene cyclic carbonates is a straightforward and atom-economical approach to utilize CO₂. Interestingly, α -alkylidene cyclic carbonates represent a notable class of heterocyclic compounds with extensive applications in chemical and medical chemistry.^[108] In this regard, Mondal et al. developed a bimetallic metallogel-based system for CO₂ fixation via the conversion of propargylic alcohols to corresponding cyclic carbonate derivatives.^[76] Silver nanoparticles were stabilized using an iron-mediated gel matrix. **L38** (Figure 11) was used as a gelator to self-assemble with Fe(III) ions. Excellent CO₂ conversion at room temperature through the cyclization of propargylic alcohols (~99%) was induced by the combined effects of the N-rich framework and the alkyne-activating affinity of AgNPs.

Cyclic sulfites are one of the effective classes of organic compounds, which are reactive toward nucleophiles. In the lithium-ion battery industry, sulphite-based compounds are extensively used.^[109] The reaction with epoxide and sulfur dioxide (SO₂) leads to form a cyclic sulfite as the product. Typically, not too many investigations were carried out to catalyze these reactions. In this regard, a first report was documented by Karan et al. with metallogel-mediated catalyst for SO₂ cycloaddition. Copper(II) salt and **L30** (Figure 11) linker were used to create a supramolecular gel, which demonstrated effective catalytic activity for the fixation of SO₂.^[105]

(d) Nitro group reduction. The conversion of nitro groups to amines is a crucial transition in organic chemistry, commonly employed in pharmaceuticals, dye industries, agrochemicals, etc., to synthesize different fine chemicals.^[110] Lee and coworkers synthesized a tetrazole-derived gelator (**L14**; Figure 10) that integrates with silver ions (Ag⁺) to form a supramolecular gel architecture in aqueous solution under alkaline conditions.^[111] This metallogel had a distinctive fiber architecture, in which silver nanoparticles were incorporated. These nanoparticles were essential for facilitating the reduction of 4-nitrophenol (4-NP) with sodium borohydride (NaBH₄) as the reducing agent. The mechanism of this catalytic process was the adsorption of 4-NP onto the surface of silver nanoparticles, where electrons from NaBH₄ were transferred to the nitro group of 4-NP, thereby promoting its reduction to 4-aminophenol. The gel matrix stabilizes the silver nanoparticles and increases their catalytic effectiveness by creating a favorable environment for the reaction. In a distinct study, Sengupta and coworkers utilized a pyridine-pyrazole-mediated tripodal linker (**L15**; Figure 10) to form a gel with silver ions in presence of water.^[112] The pyrazole group possesses hydrogen bonding donor and acceptor sites, along with metal coordina-

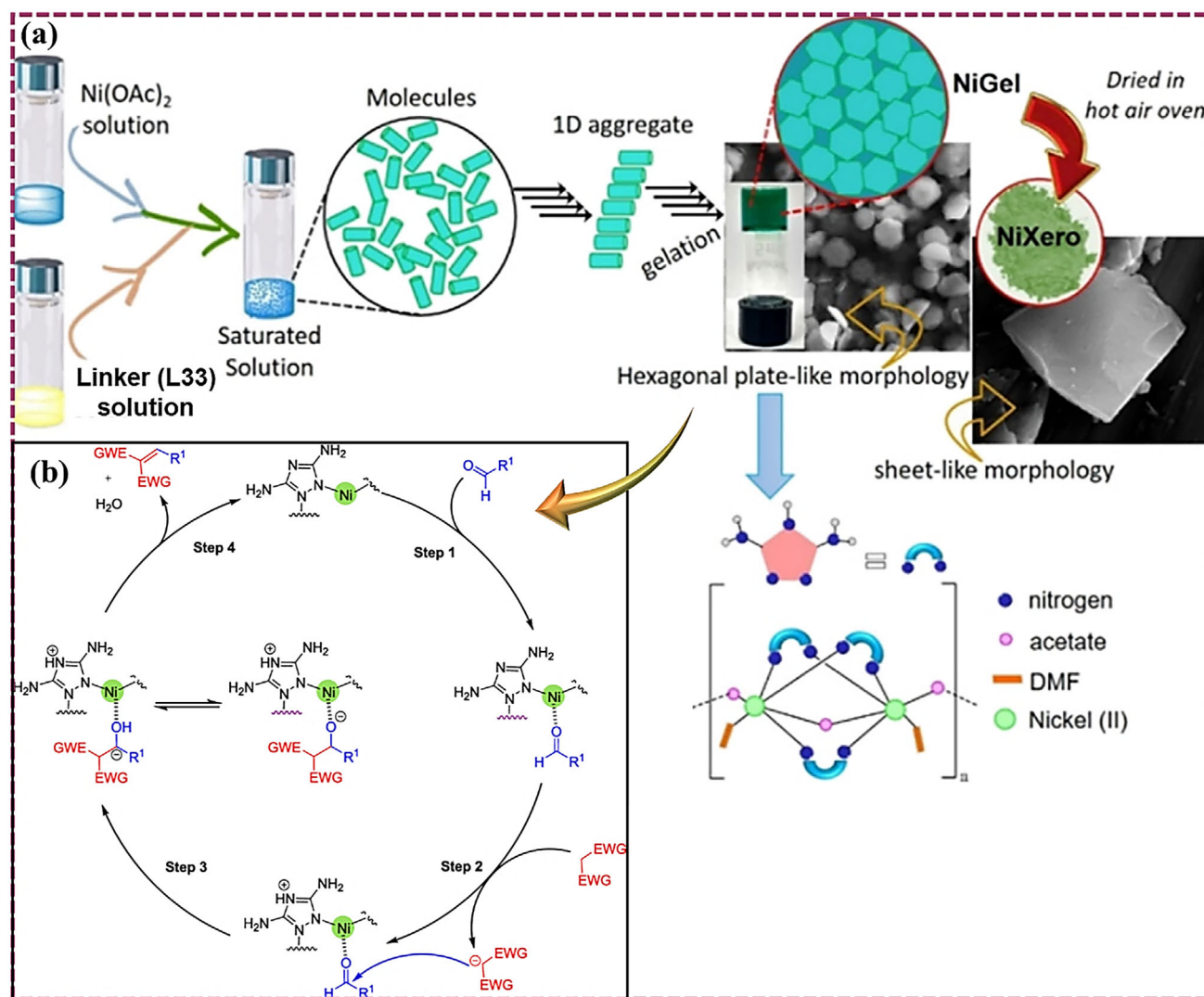


Figure 14. (a) Schematic representation of Ni(II)-mediated gel/xerogel formation and their morphological analysis. (b) CO_2 cycloaddition mechanism. Partly reproduced scheme and figure from Ref. [106]. Copyright (2023), with permission from the American Chemical Society.

tion sites. The inclusion of a pyridine moiety next to pyrazole enhances the chelation effect, which allows the incoming metal to bind concurrently to both the pyridine and pyrazole nitrogens. The synergistic effect of these centers induces the self-assembly process to form the gels. The linker not only forms metallogels with silver but also acts as an exceptional scaffold for the development of silver nanoparticles. The synthesized nanoparticles effectively catalyzed the reduction of 4-nitrophenol to 4-aminophenol. Later, Bala and coworkers developed another pyrazole-mediated linker (L28; Figure 10) and utilized it to form silver-based metallogel in water/DMF mixed solvent conditions.^[113] The gel consists of long nanofibrillar networks that function as a template for the generation of AgNPs. The silver nanoparticles-mediated gel matrix was used as a catalyst for the reduction of 4-nitrophenol. In another study, Paul and coworkers used a C3-symmetric ligand (L17; Figure 10) to produce a silver-based gel, which subsequently generated silver nanoparticles (AgNPs) when exposed to visible light.^[114] This acts as a catalyst for the reduction of sodium 4-nitrophenolate to 4-aminophenolate.

Bimetallic active moieties always give an advantage compared to single metal sites. An additional metal center can induce Lewis acidic sites, which further play an important role in catalytic conversion.^[115] In this context, Sharma et. al. synthesized a metallogel based on iron(III) and L26 (Figure 10) gelator in DMF under alkaline conditions.^[116] This gel matrix was further used as a template for the in-situ generation of silver nanoparticles. After optimizing the silver loading capacity, cubic-shaped AgNPs were utilized as an effective heterogeneous catalyst for the reduction of nitroarenes. In another study, Kyarikwal and coworkers developed a series of metallogels with $\text{Fe}(\text{III})/\text{Co}(\text{II})/\text{Cu}(\text{II})/\text{Zn}(\text{II})/\text{Ag}(\text{I})/\text{Ni}(\text{II})/\text{Fe}(\text{II})$ and L32 gelator (Figure 11 and Figure 15a).^[117] Compared to other di-/mono-valent cations, trivalent $\text{Fe}(\text{III})$ acts as a hard binding site to the nitrogen center of tetrazole and the oxygen center of the amide moieties, which facilitates the self-assembly process to form a stable supramolecular gel structure. It further stabilizes the silver nanoparticles within the gel matrix. Interestingly, silver nanoparticle-mediated iron-based gel exhibits excellent rheological behavior with self-healing properties (Figure 15b–c). This

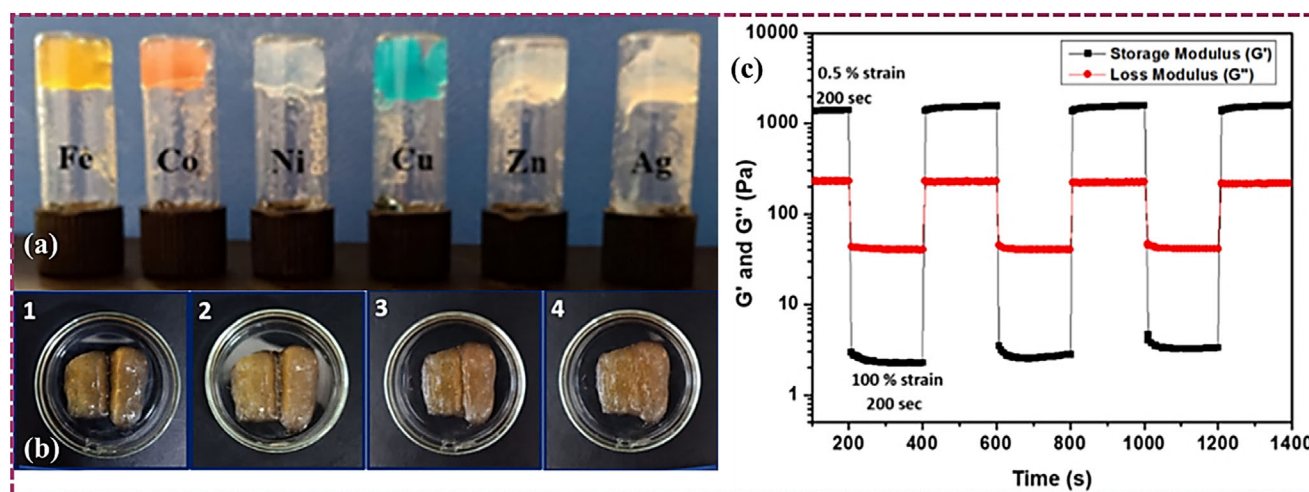


Figure 15. (a) Synthesis of metallogels with L32 gelator, (b) self-healing property of silver nanoparticle incorporated Fe(III) gel, and (c) time-dependent rheological study of silver incorporated Fe(III) gel. Partly adapted figure from Ref. [117]. Copyright (2021), with permission from the American Chemical Society.

nano-metallogel was used for the reduction of nitroaromatic compounds. The mesoporous architecture of the nanocomposite improves the diffusion of the substrate, which impacts the catalytic conversion. The study shows nearly 100% conversion in 25–35 min with good recyclability (up to 4–5 cycles), which suggests the efficacy of the catalyst. However, the efficiency was decreased after consecutive cycles due to the aggregation and leaching of silver. To solve these leaching as well as aggregation issues, recently, Nautiyal and coworkers designed another metallogel system, where the framework was stabilized by the incorporation of an additional gelator with N-rich functionalities. This induces hydrogen bond donor–acceptor sites, which play an essential role in the self-assembly process. In this work, the **L37** (Figure 11) gelator was added to the previously developed system.^[118] The synthesized silver nanoparticle-mediated bi-linker and bimetallic gel matrix exhibit enhanced catalytic activity for the reduction of nitroaromatics. The catalyst was recyclable for up to five consecutive cycles without losing efficiency.

Along with silver nanoparticle-mediated gels, gold nanoparticle-incorporated gel matrices also demonstrate an important role in the reduction of nitroaromatic compounds. In this regard, Kumar et. al. designed a supramolecular gel composed of a urea/amide-functionalized bis-pyridyl-based gelator (**L16**; Figure 10).^[119] The gel network further stabilizes gold nanoparticles (AuNPs) to form Au@L16-gel. Upon addition of solid $\text{HAuCl}_4 \cdot x\text{H}_2\text{O}$ to the gel, AuNPs and gold nanoclusters (AuNCs) were generated by an in-situ process, devoid of external reducing agents or stimuli such as heat, light, or pH. The gel matrix promotes the reduction of Au^{3+} to Au^0 and stabilizes the nanoparticles (typically pink in color), ensuring their homogeneous dispersion (Figure 16a; inset). High-resolution transmission electron microscopy (HRTEM) analysis and selected area electron diffraction (SAED) pattern display the formation of the gold nanoparticles in the gel matrix and the crystalline nature of the material (Figure 16a–c). In addition, UV–vis spectroscopy shows the plasmonic peak around 550 nm for gold

nanoparticles (Figure 16d). In an alkaline medium, AuNPs embedded in the gel were tested for their catalytic behavior for the reduction of the *p*-nitrophenol to *p*-aminophenol. Time-resolved UV–vis spectroscopy revealed a reduction in *p*-nitrophenol's typical absorption peak at 400 nm and the generation of a new peak at 300 nm for *p*-aminophenol. In addition, color changes from yellow to colorless, which also manifests effective catalytic transformation.

In a recent study, Deng et al. reported an iron oxide-based catalyst derived from a supramolecular metallogel.^[120] The gel was constructed through the self-assembly of Fe^{3+} ions with a gelator **L39** (Figure 11). Upon thermal treatment (pyrolysis) under a nitrogen atmosphere at 800 °C in the presence of conductive carbon black, the gel transforms into a porous, heterogeneous nanocomposite catalyst, composed primarily of $\gamma\text{-Fe}_2\text{O}_3$ and carbon. Furthermore, it was applied for the catalytic reduction of *p*-chloronitrobenzene to *p*-chloroaniline using hydrazine hydrate as a reducing agent in ethanol. The reaction shows excellent selectivity and over 99% conversion under 10 min (reaction temperature: 80 °C). The study highlights the potential of using metallogels as sacrificial templates for designing recyclable, nonprecious metal catalysts that are effective, scalable, and environmentally benign.

(e) Other reactions. In a preliminary study, Xing and coworkers reported Pd(II)-mediated metallogel, where **L2** (Figure 8) was used as a gelator.^[75] It was utilized for the oxidative conversion of benzyl alcohol to benzaldehyde. This study involved the fabrication of Pd-metallogels through the direct incorporation of palladium salt into a multidentate ligand. Interestingly, the catalytic activity of the wet gel was more effective compared to the corresponding xerogel and discrete Pd complexes due to the better diffusion of the substrate towards the metal sites. In another study, Mallick and coworkers developed both the MOF and metallogel systems, using calcium acetate and **L12** (Figure 8) gelator.^[19b] Gel formation transpires solely in pure DMF, where calcium ions coordinate with the ligand to

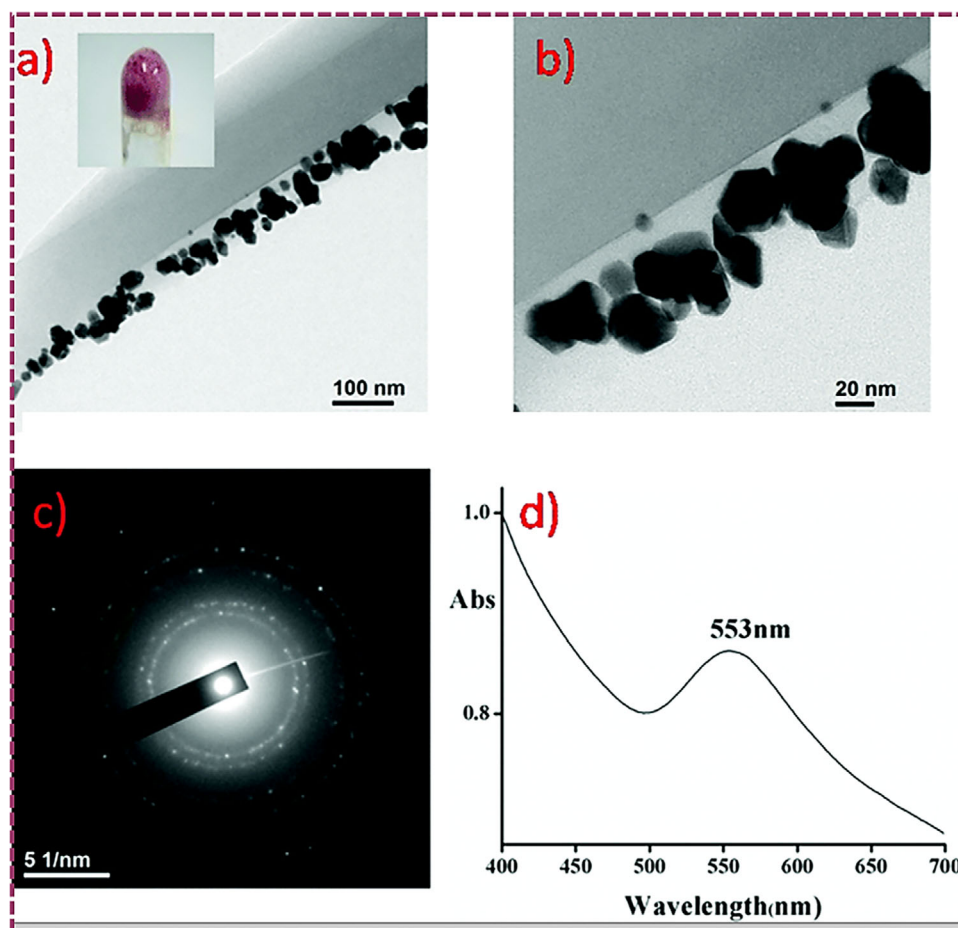


Figure 16. (a) TEM analysis of the distribution of gold nanoparticles on Au@L16-gel fiber (inset pink coloration of AuNPs-gel). (b) A zoomed-in view of AuNPs on gel fiber. (c) SAED pattern of gold nanoparticles of Au@L16-gel. (d) UV-vis spectra of the Au@L16-gel. Reprinted figure from Ref. [119]. Copyright (2014), with permission from the Royal Society of Chemistry.

establish a self-assembled fibrillar network. In contrast, a mixed solvent system comprising DMF and water facilitates the crystallization to form MOF (Figure 17). The catalytic efficacy of the gel was examined in the hydrosilylation of benzaldehyde with diphenylsilane. The reaction was performed in DMSO at 65 °C under Ar atmosphere. The calcium ion serves as the active site, utilizing its Lewis acidic center, and the gel's porous structure promotes the interaction between benzaldehyde and diphenylsilane. The reaction exhibits a turnover frequency ($\text{TOF}_{\text{S}_{1/2}}$) of 1.09 h^{-1} for the gel, surpassing that of the crystalline MOF ($\text{TOF}_{\text{S}_{1/2}} = 0.71 \text{ h}^{-1}$) and xerogel ($\text{TOF}_{\text{S}_{1/2}} = 0.74 \text{ h}^{-1}$). In a distinct study, Hosseini-Monfred and coworkers reported an iron(III) metallogel.^[121] Iron nitrate and L13 (Figure 8) linker were used to form the supramolecular gel. This gel serves as a catalyst for the selective oxidation of several alcohols, such as benzyl alcohol and cyclohexanol, that utilize 10% aqueous hydrogen peroxide (H_2O_2) as the oxidizing agent in an aqueous solution. This catalytic system functions under mild circumstances and uses nontoxic reagents, which makes it a promising alcohol oxidation alternative in organic synthesis. However, the efficiency as a heterogeneous catalyst was decreased by 20 % after the third cycle due to leaching or structural changes. In a separate study, Bala et al. utilized AgNPs-mediated gel matrix (L28 used as a gelator; Figure 10)

for the reduction of methylene blue dye as well as in Cr (VI).^[113] Liu and coworkers designed a porphyrin-based gelator (L29) (Figure 11) to form a gel structure with $\text{Rh}_2(\text{OAc})_4$ in a DMF/water solvent mixture (Figure 18a).^[122] Furthermore, the aerogel, with its high surface area and thermal stability, acts as a catalyst for the hydrosilylation of aldehydes and ketones under ambient temperatures, where PhSiH_3 was used as a reducing agent. The porous architecture of gel facilitates effective reactant diffusion and inhibits catalyst aggregation, hence providing high turnover and recyclability. The catalyst functions effectively with modest loadings (0.1–0.4 mol%) to give high yields (89%–99%) within 7 h (Figure 18b). Later, the L29 gelator (Figure 11) was also used by Zhang et al. to synthesize cobalt/aluminum-mediated gel.^[123] A porous cobalt(II)-based metal-metalloporphyrin gel was produced by combining cobalt(II) tetrakis(4-carboxyphenyl)porphyrin with aluminum nitrate in ethanol. The gelation process was facilitated by robust ligand-metal coordination interaction and the consequent aggregation of porphyrin-Al clusters, which resulted in a 3D network of cross-linked fibers. The hierarchical porosity enhances substrate transport and elevates the density of active sites. Structural investigation through different spectroscopic studies reveals that the gel network features cofacially aligned porphyrin rings stabilized by twisted Al-

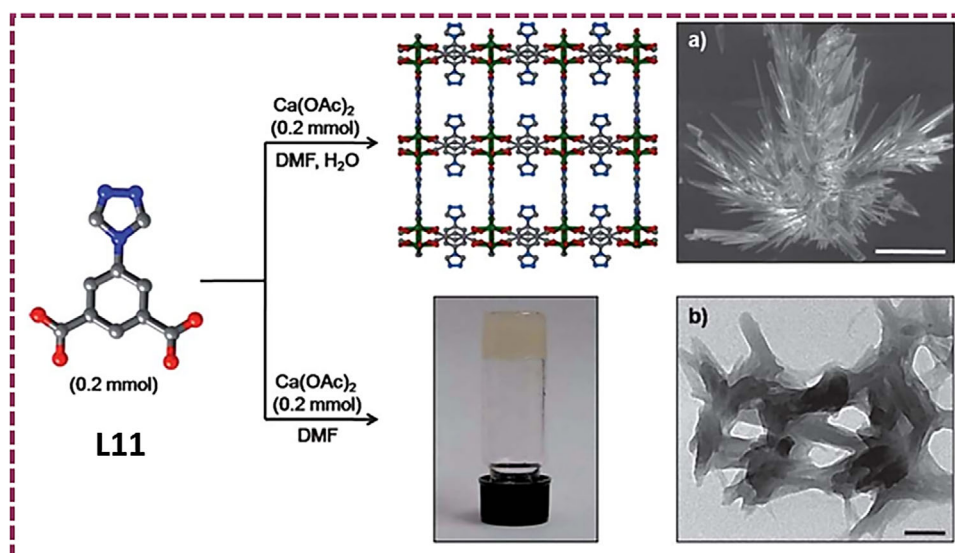


Figure 17. Synthesis of Ca-based metallogel/MOF with L12 linker and their morphological analysis (FESEM). Reproduced figure from Ref. [19b]. Copyright (2012), with permission from the Royal Society of Chemistry.

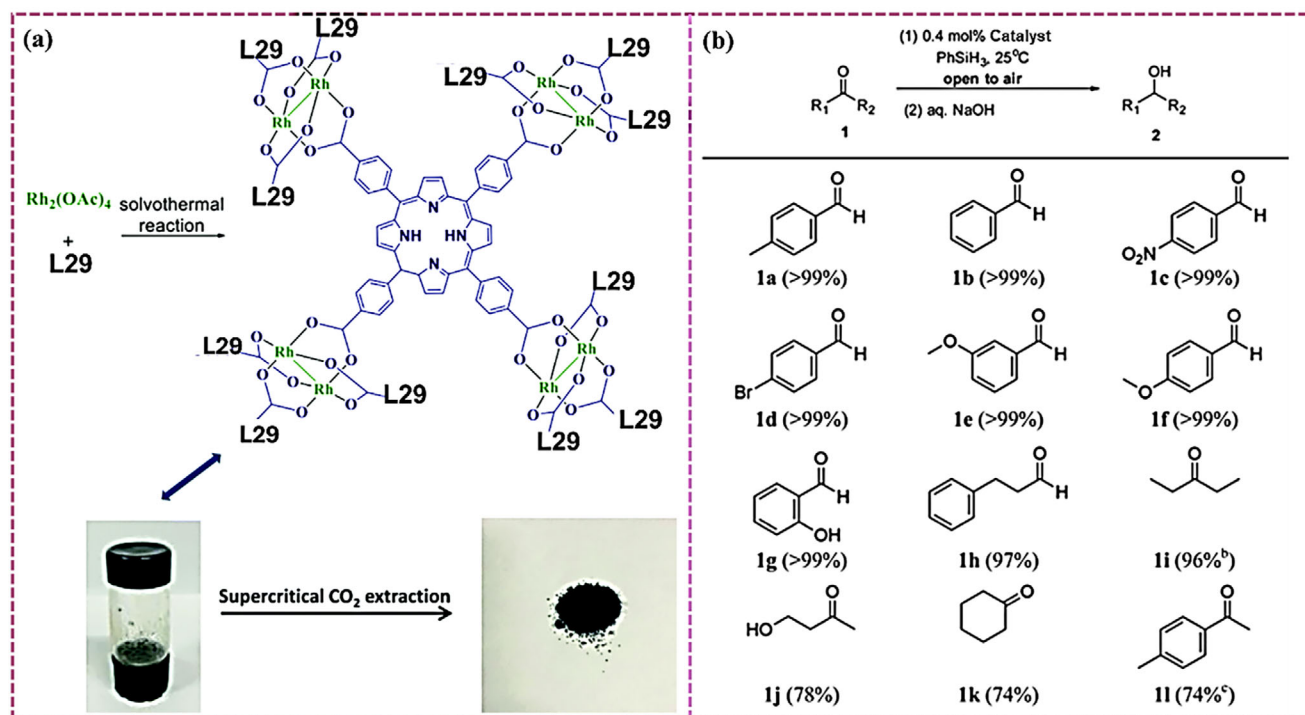


Figure 18. (a) Schematic representation of binding with Rh ions and porphyrin-based gelator L29 and (b) substrate scope for the reaction (reaction condition: PhSiH₃ (2.0 mmol), carbonyl substrate (1.5 mmol), catalyst (0.4 mol%), CH₂Cl₂ (2 mL), ambient temperature. Partly adapted scheme and figure from Ref. [122]. Copyright (2018), with permission from the Royal Society of Chemistry.

O–Al clusters (Figure 19). This framework was used in the Diels–Alder reaction, a cycloaddition involving a diene and a dienophile that yields cyclic adducts. This reaction demonstrates exceptional activity, which exhibits a 72% yield and 85% endo selectivity of the product over 48 h. Nanoscale catalytic pocket emphasizes selectivity toward kinetically controlled endo products. In a recent study, Saha et. al. developed a gel as a heterogeneous catalyst and utilized it for the Knoevenagel condensation reaction.^[106] L35 (Figure 11) gelator and

nickel acetate were used to synthesize the supramolecular gel. The catalyst demonstrates exceptional selectivity (99%) and high yield (97%) during 4 h in an aqueous environment.

3.2. Photocatalysis

A considerable effort has been undertaken to design and synthesize stable and cost-effective photocatalyst materials to attain

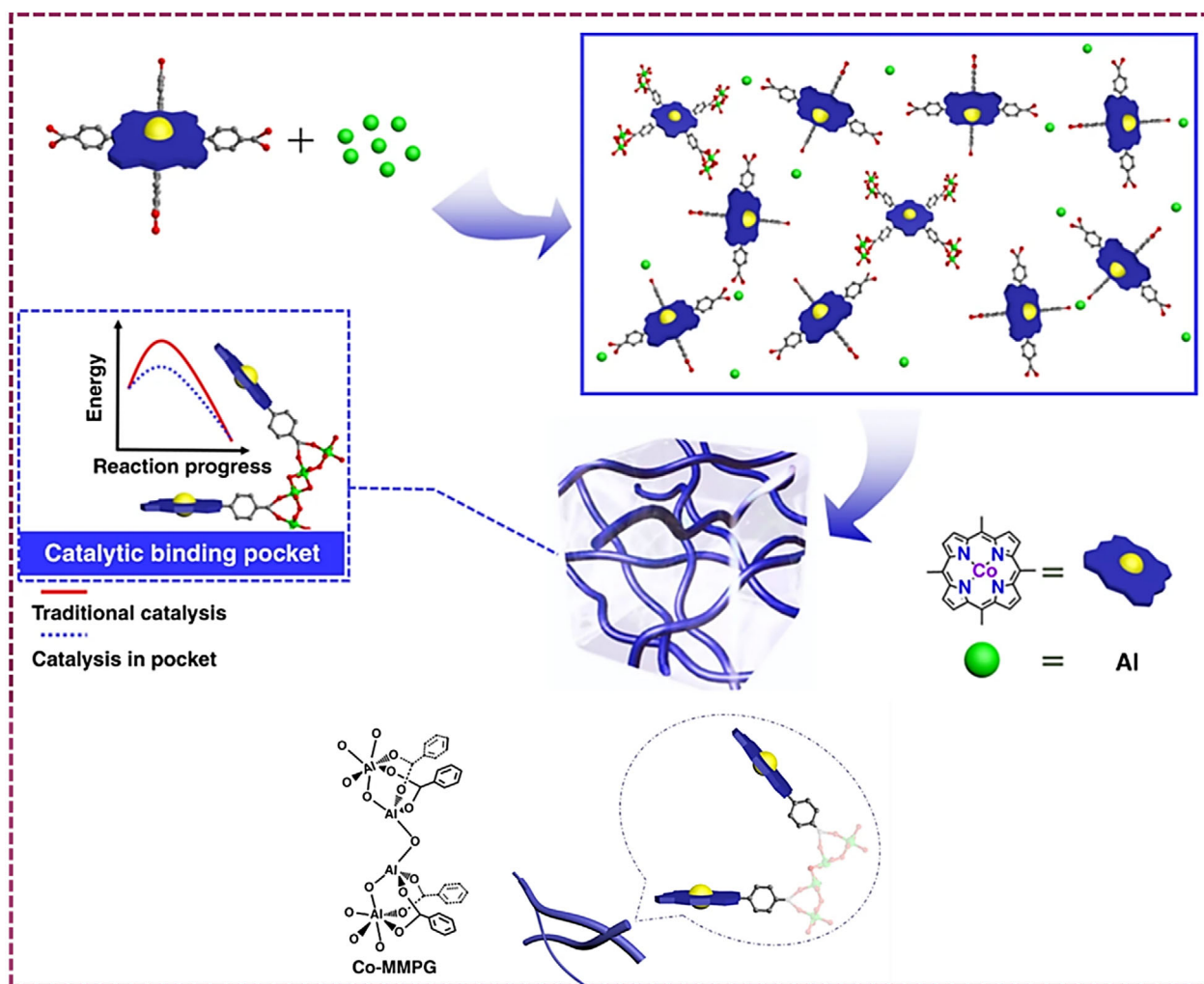


Figure 19. Schematic representation of the binding mode and structural integrity of the framework with catalytic reaction profile diagram. Reprinted figure from Ref. [123]. Copyright (2019), with permission from Springer Nature.

superior catalytic performance. Modulating noncovalent interactions, such as hydrogen bonding, π - π interactions, and van der Waals forces, allows for fine adjustment of the nanostructuring of supramolecular frameworks, which in turn greatly affects catalytic performance.^[124] Supramolecular gels are used as photocatalysts in recent studies (Table 3). The polymeric structure, containing entrapped solvent, enhances photocatalytic activity by facilitating dispersion in the reaction medium and enabling substrate diffusion to the catalytic sites.^[125]

In this context, Wang et al. reported a Cr(III)-metallogel where **L24** (Figure 10) and **L41** (Figure 20) were used as LMWGs.^[126] It was utilized as a visible-light-driven photocatalyst for the degradation of organic dyes [including methyl orange (MO), Rhodamine B (RhB), and methylene blue (MB)] in the presence of H_2O_2 under light-emitting diode (LED) and natural light irradiation. By absorbing visible lights, electrons were excited from the valence band (highest occupied molecular orbital; HOMO) of oxygen 2p orbitals to the conduction band (lowest unoccupied molecular orbital; LUMO) of Cr(III) orbitals, generating holes. These holes oxidize H_2O to hydroxyl ($\bullet\text{OH}$) radicals. On the other hand, molecular oxygen was reduced to superoxide radi-

cals ($\text{O}_2^{\bullet-}$) by excited electrons. The produced $\bullet\text{OH}$ radicals act as the main reactive species, which allows the breakdown of dye molecules into nontoxic products.

In a similar study, Sarma and coworkers developed soft supramolecular gels for photocatalytic dye (MO, MB) degradation, where nucleobases (**L42** and **L43**) (Figure 20) were used with zinc metal ions to form soft metallogels.^[127] The supramolecular interactions and metal-ligand coordination bond form Zn CPs with a hierarchical flower-like morphology, while the nanofibrous structure was generated by the Zn(II)-cytosine and Zn(II)-guanine gels (Figure 21a-c). Under UV light ($\lambda_{\text{max}} = 365 \text{ nm}$), the generated reactive oxygen species (ROS) can break down the toxic dye molecules into water and carbon dioxide.

In a distinct study, Song et al. employ a polydiacetylene (PDA)-based gel system, specifically engineered with terpyridine-diacetylene (TPY-DA) ligands (**L44**; Figure 20).^[128] The terpyridine site was well capable of binding with noble metal ions, such as Au^{3+} and Ag^+ to form supramolecular gels. In situ reduction by using sodium borohydride leads to the generation of embedded Au/Ag nanoparticles within the gel matrix. This photocatalyst

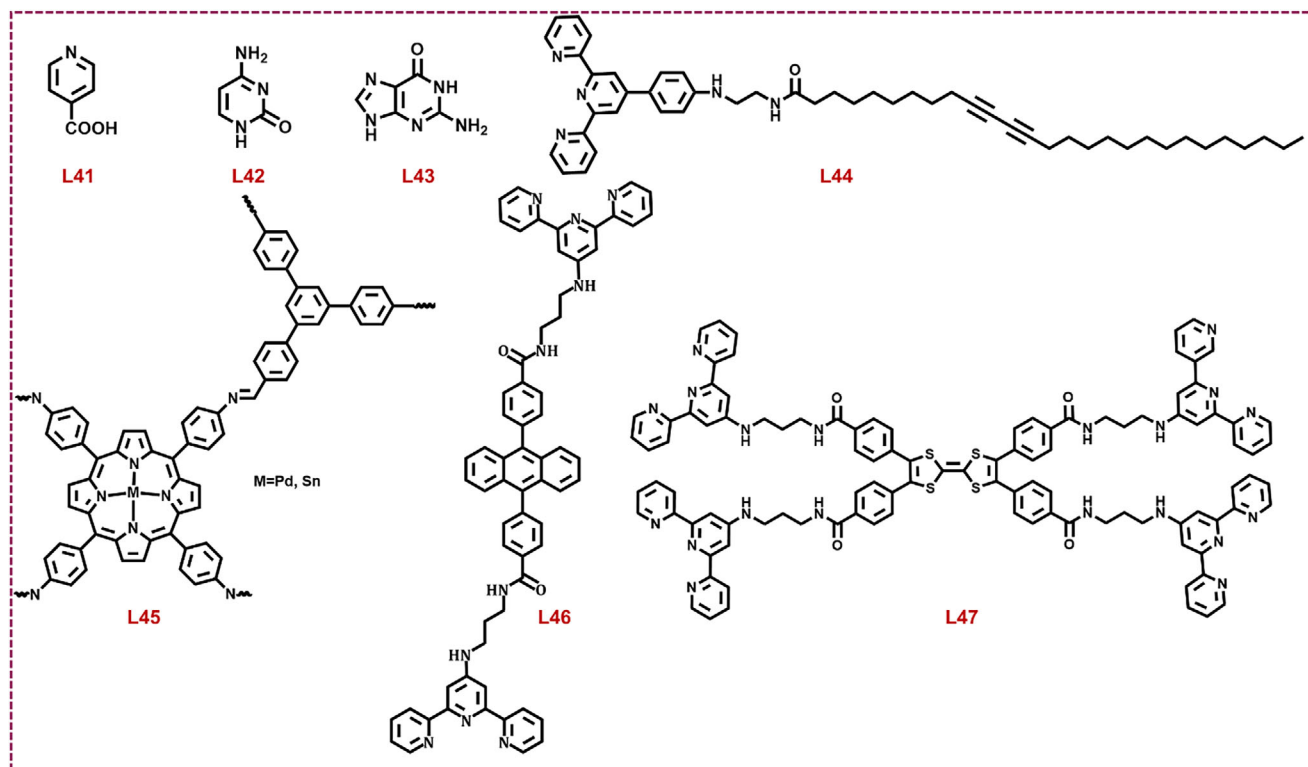


Figure 20. Gelators from L41–L47 were used to synthesize metallogels for diverse photocatalytic reactions.

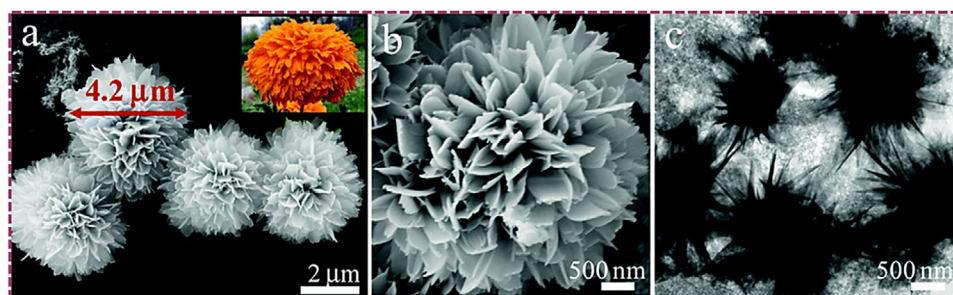


Figure 21. (a, b) FESEM and (c) TEM images of the gel (Zn-nucleobase gel) show nanoflower-like morphology. Adapted from Ref. [127]. Copyright (2018), with permission from the Royal Society of Chemistry.

was utilized for nitro group reduction under visible light and in the presence of NaBH_4 reducing agent. Importantly, the surface plasmon resonance (SPR) effect from silver/gold nanoparticles embedded gel matrix prompts to generate electron-hole pairs under visible light, which leads to a multistep electron transfer process. These photogenerated electrons were transferred to the nitro group to form an intermediate, which further promotes the reduction process. Along with this, holes react with water to make hydroxyl radicals to break down remaining pollutants.

Demand for sustainable economic growth and the gradual depletion of nonrenewable energy sources have recently prompted a rise in the quest for renewable energy.^[129] Furthermore, the development of sustainable and green energy sources is imperative due to the rising environmental pollution caused by the burning of fossil fuels.^[130] In light of this, converting solar energy into fuels, specifically, the reduction of water and CO_2 has become a great way to store intermittent energy.^[131]

Inspired by natural photosynthesis, the covalent linkage of the light-absorbing unit (photosensitizer) and active catalytic centers within a solvated macromolecular assembly represents a promising strategy that has recently garnered attention for improving photocatalytic performance.^[132] The recent development of soft metallogels has made a significant step in this photocatalytic research. The nanostructured architecture of the supramolecular framework can be precisely adjusted by modulating noncovalent interactions, which significantly influence catalytic efficiency. In this regard, Liao et al. developed porphyrin-based imine gels as photoactive scaffolds for hydrogen evolution under visible light.^[133] The gels were formed by reacting metalated porphyrins (Pd) with triazine-based aldehydes (L45; Figure 20), yielding a porous network with extended π -conjugation and abundant coordination sites. Upon doping with Pt nanoparticles, these gels served as both light-harvesting antennae and electron conduits. It facilitates photogenerated charge transfer to proton reduc-

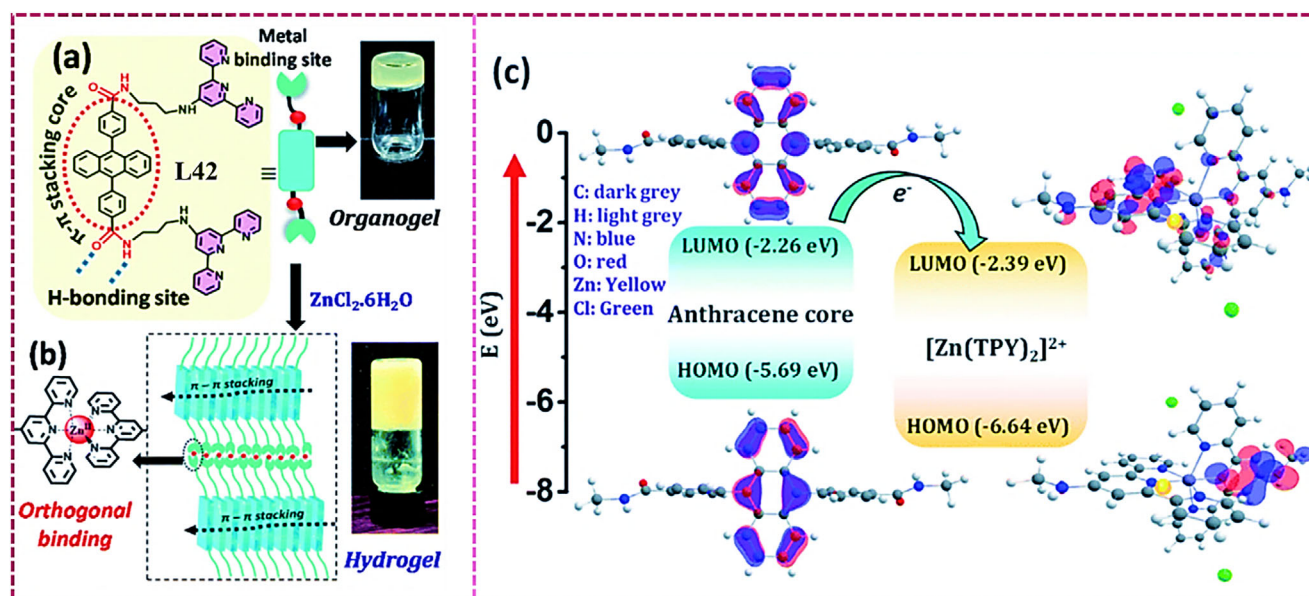


Figure 22. (a, b) Schematic representation of gel synthesis. (c) HOMO-LUMO gap of the light-harvesting core (anthracene moiety) and binding motif (Zn-terpyridine moiety). Reproduced figure from Ref. [125]. Copyright (2021), with permission from the Royal Society of Chemistry.

tion sites. The photocatalytic system, using sodium ascorbate as a sacrificial electron donor, demonstrated an impressive hydrogen evolution rate over multiple cycles. The wet gel structure significantly enhanced performance over the dried form due to improved proton transport and photonic interaction. This work opens a new avenue for soft-materials-based photocatalysts integrating molecular design, gel chemistry, and visible-light responsiveness.

In another study, Verma and coworkers developed a strategy to design a linker (L46) (Figure 20) with an anthracene-mediated light-harvesting constituent.^[125] The terpyridine moiety covalently attached to the anthracene section can coordinate with zinc ions to generate an active catalytic site (Figure 22a,b). The catalytic mechanism entails the activation of the anthracene moiety following the absorption of visible light, which functions as a light-harvesting framework. It promotes the excited electron to active catalytic sites of Zn(II)-terpyridine centers and facilitates the reduction of protons (H^+) to hydrogen (H_2) by a multistep electron transfer process. Along with this, the photoexcited electrons reduce water molecules to produce hydrogen gas, while triethylamine (TEA) acts as a sacrificial electron donor to restore the catalyst.

A density functional theory (DFT) study also supports the photosensitization process. The HOMO-LUMO gap was calculated for a separate light-harvesting core (anthracene unit) and zinc-terpyridine moiety ($[\text{Zn}(\text{TPY})_2]^{2+}$). The result suggests favorable conditions for excited-state electron transfer, which facilitate the photocurrent generation within the framework structure (Figure 22c).

Later, Verma and coworkers developed a highly porous, nanofibrous structure with excellent light-harvesting properties and electron mobility using a soft gel matrix.^[134] As a light-harvesting unit, the tetrathiafulvalene moiety was used as a core of the LMWGs (L47) (Figure 20), and extended with terpyridine ends. The terpyridine can easily coordinate with zinc(II), which

generates an active catalytic center for efficient photocatalysis (Figure 23a). Micrographic study (FESEM and TEM analysis) suggests that the synthesized xerogel exhibits an entangled network morphology composed of nanoribbons. In addition, the height and diameter of the nanoribbons were determined to be around 7 and 40–80 nm, respectively, via atomic force microscopy (AFM) analysis (Figure 23c–h). In this work, they use the zinc-based gel matrix as a template to incorporate the Pt nanoparticles, which deliberately enhances the catalytic efficiency. The formation of stable Pt nanoparticles was confirmed by HRTEM and FESEM analysis. The size of the nanoparticles was found to be in the range of 2–3 nm. SAED pattern shows the d-spacing value of 0.23 nm and lattice fringes confirm (111) planes for the presence of Pt nanoparticles (Figures 23b and 23i–k). It diminishes electron-hole recombination and alters CO_2 reduction selectivity from CO to CH_4 by bringing further active sites, which optimize the binding energy to generate the intermediate.

In a separate study, they also reported a Ru(II)-based metallogel which was utilized in photocatalytic CO_2 reduction.^[135] As a light-harvesting moiety, in this work, they used a porphyrin core mediated linker extended with terpyridine end (L48) (Figure 24). Depending on the utilization of sacrificial electron donors, the excited Ru(II) species undergoes sequential electron transfers to CO_2 , creating intermediate species including carbon dioxide radical anion ($\text{CO}_2^{\cdot-}$), formate (HCOO^-), carbon monoxide (CO), and methoxy radical (CH_3O). These species are then reduced and protonated to generate CO or CH_4 .

In a distinct study, Yang et al. developed a novel approach for efficient photocatalytic CO_2 reduction using cobalt-metallogel derived from glutamic acid-based lipid molecules (L49; Figure 24).^[136] These amphiphilic molecules, possessing long hydrophobic chains and pyridine-mediated headgroups, coassembled with Co^{2+} ions to form bilayer nanostructures with tightly packed alkyl chains. This generates a hydrophobic microenvironment that enhances CO_2 diffusion and stabilizes

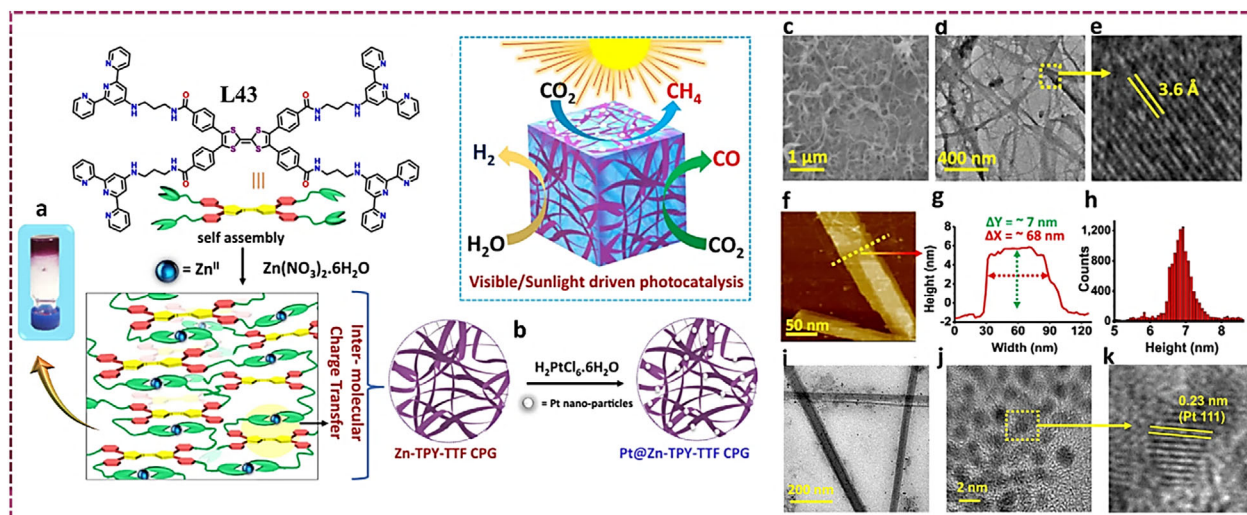


Figure 23. (a) Schematic representation of Zn-mediated gel synthesis and (b) Pt incorporated into the gel matrix. (c) FESEM, (d) TEM, and (e) HRTEM images. (f–h) Atomic force microscopy (AFM) images with height profile of Zn gel. (i) TEM and (j, k) HRTEM analysis of Pt incorporated Zn gel. Partially reproduced figure from Ref. [134]. Copyright (2021), with permission from Springer Nature.

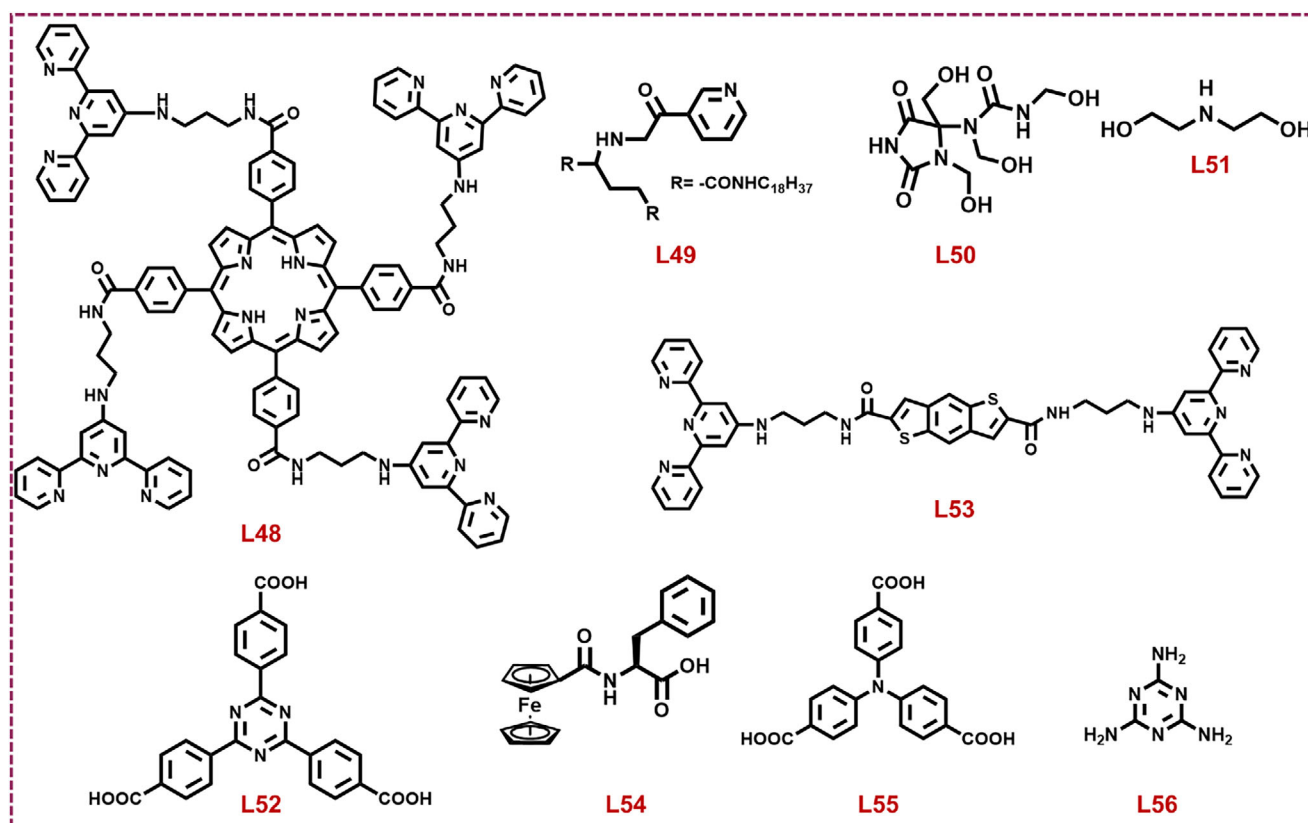


Figure 24. Gelators from L48–L56 were used to synthesize metallogels for diverse photocatalytic and electrocatalytic reactions.

catalytic sites through a synergistic binuclear cobalt configuration. The photocatalyst exhibits a remarkable CO generation rate of 208,724 μmol g⁻¹ within 24 h and a high CO/H₂ selectivity of 90%. The nanoribbon structure of the gel network facilitates efficient mass transfer and active site accessibility. Photophysical characterizations reveal narrow bandgaps (~1.84 eV), excellent light absorption, and favorable energy

alignments for CO₂ reduction. Importantly, the gels demonstrated recyclability, high structural stability, and selective CO generation without forming other reduction products like CH₄ or MeOH. This work presents a bioinspired soft-material platform that mimics natural lipid bilayers, setting a new direction in designing lipid-like metallogels for efficient solar-to-fuel conversion.

In a recent study, Alam and coworkers synthesized a neodymium-containing metallogel where diazolidinyl urea and diethanolamine (**L50** and **L51**) (Figure 24) were used as LMWGs.^[137] The gel demonstrates exceptional self-healing and load-bearing capacities. Interestingly, this soft material was molded into different shapes to demonstrate a smart tunable entity. Pyrolysis at 600 °C under an inert atmosphere transforms the xerogel into a highly porous neodymium-doped nitrogen-rich carbon aerogel. A hierarchical porous structure with a high surface area enhances CO₂ adsorption and activation efficiency. The material serves as an effective photocatalyst for the photocatalytic reduction of CO₂ to CO. Water was utilized as the electron donor under visible light irradiation without the need for sacrificial agents. Upon the absorption of visible light, photo-generated electron-hole pairs are formed. The excited electrons were transferred from the conduction band to adsorbed CO₂ species, which leads to the formation of intermediates such as carbonate (CO₃²⁻), bicarbonate (HCO₃⁻), and HCOO⁻. After that, these intermediates were then transformed into CO via multi-electron transfer processes. In-situ diffuse reflectance infrared Fourier transform (DRIFTS) study confirms the generation of those reactive intermediates during the reaction studies.

In a distinct study, Gao et al. developed multifunctional magnetic metallogel composites encapsulated within sodium alginate (SA) beads (Fe₃O₄/metallogels/SA) for efficient removal of chlortetracycline hydrochloride (CTC), a persistent antibiotic pollutant.^[138] The **L52** gelator (Figure 24) was utilized to form metallogels with Fe³⁺/Al³⁺ ions. These metallogels provide high surface areas and visible-light-active Fe–O or Al–O clusters, while encapsulation in SA improved stability, handling, and recyclability. Encapsulation of Fe₃O₄ magnetic nanoparticles enhances the electron transfer ability of the composite material. The materials show excellent thermal, chemical, and magnetic properties, which enable rapid recovery using an external magnet. Degradation pathways and toxicity assessments revealed environmentally benign by-products. This work provides a scalable, green solution for wastewater treatment and demonstrates how integrating magnetic separation, light-activated catalysis, and biodegradable supports can overcome the limitations of powdered nanomaterials in real-world applications.

Later, Alam and coworkers developed another metallogel system, which was fabricated with silver nanoparticles. The gel was synthesized from silver nitrate and **L40** (Figure 11) gelator.^[107] It exhibits effective photocatalytic CO₂ reduction, with a conversion rate of 18.6 μmol g⁻¹ and approximately 85% selectivity for CO under ambient conditions without a sacrificial agent. The synergistic interplay between the plasmonic effect from silver nanoparticles and efficient charge carrier dynamics results in high catalytic activity for CO₂ photoreduction. In a very recent study, Mondal et al. designed a gelator with a photoactive moiety to form a soft metallo-supramolecular gel.^[139] The study introduces a novel low molecular weight gelator (**L53**; Figure 24), which couples with a benzo[1,2-b:4,5-b']dithiophene (BDT) chromophore with terpyridine ligands via alkyl amide linkers. Self-assembly of this molecule with Co²⁺ ions produced a coordination polymer gel with a 3D, fibrous nanostructure. Under visible light irradiation, the metallogel demonstrates

remarkable catalytic activity, that can able to convert CO₂ into CO with 99% selectivity. Even at reduced CO₂ concentrations (5% CO₂ in Ar), the catalyst maintained high activity (1.9 mmol g⁻¹ CO in 10 h) and over 94% selectivity. Spectroscopic analyses, including DRIFT, femtosecond transient absorption (fsTA), and DFT simulations, were used to elucidate the reaction mechanism. It confirms the effective charge separation and a favorable energy profile. This work exemplifies a strategic integration of photoactive organic moieties and catalytic metal centers in soft materials, advancing the development of gel-based materials for solar fuel generation.

3.3. Electrocatalysis

Inorganic–organic hybrid materials have been widely used as electrocatalysts recently.^[140] In contrast, metallogels have recently emerged in the realm of electrochemical studies. Table 4 demonstrates recent research interests in soft metallogels in electrocatalytic investigations. Generally, the high-temperature processing of these gel materials results in the creation of heteroatom-mediated carbonized substances.^[141] It produces a highly porous nanostructured network that may influence the surface area and active metal sites of the materials. This pertains to the electrochemical catalytic behaviors.^[142]

He et al. reported a facile one-step synthesis of Fe₃O₄/N-doped graphene aerogels using a supramolecular hydrogel composed of ferrocenoyl phenylalanine (**L54**; Figure 24) and graphene oxide (GO).^[143] Graphene oxide (GO) promotes sol–gel transitions at low concentrations, whereas hydrothermal treatment facilitates the in situ oxidation of ferrocene to Fe₃O₄ nanoparticles and the reduction of GO to graphene. This results in the formation of aerogels with uniformly distributed Fe₃O₄ nanocrystals anchored on 3D graphene networks. The material exhibits superior oxygen reduction reaction (ORR) activity in comparison to commercial Pt/C. The improved charge mobility, increased porosity, and robust metal–support interaction play important roles in ORR activity. The research introduces an effective and scalable approach for generating metal oxide/carbon composites from a single hydrogel precursor, which establishes a novel framework for cost-effective, morphology-controlled catalyst fabrication. In a distinct study, Dhara et al. reported metallogels from Fe(III) and Al(III) ions with **L55** (Figure 24) ligands and analyzed their varied physicochemical properties.^[144] Despite originating from different elemental groups (Fe: d-block, Al: p-block), both metals form metallogels with stable +3 oxidation states. The **Fe–L55** gel exhibits significantly enhanced redox activity, electrical conductivity, and oxygen evolution reaction (OER) catalytic performance compared to the **Al–L55** gel. Fluorescence studies showed cyan-emission for both **L55** and **Al–L55** under a UV source (λ_{ex} = 365 nm), whereas **Fe–L55** didn't show any emission. The DFT calculations attributed these differences to electronic configurations and coordination environments. **Al–L55** shows a spindle-like structure. Although nanofibers with a more porous structure were observed for **Fe–L55**. Furthermore, porous morphology and active Fe-centers promote easy accessibility for reactants, which leads to bet-

ter catalytic activity for OER reactions. The results underscore the impact of metal choice on the electronic and catalytic behavior of metallogels and offer insights into tuning properties for targeted catalysis applications. In another study, Jiang et al. introduced a unique gel-assisted synthesis for creating a composite electrocatalyst composed of cobalt phosphide (Co₂P) nanoparticles anchored on cobalt/nitrogen/phosphorus codoped graphene (CoNPG).^[145] A supramolecular hydrogel was formed by melamine (**L56**; Figure 24), cobalt nitrate, phosphoric acid, and graphene oxide. After pyrolysis, followed by acid treatment, leads to form a highly active and durable bifunctional material for both ORR and OER. The pyrolysis was carried out at different temperatures (800, 900, and 1000 °C) to obtain multiple catalysts such as Co₂P@CoNPG-800, Co₂P@CoNPG-900, and Co₂P@CoNPG-1000, respectively. Among these, Co₂P@CoNPG-900 shows the best catalytic activity for OER/ORR. The synergy between Co₂P nanocrystals and the Co-Nx/P-doped carbon matrix enhanced charge transfer and stabilized the electrocatalytic sites. Iron in mixed valences may offer redox-active sites for oxygen adsorption, which can enhance the ORR activity. However, these Fe/Fe-oxide particles exhibit poor charge-transfer characteristics and experience agglomeration during synthesis. A proficient strategy has been implemented to deposit Fe/Fe-oxide particles onto carbon materials, particularly carbon nanotubes (CNTs), which possess sp²-C networks. It enhances electronic conductivity and concurrently mitigates their agglomeration. In this context, Wang et al. utilized Fe-based metallogels (**L13 gelator**; Figure 8) as sacrificial templates to prepare highly active oxygen reduction reaction (ORR) catalysts by pyrolyzing them with urea and nitrogen-doped carbon nanotubes (NCNTs).^[146] The resulting composite featured core-shell Fe-Fe₂O₃ nanoparticles (~10 nm) encased in N-doped carbon shells and anchored onto NCNTs. This architecture facilitated efficient charge transfer, high dispersion of catalytic centers, and excellent stability. The catalyst showed an onset potential of 0.92 V, high durability (91.7% current retention after 20,000 s), and methanol tolerance. The study showcases how metallogel-derived nanostructures can be tailored for high-performance, cost-effective fuel cell technologies. In a separate study, Saha and coworkers reported a Co(II)-based organogel (Co-Gel) using **L35** (Figure 11) gelator.^[147] The Metallogel shows self-healing and thermal responsiveness behavior. Hydrogen bonding and π - π stacking interactions play crucial roles in the stabilization of the gel networks. Upon drying, the gel was converted into xerogel, which retained the porous structure and Co²⁺ sites. Further calcination of the xerogel leads to the formation of Co₃O₄ nanoparticles. Both xerogel and Co₃O₄ were tested for OER in acidic and alkaline media. Interestingly, xerogel performed better in alkaline conditions with a Faradaic efficiency of 91.7%, while Co₃O₄ was more stable under acidic conditions. The structural differences and electronic environments of the two materials led to this divergence in catalytic behavior. This is among the first studies to directly compare a metallogel and its derived oxide for dual-environment electrocatalysis, revealing valuable insights into phase-specific activity tuning. In further advancement, they modified the loading of heteroatoms onto graphitized carbon supports.^[148] The cobalt nanomaterials were encapsulated in nitrogen- and oxygen-

doped carbon material via the pyrolysis of Co-gel system. By varying the pyrolysis atmosphere (e.g., inert, reduced, and mixed air), heteroatom doping level, and carbon structure were controlled, which forms materials with different catalytic profiles. Pyrolysis under the N₂ atmosphere produces Co(o) nanoparticles embedded in carbon structure, while partial oxidation by mixed air flow generates a mixture of nanoparticles with varying oxidation states. Importantly, Co(0) nanoparticles doped carbon structure shows better performance than cobalt-oxide nanoparticles doped catalyst. It exhibits a low OER overpotential of 378 mV and a TOF of 0.012 s⁻¹. The dual doping enhanced charge mobility, active site density, and corrosion resistance. And it outperforms Co₃O₄ derived from the same precursor. This work underscores the role of controlled doping and carbon encapsulation in maximizing the electrocatalytic efficiency of metallogel-derived nanomaterials for water-splitting applications. Shang and coworkers demonstrated a strategic use of metallogel as a sacrificial template for synthesizing bifunctional oxygen electrocatalysts.^[149] **L57** (Figure 25) gelator was coordinated with Co²⁺ ions to form a stable gel through self-assembly in aqueous conditions. After freeze-drying, the gel was pyrolyzed under nitrogen at 900 °C to produce porous nitrogen-doped carbon structures embedded with finely dispersed Co nanoparticles (CoNC-MOG-9). The BET surface analysis, XRD, and TEM reveal a nanosheet architecture with high surface area and abundant Co-Nx sites, which play a significant role in enhancing the electrochemical active sites. Electrochemical tests indicate high ORR activity with a half-wave potential of 0.815 V and efficient OER with an overpotential of 0.40 V at 10 mA cm⁻². The material demonstrates superior power density and stability when incorporated into a solid-state Zn-air battery. This displays the feasibility of employing basic bioderived gels for the scalable and economical production of high-performance nonprecious metal catalysts. In a distinct study, Ni-based supramolecular gel was utilized by Saha and coworkers for hydrogen evolution reaction (HER)/OER applications.^[150] During pyrolysis in an inert environment at 800 °C, the gel matrix transformed to bifunctional electrocatalysts composed of Ni(0) nanoclusters encased in N, O-doped graphitized carbon layers. The gel was synthesized using Ni(II) metal ions with a triazole-based ligand (**L35**; Figure 11). It self-assembles into a stable framework through hydrogen bonding and metal-ligand coordination interactions. During the pyrolysis process, the framework went through controlled decomposition to form a highly conductive graphitic carbon structure with uniformly dispersed Ni nanoparticles. The catalytic mechanism for the HER adheres to the Volmer-Heyrovsky route, wherein water molecules are initially adsorbed onto the catalyst surface and then reduced to generate adsorbed hydrogen intermediates (H_{ads}) through electron transfer from nickel active sites. The intermediates then combine (Heyrovsky step) to produce molecular hydrogen (H₂). The mechanism for OER entails the adsorption of hydroxide ions (OH⁻) onto partially oxidized nickel species, resulting in the formation of NiOOH as an active intermediate, which subsequently undergoes further oxidation to produce O₂ through a series of proton-coupled electron transfer (PCET) steps. In a recent study, Wagh and coworkers developed a novel bioinspired nickel-based metallogel electro-

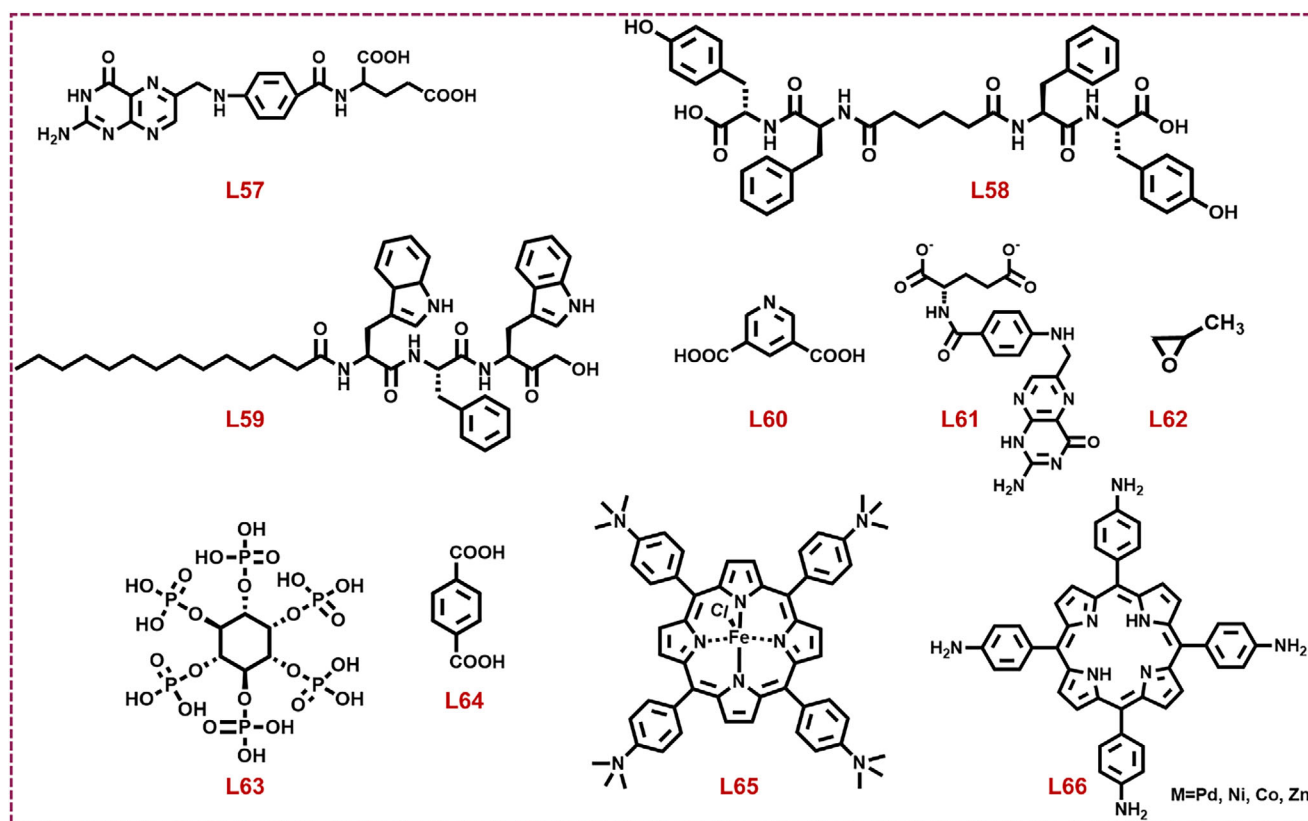


Figure 25. Gelators from L57–L66 were used to synthesize metallogels for different electrocatalytic reactions.

catalyst, which is derived from a self-assembling boladipeptide consisting of L-tyrosine, adipic acid, and L-phenylalanine (L58; Figure 25).^[151] Through a sonication-assisted synthesis in aqueous media, Ni^{2+} ions coordinated with the deprotonated carboxylates of the peptide to yield a nanofibrillar gel structure. The xerogel demonstrates exceptional OER activity, which requires only a 164 mV overpotential to reach 10 mA cm^{-2} current density in 1 M KOH. The Tafel slope of 74 mV dec^{-1} indicates rapid catalytic kinetics.

The high surface area ($10.5 \text{ m}^2/\text{g}$), amorphous structure, and the dynamic electron transfer between Ni^{2+} and surrounding peptide ligands facilitate this fast reaction kinetics. Detailed morphological and spectroscopic characterizations, including SEM, TEM, AFM, confocal microscopy, XPS, X-ray absorption near edge structure (XANES), and extended X-ray absorption fine structure (EXAFS), confirm a dense nanofibrillar network, uniform elemental distribution, and stable Ni^{2+} coordination within an octahedral environment. The electrocatalyst also exhibits excellent long-term stability over 100 h without structural or compositional degradation. Theoretical DFT calculations supported experimental observations, that affirm the catalyst's favorable energetics for OER intermediates. In a very recent study, Mondal and coworkers developed silver-containing metallo hydrogel (Ag-Gel) by incorporating silver ions (Ag^+) into a peptide-based amphiphilic gelator (L59; Figure 25), in phosphate buffer at pH 7.46.^[152] In the presence of sunlight, the photoreduction process converts Ag^+ ions into AgNPs within the nanofibrous hydrogel matrix. It forms AgNP-Gel (Figure 26a), which functions as an effective

electrocatalyst for the HER in acidic conditions ($0.5 \text{ M H}_2\text{SO}_4$). It demonstrates an overpotential of 480 mV at a current density of 10 mA cm^{-2} and a Tafel slope of 252 mV dec^{-1} , indicating relatively rapid charge transfer kinetics. Electrochemical impedance spectroscopy (EIS) experiments reveal a minimal charge transfer resistance (R_{ct}) of 15.1Ω , which emphasizes the effective electron transport within the gel matrix (Figure 26b–e). The nanofibrous architecture of the hydrogel offers an extensive surface area, enhancing proton transport and stabilizing the silver nanoparticles. Importantly, it prevents aggregation and leaching during electrolysis.

(a) In multimetallic systems: Researchers have also tried to decorate the catalyst as multi multimetallic system rather than a single metal site.^[153] In this context, mixed metallic soft gels have been utilized to increase the active centers in a specific catalyst, which subsequently impacts product formation. Shijina and coworkers developed a Fe–N-doped porous graphitic carbon electrocatalyst through the pyrolysis (at 900°C) of an interpenetrating polymer network.^[154] The composite material was composed of a melamine-formaldehyde resin and an iron-based metallogel (L13 was used as a gelator; Figure 8). Along with this, naphthalene was used as a porogen. After pyrolysis of these composite materials, it leads to form a hierarchical highly porous moiety enriched with graphitic carbon structure and pyridine N-sites. The resulting Fe-MOG-MFN-C material features a hierarchical porous structure with a high surface area. Graphitic carbon structure enriched with pyridinic nitrogen

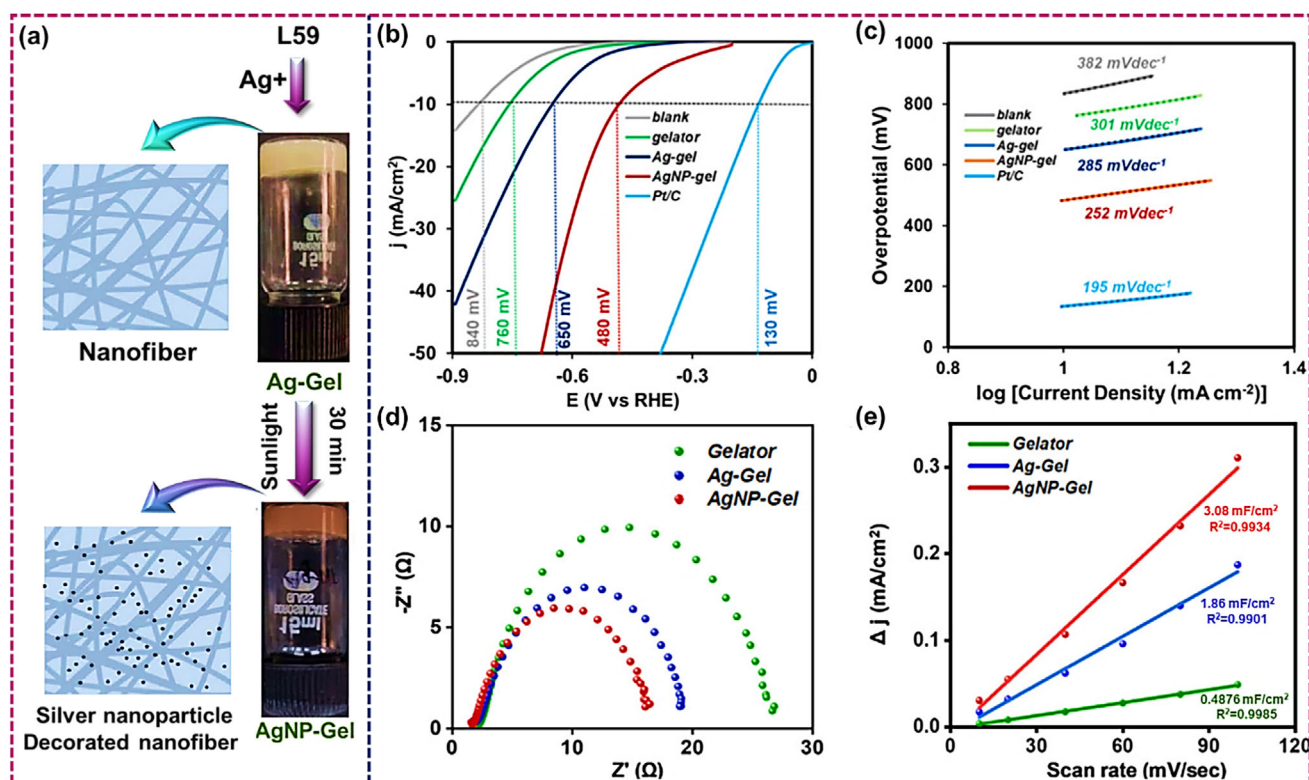


Figure 26. (a) Schematic design of AgNPs mediated gel synthesis, (b) linear sweep voltammetry (LSV), (c) Tafel slopes, (d) electrochemical impedance spectroscopy (EIS) curves, and (e) double-layer capacitance (linear fit) for the respective catalysts. Partially adapted scheme and figure from Ref. [152]. Copyright (2024), permission from the American Chemical Society.

sites enhances its catalytic properties. This material serves as an efficient electrocatalyst for the ORR in alkaline media (0.1 M KOH), exhibiting an onset potential of 0.91 V versus RHE and a half-wave potential of 0.85 V, comparable to commercial Pt/C catalysts. The catalytic mechanism involves the adsorption of O₂ onto the Fe-N_x coordination sites, with Fe serving as the primary active site, promoting O₂ activation through electron transfer. It results in the generation of intermediates such as superoxide (O₂⁻), peroxide (OOH⁻), and hydroxide (OH⁻). The reaction proceeds through a four-electron transfer mechanism, wherein O₂ was immediately reduced to OH⁻, without the generation of H₂O₂ intermediates. The Fe-N coordination sites and graphitic carbon matrix collaboratively facilitate charge transfer and electron delocalization, hence improving catalytic activity. In another study, the mixed metal-mediated gel was used for effective OER by Cao et al.^[155] Iron/cobalt/nickel-based trimetallic gel was synthesized using the L38 linker (Figure 11). Multiple gel systems were developed using different ratios of these metal ions. Gels were prepared by keeping the ratio of the metal ions Co/Fe/Ni in 5:1:4, 4:2:4, 3:3:4, and 2:4:4 molar ratios, which resulted in the formation of CoFeNi-1, CoFeNi-2, CoFeNi-3, and CoFeNi-4 metallogels, respectively. During calcination, the metallogels precursor transform into a spinel-type oxides (CoFeNi-O-1, CoFeNi-O-2, CoFeNi-O-3, and CoFeNi-O-4). Among all, CoFeNi-O-1 shows the best result for the OER in alkaline conditions (1.0 M KOH). The synthesized gel shows a bulk-like structure while after heating it gives an interconnected network structure. The micrographic study further reveals the

generation of nanoparticles. The SAED pattern displays the polycrystalline nature of the materials. Energy-dispersive X-ray spectroscopy (EDS) analysis further confirms the homogeneous distribution of the Co/Fe/Ni/O in the catalyst. Electrochemical evaluation indicates that the optimized CoFeNi-O-1 attains an overpotential of 244 mV at 10 mA cm⁻² and a low Tafel slope of 55.4 mV dec⁻¹, surpassing commercial RuO₂ catalyst. The catalyst's porous nanostructure promotes mass transfer, increases active site accessibility, and facilitates high efficiency for OER (Figure 27a-d).

In a distinct study, Guo and co-workers developed a green, self-templated carbonization approach to synthesize transition metal phosphide (TMP) nanoparticles embedded in nitrogen/phosphorus dual-doped carbon quasiaerogels using bimetallic metallogels as precursors.^[156] The approach used guanosine monophosphate (L40; Figure 11) as a heteroatom source and ligand, avoiding harmful phosphating chemicals in the process. This leads to form well-dispersed CoP, FeP, and Ni₂P nanocrystals embedded in 3D conductive frameworks with high porosity and abundant active sites. The catalyst exhibited excellent bifunctional performance with a half-wave potential of 0.85 V for ORR and a low overpotential for HER across pH ranges (230 mV in acid, 290 mV in alkaline, and 352 mV in neutral media). It also demonstrates remarkable durability with 96.7% retention after 50,000 s. These heterostructures represent a promising alternative to noble-metal catalysts for sustainable energy applications like fuel. In a separate study, Xiao et al. reported a

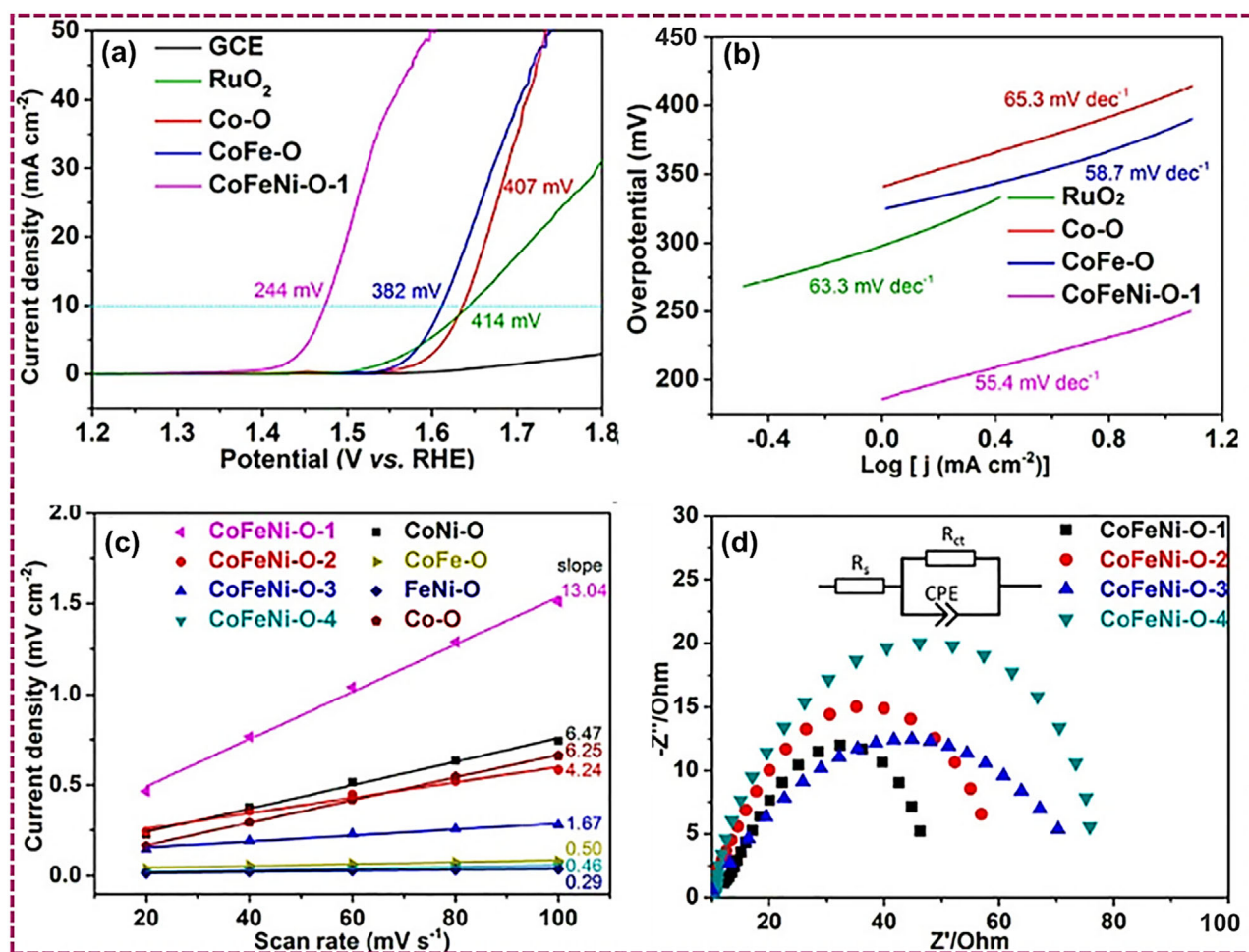


Figure 27. (a) LSV curves, (b) Tafel slopes, (c) current density differences, and (d) EIS diagrams of synthesized catalysts (CoFeNi-O-1, CoFeNi-O-2, CoFeNi-O-3, and CoFeNi-O-4), and reference (RuO₂). Partially adapted figure from Ref. [155].

bottom-up approach to design highly efficient HER electrocatalysts using metal-organic nanofiber gels.^[21] These were synthesized by coordinating Pd²⁺ with L60 (Figure 25) and transition metal ions like Co²⁺, forming an extended fibrous network under ambient conditions. The Pd-Co nanofibers were deposited on nickel foam and subjected to in situ electrochemical activation. Furthermore, Pd²⁺ was reduced to Pd⁰ nanoparticles that decorated the fibrous support. This transformation enhances electrical conductivity and exposes more active Pd sites. Postactivation manifests better catalytic activity, which even outperforms the activity of Pt/C at higher current density. The catalyst exhibits an overpotential of just 57 mV at 10 mA cm⁻² and a Tafel slope of 55 mV dec. The study offers a compelling route to reduce precious metal usage while boosting catalytic efficiency through gel-based nanostructuring and electrochemical tuning. Zhu et al. reported a zinc/cobalt-based metallogel, where folate dipotassium salt was used as a ligand (L61; Figure 25). It serves as a versatile precursor for fabricating electrocatalysts via pyrolysis.^[157] The metallogel was thermally converted into cobalt/nitrogen dual-doped porous carbon nanosheets (Co/N@PCS), featuring a hierarchical 3D lamellar framework. The formation of this gel was facilitated through coordination bonding among Zn²⁺/Co²⁺ and L61, wherein Zn was preferentially incorporated due to its

stronger coordination ability. The Co/N@PCS composite showed high surface area (~747 m²/g), excellent graphitization, and uniformly distributed active Co/N sites. Its porous carbon structure and well-exposed Co sites delivered outstanding ORR catalytic performance, with a half-wave potential of 0.87 V versus RHE and superior methanol tolerance and durability compared to Pt/C. In another study, Wang and coworkers devised an unconventional gelation method based on solvent dispersion, where propylene oxide (L62; Figure 25) was used to induce gel formation from a Ni-Fe precursor solution.^[158] The process utilizes the nucleophilicity of propylene oxide to trigger network assembly in an ethanol/water medium at room temperature. The optimal Ni₂Fe-gel featured a sponge-like porous structure and a high surface area of 216.9 m²/g. The synergistic interaction between Ni and Fe centers manifests superior OER activity. The current density of 10 mA cm⁻² was achieved for an overpotential of 245 mV in alkaline media. Compared to conventional hydrothermal or electrodeposition techniques, this method offered significant advantages in simplicity, control, and scalability. The results validate solvent-induced gelation as an effective and underexplored pathway for crafting high-performance electrocatalysts. Xiao et al. developed a novel class of multimetallic aerogels (MG-FeNiCo) by integrating Fe³⁺, Ni²⁺, and Co²⁺ ions with L13

(Figure 8) via a one-pot self-assembly process.^[159] Unlike traditional coassembled structures, these materials exhibit unique self-sorting behavior, forming a hybrid morphology that consists of nanoparticles, thick tapes, and thin nanoribbons. The resultant MG-FeNiCo aerogels possess a low density (52.8 mg cm^{-3}) and extraordinary mechanical strength, capable of supporting 770 times their weight. Their OER performance was particularly remarkable, with an overpotential of just 248 mV at 20 mA cm^{-2} and a low Tafel slope of 49 mV dec^{-1} , and well comparable with commercial RuO_2 catalysts. This high activity was attributed to the synergistic redox interplay between $\text{Fe}^{3+}/\text{Fe}^{2+}$ and $\text{Ni}^{3+}/\text{Ni}^{2+}$ states, improved electron transfer, and the abundance of active sites resulting from their partially amorphous, hierarchical structure. Furthermore, doping with graphene oxide (GO) enhances electrical conductivity and catalytic durability. EIS and XPS analyses confirm lower charge-transfer resistance and better electronic states compared to bimetallic counterparts. In another study, Zhang et al. demonstrated a straightforward method for fabricating bimetallic Ni-Fe-based metallogel as efficient electrocatalysts for overall water splitting.^[160] These gels were synthesized at room temperature in aqueous media using **L38** gelator (Figure 11), which coordinated with transition metals. $\text{Ni}_{n-6}\text{Fe}_{n-4}$ -metallogel was synthesized by varying stoichiometric ratios of metal ions and gelator. Typically, $20 \mu\text{L}$ of a 20 mM solution of each metal ion and gelator was added to prepare a bimetallic gel system. It exhibits excellent electrocatalytic performance for the OER with an impressively low overpotential of 285 mV at 10 mA cm^{-2} , and an ultralow Tafel slope of 33 mV dec^{-1} . It also shows moderate HER activity, which facilitates complete water splitting with a cell voltage of just 1.61 V and exceptional long-term stability over 20 h. The synergistic interplay of Ni and Fe, along with a highly porous nanofiber structure and nitrogen-rich ligands, was crucial to the material's exceptional catalytic performance. In a separate study, Feng et al. developed Fe-Co bimetallic gels using **L63** (Figure 25), a naturally derived phosphorus-rich ligand with strong chelating capability.^[161] The gel was formed under mild aqueous conditions, where **L63** was coordinated with Fe^{3+} and Co^{2+} ions in various molar ratios. These gels were converted into aerogels via freeze-drying and then chemically reduced using NaBH_4 , a strategy that retained the original porous morphology while inducing mixed-valence states of Fe and Co. Structural analysis confirms the presence of active Fe(II)/Fe(III) and Co(II)/Co(III) centers, and electrochemical measurements in alkaline solution reveal outstanding OER performance. The combination of **L63**, Co, and Fe in a 1:2:2 molar ratio exhibits the most superior electrochemical activity. It shows an overpotential of 257 mV at 20 mA cm^{-2} and a low Tafel slope of 36 mV dec^{-1} . The reduction method proved superior to pyrolysis by preserving catalytic accessibility. Song et al. reported the fabrication of a novel bifunctional electrocatalyst through the carbonization of FeCr-doped Ni-**L13** aerogels.^[162] The resulting metal-carbon composite features a tubular morphology with small, encapsulated metal nanoparticles and a hierarchically porous carbon framework. Through epoxide-induced gelation and supercritical drying, the aerogel architecture inhibited metal agglomeration and facilitated the in-situ development of conductive carbon

tubes. Doping with trivalent metals was crucial for controlling the morphology of porous networks and the active sites. A thorough evaluation of catalytic performance indicates that Fe doping significantly enhances OER activity, potentially due to partial charge transfer between Fe and $\text{Ni}^{3+}/\text{Ni}^{4+}$. Additionally, Cr-doping regulates the dimensions of nanocomposites as well as augments the HER activity through a synergistic mechanism. The catalyst exhibited low overpotentials for HER (137 mV) and OER (220 mV), which achieves full water splitting at a cell voltage of just 1.54 V with excellent 50-h operational stability. In another study, Zhang et al. investigated a novel design paradigm for selective 2e^- oxygen reduction to H_2O_2 utilizing an oxygen-rich gelator (**L38**; Figure 11) and transition metal modulation (Fe, Co, and Ni) in metallogels.^[163] The optimal $\text{Fe}_{n-1}\text{Co}_{n-9}$ -metallogel ($50 \mu\text{L}$, 20 mM of Fe^{3+} ; $450 \mu\text{L}$, 20 mM of Co^{2+} ; $500 \mu\text{L}$, and 20 mM of gelator) displays a 93% H_2O_2 selectivity across 0.15–0.65 V and an electron transfer number of ~ 2.1 , which confirms the 2e^- pathway dominance. It provides a highly controllable and scalable alternative to oxidative post-treatment methods, which significantly contributes to decentralized, clean H_2O_2 generation.

Significant efforts have been dedicated to the development of the fuel cell industry.^[164] The direct methanol fuel cell (DMFC) stands out among fuel cell types as a promising candidate for future applications due to its high energy density, straightforward design, and efficient operation.^[165] It is crucial to investigate anode electrocatalysts for the methanol oxidation reaction (MOR), a critical process for direct methanol fuel cells (DMFCs).^[166] In this regard, Wang et al. developed an efficient electrocatalyst for methanol oxidation reaction (MOR) using trimetallic metal-organic gel.^[167] Thermal agitation at 160°C for 3 h in DMA solvent was used to form the gel, where aluminum/copper/nickel were used as metal sources, and **L64** (Figure 25) was used as a linker. In the multistage catalytic mechanism, the $\text{Ni}^{2+}/\text{Ni}^{3+}$ redox cycle was utilized to oxidize methanol. The next step was to adsorb and dehydrogenate methanol molecules. This creates reaction intermediate species. These proceed through additional oxidation to produce CO_2 and liberate electrons. Copper sites improve the oxidation process by increasing the efficiency of charge transfer and electrical interactions with nickel sites.

(b) Supramolecular rigid structure supported systems: Although talking about electrochemical or photochemical-based applications, porphyrin-based organic gelator-mediated frameworks show exceptional activity toward HER/OER/ORR applications.^[168] Extended conjugation in the gelator system leads to a high faradic yield with low overpotential, which offers a great platform to build robust electrocatalysts.^[169] Recently, researchers have used porphyrin-based gelators to synthesize soft gels and utilized them in electrochemical applications. In this context, Choi et al. reported a breakthrough in carbon dioxide conversion by engineering a 3D iron porphyrin (**L65**; Figure 25)-graphene hydrogel (FePGH) capable of electroreducing CO_2 to CO with exceptional efficiency.^[170] The catalytic architecture integrates a redox-active porphyrin complex with a conductive graphene hydrogel matrix, yielding a high surface area, accessible active sites, and resilient

electron routes. FePGH achieved $\sim 96.2\%$ faradaic efficiency for CO production at a low overpotential of 280 mV, along with long-term durability over 20 h and a cathodic energy efficiency of 79.7%. The 3D structure enables better CO₂ transport and suppresses competing hydrogen evolution. This study emphasizes a scalable approach for effective CO₂ value and presents graphene hydrogel matrices as innovative platforms for molecular electrocatalysis. In another study, Cai and coworkers developed a porphyrin-based imine gel using **L66** (Figure 25) gelator and ferrocene-1,1'-dicarbaldehyde.^[171] Diverse gels were synthesized by incorporating different metalloporphyrins ($M = \text{Ni}^{2+}$, Co^{2+} , Pd^{2+} , and Zn^{2+}), which form porous nanostructures interconnected with nanoparticles of 20–50 nm in diameter. Among them, Co-based material shows the highest catalytic activity. In case of HER application, it exhibits the lowest overpotential (470 mV) as well as Tafel slope (110 mVdec⁻¹) values among all, which shows fast electrocatalytic kinetics for cobalt-mediated gel. The lowest band gap was observed for Co-mediated gel, which suggests that the surface trans effect may impact the electronic structure of Co centers and their capacity to stabilize chemical intermediates. This may lead to enhancing the electrocatalytic performance of Co-based gel as compared to others.

Along with porphyrin-mediated supramolecular structure, terpyridine-based coordination-driven polymers also display significant advancement in catalytic research.^[172] The affinity to form strong coordination with distinct metal ions (such as Ru, Fe, Co, and Zn), the ability to provide additional stability through hydrogen bonding, and π - π -stacking make this moiety the preferred choice to synthesize polymeric gel materials. This helps in electron transfer ability throughout the 3D-connected polymeric network and plays a crucial role in enhancing the electrochemical activity of the materials. In this regard, Liu et al. explored the electrocatalytic potential of coordination polymers formed from terpyridine-based gelators (**L67** and **L68**; Figure 28) and cobalt ions.^[173] Chloride and acetate salts of cobalt ions were utilized to examine the gelation ability of these gelators. The **L67** shows the best gelation ability in the presence of chloride salt due to less steric hindrance of triterpyridine moiety and the existence of $\text{tpyCo}^{2+}\text{-OH}_2$ units. It promotes better hydrogen bonding ability throughout the 3D network structure. Moreover, it demonstrates superior electrical conductivity with an interconnected porous structure, which makes it a suitable candidate for oxygen evolution catalysis. The optimized catalyst demonstrates a low overpotential of 320 mV at 10 mA cm⁻² and sustained stability over 2000 cycles. Spectroscopic and computational analyses reveal that the highly active tpy-Co^{2+} (3N-Co) configurations serve as the active centers. This study offered a significant leap in applying supramolecular coordination complexes to practical energy devices, showing how soft, self-assembled materials can rival or outperform traditional crystalline frameworks. In another study, Liu et al. synthesized terpyridine- Co^{2+} (Tpy-Co^{2+}) low-molecular-weight gelator (**L69**; Figure 28) that forms supramolecular hydrogels through a unique “bridge bond” interaction involving hydrogen bonding between Cl^- ions and H_2O (Figure 29).^[174] The hydrogen bond and π - π conjugation exhibit

a synergistic influence on gelation. The “bridge bond” interaction links with the adjacent structural units to form a rigid network. This structural innovation enables the creation of a 3D conductive hydrogel framework with exceptional electrocatalytic activity for OER and ORR. The spatial confinement effect through a large gelator exhibits excellent electron transport ability. It shows the lowest overpotential (264 mV at 10 mA cm⁻²) and supports a liquid Zn-air battery with ultralong cycling stability exceeding 1100 h and round-trip energy efficiency of 65.3%. Additionally, the material proves effective in quasi-solid-state configurations, which maintain stability at both room and sub-zero temperatures (-40°C). The study not only elucidates the gelation mechanism driven by π - π conjugation and hydrogen bonding but also showcases the practical viability of these hydrogels in flexible electrochemical applications, which opens avenues for wearable energy storage systems.

(c) Porous framework-supported systems: The development of MOF/ZIF-based gels significantly influences catalytic research.^[175] It aids in addressing multiple problems, such as leaching and structural disintegration. The gel component of MOF/ZIF-based hydrogels and aerogels offers structural support to the frameworks, which improves their stability during the recyclability test. In this regard, Sun and co-workers developed a novel hybrid photoelectrocatalyst by integrating UiO-67 MOF (using **L70** gelator; Figure 28) nanoparticles with photonic crystal matrices inspired by butterfly wing structures.^[176] Using metal-organic gelation, the photonic substrate was uniformly anchored onto the MOFs and formed a highly ordered and responsive material. The composite system functions as an efficient photocathode for hydrogen evolution under visible light, leveraging the light-trapping and energy-transfer capabilities of the photonic crystal. Mott-Schottky analysis shows it functioned as an n-type semiconductor with a significantly reduced bandgap (~ 0.75 eV). Under illumination, the current density increases from 3.2 to 7.0 mA cm⁻² at -0.6 V, and carrier density increases over 2-fold within 30 min. This unique synergy between MOF chemistry and bioinspired photonic structures opens new directions for artificial photosynthesis and solar-to-hydrogen conversion, addressing key limitations in light capture and catalytic efficiency. In another study, Gu and coworkers developed a hierarchical assembly technique where coordination-driven guanosine-based metallo gel was utilized as a robust host material for ZIF-67.^[177] The linker **L71** (Figure 28) was used as a gelator, and Zn^{2+} ions as the metal source to form coordination-driven nanostructure gels. The cobalt-embedded porous carbon polyhedra with B, N co-doped carbon nanofibers ($\text{Co@Zn}^{2+}\text{-L71 gel/ZIF-67}$) were formed after pyrolysis of the ZIF-67 incorporated supramolecular gel in presence of Ar (Figure 30). The Co-Nx sites, obtained from the pyrolyzed ZIF-67 structure, exhibit significant catalytic activity by enhancing charge transfer efficiency and improving oxygen binding energy. The codoping of boron and nitrogen further augments the catalyst's conductivity, stability, and electron density, hence enhancing its overall performance in the ORR process.

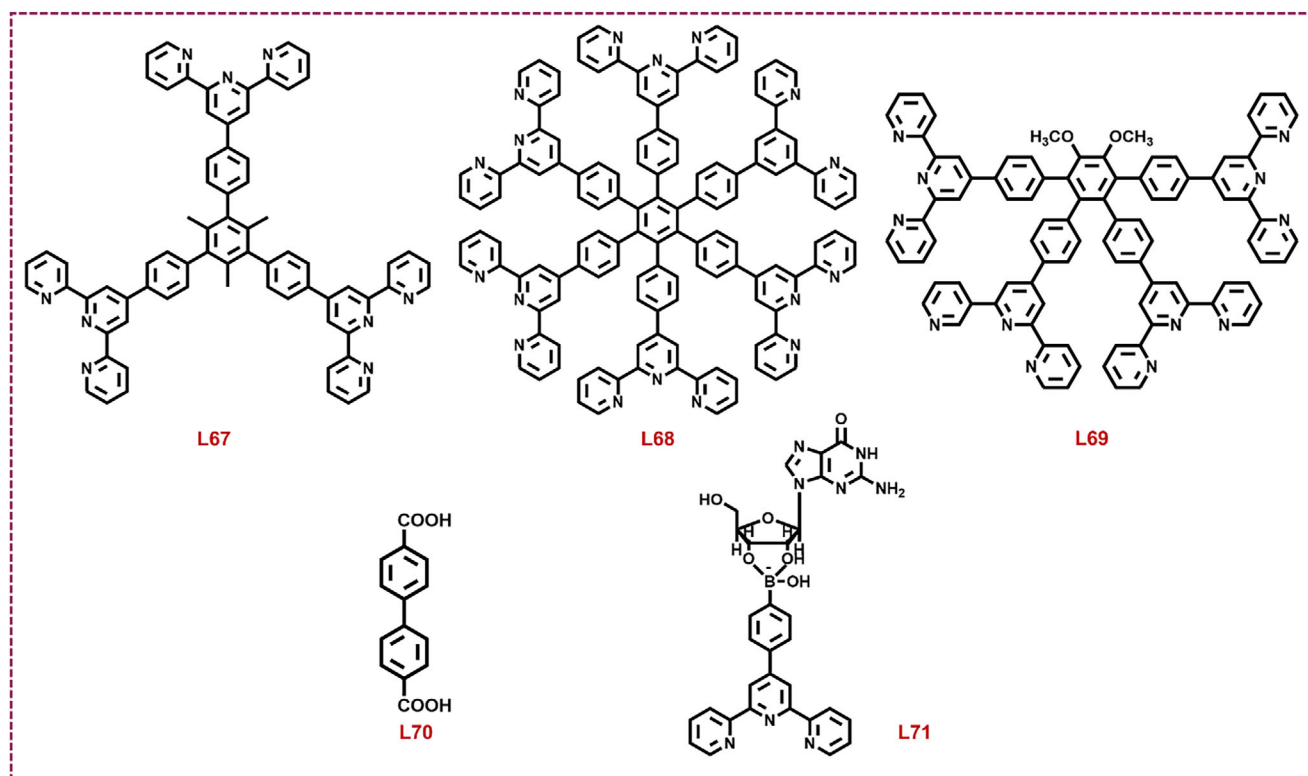


Figure 28. Gelators from L67–L71 were used to synthesize different metallogels and utilize them in electrocatalytic reactions.

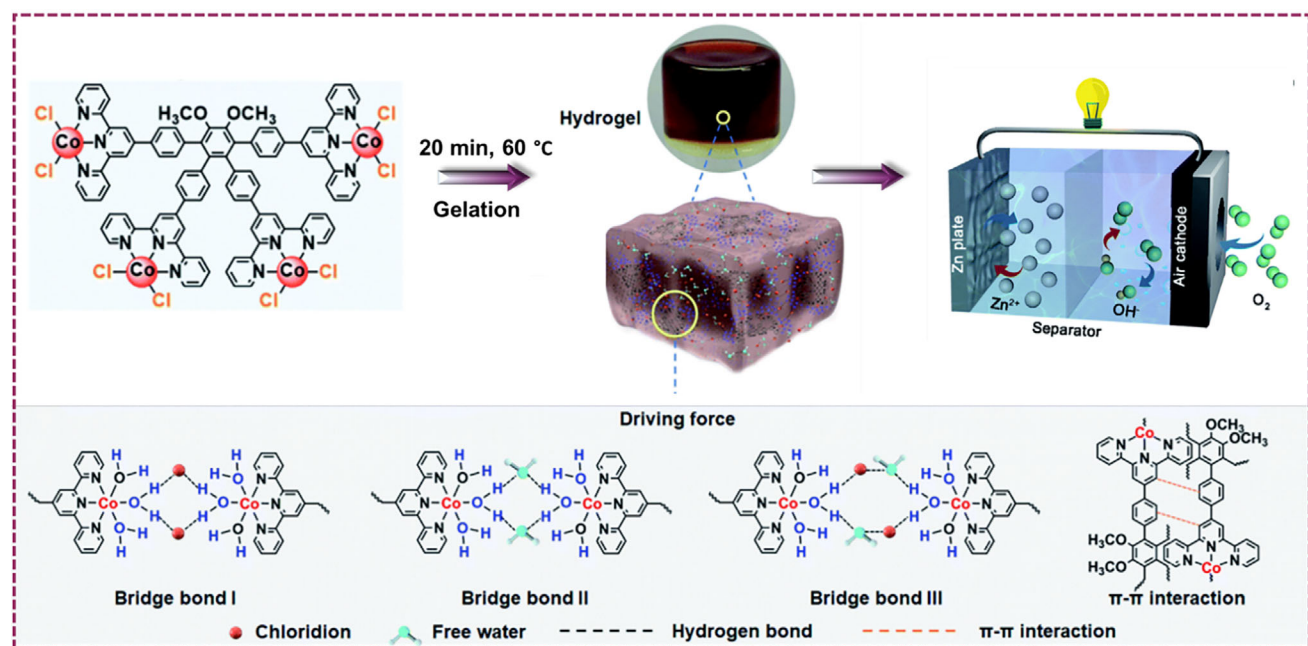


Figure 29. Schematic representation of gelation (interaction of terpyridine- Co^{2+} unit), "bridge bond" interactions, and the utilization of metallogel in Zn-air battery. Partially adapted scheme from Ref. [174]. Copyright (2022), with permission from the Royal Society of Chemistry.

3.4. Biomimetic Catalysis

Enzymes represent the most promising catalysts, as they are found in organisms and can achieve high catalytic efficiencies under physiological conditions.^[178] Natural enzymes possess

numerous potential applications; however, their practicality is often hindered by high production costs, limited stability, and extreme sensitivity to variations in conditions such as temperature or pH.^[179] Consequently, significant efforts have been made to identify synthetic enzymes capable of mimicking the cat-

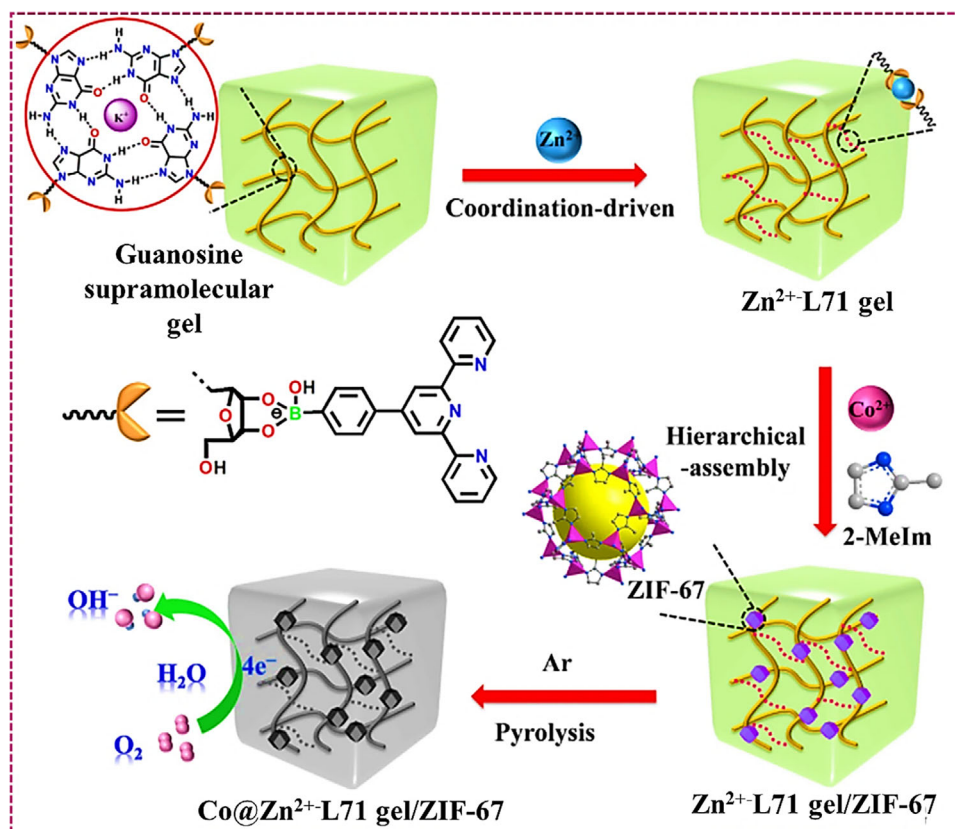


Figure 30. Schematic representation of guanosine-based gel, Zn^{2+} -L71 gel, Zn^{2+} -L71 gel/ZIF-67, and $\text{Co}@\text{Zn}^{2+}$ -L71 gel/ZIF-67. Reproduced from Ref. [177]. Copyright (2021), with permission from Elsevier.

alytic functions of natural enzymes for practical applications. In recent years, metallogels have emerged as biomimetic catalysts, effectively emulating the remarkable potency and specificity of natural metalloenzymes' catalytic activity. A multitude of metallogel systems integrating supramolecular gel networks with metal coordination chemistry have been documented to exhibit enzyme-like activity in soft materials.^[14a] In this context, Wang et al. produced a Cu^{2+} -selective metalhydrogel utilizing chiral phenylalanine-derived ligands (L72A- and L72B; Figure 31) that were functionalized with pyridyl groups.^[180] The metalhydrogel shows substantial reactivity with molecular oxygen, leading to the formation of $[(\text{L}+\text{D})\text{-L72-Cu}^{3+}\text{-O}_2]$ species. This can effectively reduce ferric cytochrome c with reactive O_2 -species by obtaining an electron from reductant ascorbic acid. This system mimics essential features of enzymatic function, that illustrate how the strategic design of chiral ligands can impart biomimetic redox properties to metallogels. In the direction of the biomimetic paradigm, Malviya et al. synthesized a Cu(II) -carboxamide-based metallogel (L73; Figure 31) that proficiently catalyzes the oxidation of catechols to quinones, mimicking the function of catechol oxidase, and exemplifies one of the initial instances of enzyme-mimicking catalysis executed entirely within a gel matrix.^[181] In a similar study, Dominic Kurbah and coworkers developed a dicopper carboxylate metallogel with bipyridine (L74; Figure 31) and benzoic acid (L75; Figure 31) ligands by aerobically oxidizing 3,5-di-*tert*-butylcatechol under mild conditions. This metallogel demonstrated catechol oxidase

mimicking activity and provided thorough enzyme kinetics to validate its catalytic efficacy.^[182] Enzyme-mimicking nanomaterials (nanozymes) that are highly active, stable, and cost-effective have the potential to serve as alternatives to natural enzymes for catalyzing enzyme-like reactions. He et al. reported a Ru-based metallogel with a favorable porous architecture as an innovative nanozyme material emulating dual-peroxidase biocatalytic activities.^[183] The gel was synthesized using L76 (Figure 31) gelator and RuCl_3 . The gel exhibits inherent horseradish peroxidase (HRP)-mimetic activity, that facilitates dopamine oxidation and luminol chemiluminescence (CL) in the presence of H_2O_2 . Along with this, it was also utilized in the oxidation of nicotinamide adenine dinucleotide (NADH) by H_2O_2 . A highly functional NAD + cofactor was produced by oxidizing NADH by Ru-metallogels, which exhibited strong NADH peroxidase-mimic activity. The kinetic study shows very high catalytic velocity, with excellent binding affinities of Ru-metallogel, and the catalytic process follows the usual Michaelis–Menten behavior. In addition to exhibiting exceptional catalytic activity and dual-peroxidase mimic capabilities, this Ru-metallogel sidesteps the difficult fabrication processes and harsh synthesis conditions. In a distinct study, Kurbah et al. developed an innovative and effective protocol for the Bromo peroxidase-like activity utilizing a straightforward $\text{VO}_2\text{-L77}$ (Figure 31) metallogel as the catalyst.^[184] In another study, Sarkar et al. synthesized a nanofibrous Cu(II) metallogel through the combination of L78 and L79 (Figure 31). This metallogel functions as a phenoxazinone synthase, accelerating the

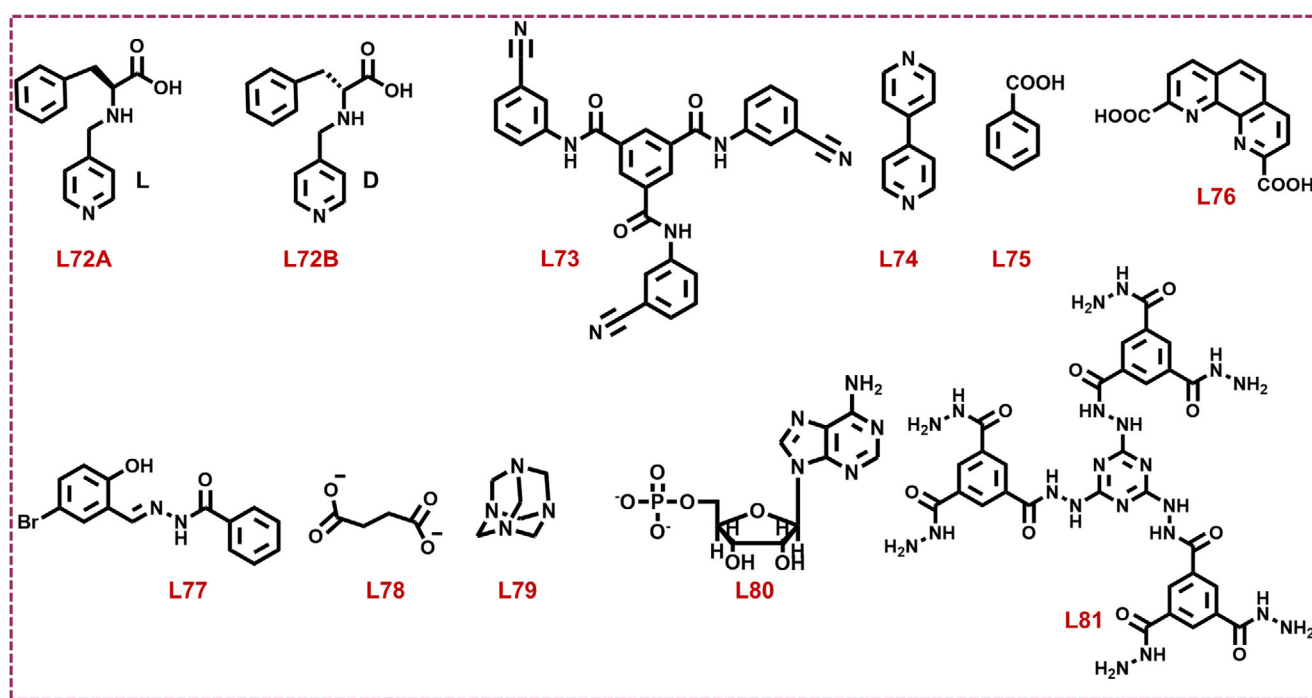


Figure 31. Gelators from L72–L81 were used to synthesize different metallogels and utilize them in biomimicking catalytic reactions.

oxidative transformation of *o*-aminophenol to phenoxazinone following a Michaelis–Menten kinetic model.^[185] Later, Agarwal et al. reported Co-L80 supramolecular hydrogel (L80; Figure 31) for multinanozymatic activity. It mimics catalase at neutral to basic pH and peroxidase at acidic pH, with additional phenoxazinone synthase-like activity. By lowering ROS-induced cellular stress, this metallogel additionally showed biological relevance, underscoring its potential for use in medicine.^[41a] In a recent study, Munjal et al. reported a siderophore-inspired Fe (III)-based metallogel was developed by L81 and L13 (Figure 31 and Figure 8) gelators. This metallogel mimics the transport and iron sequestration behavior of natural siderophores, allowing for selective Fe³⁺ scavenging and redox-responsive release, thereby reflecting both structural and functional biomimicry.^[47]

4. Critical Analysis

Despite the ongoing growth in the realm of metallogels, it is evident that their research remains in the nascent stages. The complete understanding of the metal–ligand environment within polymeric structures remains elusive. There are still numerous loopholes where the discussion can be carried out. The gap in these investigations hinders the precise determination of structure–property correlations, which restricts access to valuable information for subsequent enhancements. Spectroscopic techniques such as near-edge X-ray absorption fine structure may contribute to obtain information about the immediate vicinity of the metal centers. Methods that are commonly used in the field of MOF community, such as elemental analysis, have the potential to extract information regarding the linker-to-metal ratios in the structure. Along with this, control over morphology and porosity is crucial in soft material research. Much more

research effort is needed in these aspects of regulating and modulating metallogels. Hence, there is a need to tune the design principles to provide control over the surface chemistry and morphological variations.

The intricacy of catalytic processes facilitated by metallogels has progressively escalated, and it is plausible to anticipate that metallogels will persist in providing the answers to challenges in catalytic organic transformations. However, from the standpoint of an organic chemist, there has been relatively little investment in the research and development of metallogels compared to homogeneous catalysts. It is necessary to thoroughly examine their actual capabilities, shortcomings, and limitations as catalysts for organic synthesis. Although, researchers have started to develop new strategies to build efficient catalysts for diverse organic transformation reactions. To this end, relevant efforts need to be manifested more strongly towards C–H activation, enantioselective processes, and other complex biomimicking transformations.

On the other hand, the wide research in the context of electro/photocatalytic applications is still in its early stages. Studies on ORR, OER, and HER have been conducted; however, the use of these gels has not been extensively investigated for other electrocatalytic reactions, such as nitrogen reduction reactions and other battery-related applications. Easy tunability and bulk phase production may outperform the other inorganic–organic hybrid materials in next-generation electrocatalytic device integration. Apart from electrocatalytic investigations, photocatalytic studies are also not well-established in the field of metallogel-mediated catalytic transformations. In recent years, there has been an upsurge in solar cell-based energy research within the MOF community. Meanwhile, these soft materials are a little behind in marking their existence. In this regard, the hybrid metallogels based on photoactive materials and those includ-

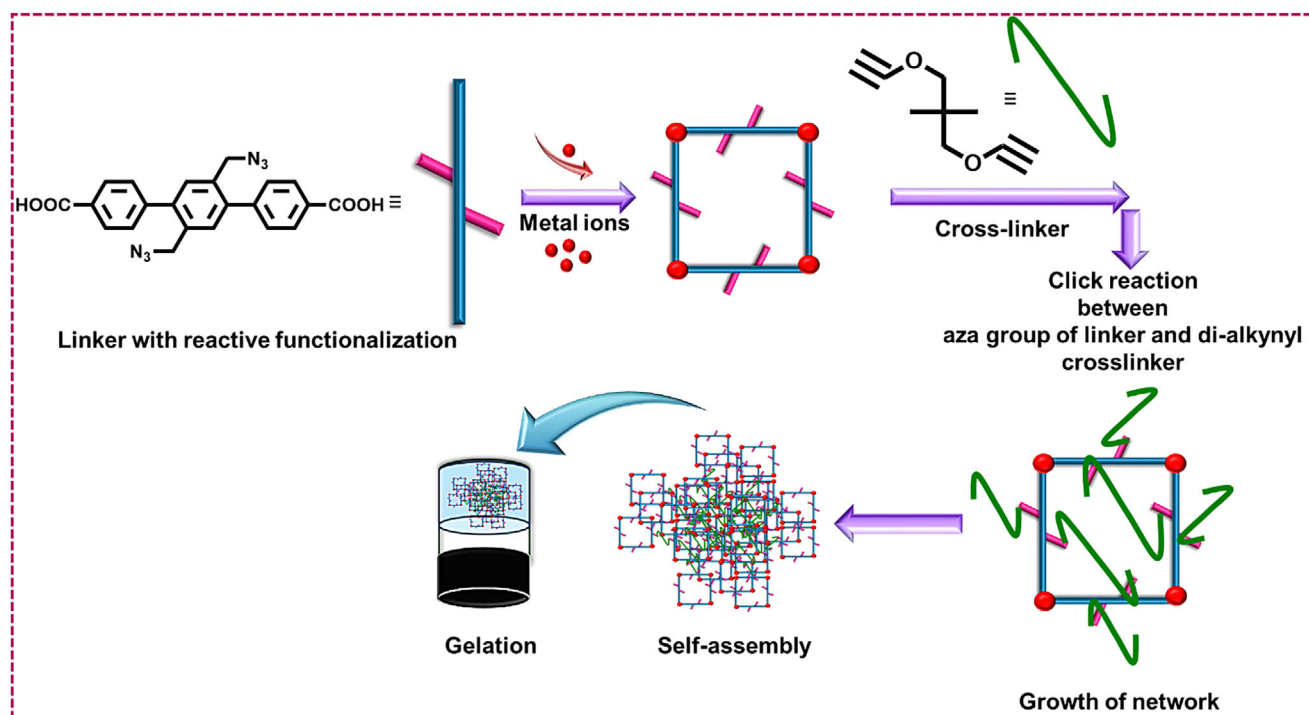


Figure 32. Schematic representation of gelation by cross-linker method, where reactive functional species can bind with the cross-linker group via definite reaction conditions and enhance the strength of gel networks.

ing conjugated linkers could surmount the current limits of these metallogels. The photoactive substance will enhance the photoactivity of metallogels, while the conjugated linker will promote the separation of photogenerated charge carriers.

Leaching is a prevalent issue in metallogel catalysis, especially when the metal centers responsible for catalysis are inadequately bound within the gel matrix. Its low catalytic performance and lack of recyclability limit its use in cutting-edge heterogeneous catalytic research.^[84] The gel framework could be made more stable with the introduction of a cross-linker method, which could be useful for advanced catalytic research.^[186] The additional bridging cogelator can covalently cross-link within the gel network structure to enhance stability, which restricts further leaching of metal ions. Gel matrix with reactive functionalized organic linker can interact with external cross-linking agents via definite reactions, as shown in Figure 32.^[187] It demonstrates enhanced structural stabilization by limiting the disintegration of the framework's backbone. Alternatively, in a "hybrid metallogel" system, MOF nanoparticles are confined in a gel matrix via physical or chemical crosslinking. This particle can be incorporated through the in-situ gelation method or postsynthetic modification. This facilitates uniform dispersion of one or more metal sources across the gel matrix and assembles multiple metal components at the nanoscale with high homogeneity.^[59]

The creation of hybrids or composites, such as carbon/metal oxide compounds, has led to several exciting discoveries in energy storage, conversion, and catalysis.^[188] Like MOF chemistry, metallogels can also be utilized to make porous carbonaceous material composites.^[189] Different nanoparticles can be loaded within the aerogel framework. Metal-mediated coordi-

nation polymer material most often shows poor charge carrier capacity and is also constrained by aggregation and leaching issues. Meanwhile, postthermal treatment of these materials demonstrates improved stability under extreme conditions and augments the accessibility of catalytically active areas within the hierarchical porous structure.^[14e] The high-temperature calcination effectively restricts the aggregation and leaching of metallic components. Overall, these phenomena impact catalytic cyclic stability and applicability.

5. Conclusion and Prospects

Metallogels represent a fascinating category of soft and smart materials that employ a "bottom-up" methodology to assemble polymeric structures from small gelators. The interplay of noncovalent interactions can effectively alter the properties of polymeric structures, including their physical and optical characteristics. Their synthesis, manufacturing, and nanocompositing or hybridization with other materials have advanced significantly in the past decade, primarily resulting in new classes of materials. Regardless of the challenges, the numerous applications of metallogels demonstrate their practicality. Considering the wide range of uses for metallogels, we anticipate that synthesis engineering is one of the most exciting new paths in this field, which can transform metallogels. This allows more precise control over the synthesis of nanostructured gel, potentially propelling the development of commercially viable products for catalytic transformation and energy storage. This review primarily focuses on providing a summary of the crucial accomplishments in the fields of metallogel and catalysis. By

imparting catalytic sites, such as active metal ions, MNPs, and gelators with active functionality into the gel matrix, metallogels might be viewed as attractive candidates for catalysts with diverse advantages. A comprehensive discussion on various catalytic studies and recent advancements was summarized appropriately. The synthesis approach of metallogelators and their structural description, diverse interactions that play a crucial role in the self-assembly process, were discussed. Finally, distinct catalytic conversions are presented in a tabular style for the reader's convenience. In addition to significant efforts in environmental conservation and green chemistry, metallogels will undoubtedly offer a novel methodology for the design and synthesis of more versatile and resilient supramolecular catalysts with high atom economies in the near future.

Acknowledgments

S.M. and J.R. express gratitude to the Indian Institute of Technology Patna for providing the requisite resources. D.S. acknowledges the Science & Engineering Research Board (SERB) of the Government of India for providing a research grant under sanction CRG/2023/003002.

Conflict of Interests

The authors declare no conflict of interest.

Keywords: Heterogeneous catalysis • Metallogels • Self-assembly • Soft materials • Supramolecular gels

- [1] P. Terech, R. G. Weiss, *Chem. Rev.* **1997**, *97*, 3133–3160.
- [2] P. Dastidar, S. Ganguly, K. Sarkar, *Chem. Asian J.* **2016**, *11*, 2484–2498.
- [3] T. Graham, *Phil. Trans. R. Soc.* **1861**, *151*, 183–224.
- [4] D. J. Lloyd, *Colloid Chem* **1926**, *1*, 767–782.
- [5] P. J. Flory, *Faraday Discuss.* **1974**, *57*, 7–18.
- [6] K. Almdal, J. Dyre, S. Hvidt, O. Kramer, *Polym. Gels Netw.* **1993**, *1*, 5–17.
- [7] J. V. Alemán, A. V. Chadwick, J. He, M. Hess, K. Horie, R. G. Jones, P. Kratochvíl, I. Meisel, I. Mita, G. Moad, S. Penczek, R. F. T. Stepto, *Pure Appl. Chem.* **2007**, *79*, 1801–1829.
- [8] A. Y.-Y. Tam, V. W.-W. Yam, *Chem. Soc. Rev.* **2013**, *42*, 1540–1567.
- [9] N. Alam, S. Mondal, D. Sarma, *Coord. Chem. Rev.* **2024**, *504*, 215673.
- [10] a) J. Raeburn, D. J. Adams, *Chem. Commun.* **2015**, *51*, 5170–5180; b) J. Zhang, C.-Y. Su, *Coord. Chem. Rev.* **2013**, *257*, 1373–1408; c) S. Mondal, N. Alam, S. Sahoo, D. Sarma, *J. Colloid Interface Sci.* **2023**, *633*, 441–452.
- [11] D. K. Kumar, J. W. Steed, *Chem. Soc. Rev.* **2014**, *43*, 2080–2088.
- [12] a) D. K. Smith, *Soft Matter* **2024**, *20*, 10–70; b) P. Sahoo, V. G. Puranik, A. Patra, P. Sastry, P. Dastidar, *Soft Matter* **2011**, *7*, 3634–3641.
- [13] a) P. Sutar, T. K. Maji, *Dalton Trans.* **2020**, *49*, 7658–7672; b) N. Alam, S. Mondal, S. S. Hossain, S. Sahoo, D. Sarma, *ACS Appl. Eng. Mater.* **2023**, *1*, 1201–1212; c) S. Saha, B. Pal, K. Sundar Das, P. Kumar Ghose, A. Ghosh, A. De, A. Kumar Das, P. Pratim Ray, R. Mondal, *ChemistrySelect* **2022**, *7*, e202203307.
- [14] a) H. Wu, J. Zheng, A. L. Kjøniksen, W. Wang, Y. Zhang, J. Ma, *Adv. Mater.* **2019**, *31*, 1806204; b) Z. Gao, J. Zhu, Y. Han, X. Lv, X. Zhang, F. Wang, *Polym. Chem.* **2016**, *7*, 5763–5767; c) K. C. Chang, J. L. Lin, Y. T. Shen, C. Y. Hung, C. Y. Chen, S. S. Sun, *Chem. - Eur. J.* **2012**, *18*, 1312–1321; d) Z. Liu, X. Zhao, Q. Chu, Y. Feng, *Molecules* **2023**, *28*, 2274; e) S. Ma, J. Xu, S. Sohrobi, J. Zhang, *J. Mater. Chem. A* **2023**, *11*, 11572–11606; f) B. Gupta, S. Kalyan Samanta, R. Singh, *Mater. Today* **2024**, *80*, 681–709.
- [15] E. Roduner, *Chem. Soc. Rev.* **2014**, *43*, 8226–8239.
- [16] a) C.-H. Jun, *Chem. Soc. Rev.* **2004**, *33*, 610–618; b) D. Balcells, E. Clot, O. Eisenstein, *Chem. Rev.* **2010**, *110*, 749–823.
- [17] a) S. Toledano, R. J. Williams, V. Jayawarna, R. V. Ulijn, *J. Am. Chem. Soc.* **2006**, *128*, 1070–1071; b) D. Díaz Díaz, D. Kühbeck, R. J. Koopmans, *Chem. Soc. Rev.* **2011**, *40*, 427–448; c) E. Serrano, N. Linares, J. Garcia-Martinez, J. R. Berenguer, *ChemCatChem* **2013**, *5*, 844–860.
- [18] J. K. Wychowanec, H. Saini, B. Scheibe, D. P. Dubal, A. Schneemann, K. Jayaramulu, *Chem. Soc. Rev.* **2022**, *51*, 9068–9126.
- [19] a) G. Liu, S. Li, C. Shi, M. Huo, Y. Lin, *Nanomaterials* **2023**, *13*, 1178; b) A. Mallick, E.-M. Schön, T. Panda, K. Sreenivas, D. D. Díaz, R. Banerjee, *J. Mater. Chem.* **2012**, *22*, 14951–14963; c) S. Kitagawa, *Chem. Soc. Rev.* **2014**, *43*, 5415–5418.
- [20] C. Rizzo, S. Marullo, F. Billeci, F. D'Anna, *Eur. J. Org. Chem.* **2021**, *2021*, 3148–3169.
- [21] Y. Xiao, H. Yang, X. Gong, L. Hu, Y. Tong, J. Zhang, *ACS Appl. Nano Mater.* **2020**, *3*, 2393–2401.
- [22] M. Araújo, S. Díaz-Oltra, B. Escuder, *Chem. - Eur. J.* **2016**, *22*, 8676–8684.
- [23] K. Chan, A. Zinchenko, *Waste Manag* **2023**, *164*, 20–28.
- [24] P. Slavik, D. W. Kurka, D. K. Smith, *Chem. Sci.* **2018**, *9*, 8673–8681.
- [25] T. Khandaker, M. A. A. M. Anik, A. Nandi, T. Islam, M. M. Islam, M. K. Hasan, P. K. Dhar, M. A. Latif, M. S. Hossain, *Catal. Sci. Technol.* **2025**, *15*, 1357–1389.
- [26] Y. Liao, L. He, J. Huang, J. Zhang, L. Zhuang, H. Shen, C.-Y. Su, *ACS Appl. Mater. Interfaces* **2010**, *2*, 2333–2338.
- [27] a) L. Kang, J. Chu, H. Zhao, P. Xu, M. Sun, *J. Mater. Chem. C* **2015**, *3*, 9024–9037; b) P. Serp, *ChemCatChem* **2023**, *15*, e202300545.
- [28] a) C. Liu, J. Wang, J. Wan, C. Yu, *Coord. Chem. Rev.* **2021**, *432*, 213743; b) K. Wang, Y. Li, L.-H. Xie, X. Li, J.-R. Li, *Chem. Soc. Rev.* **2022**, *51*, 6417–6441; c) S. Sahoo, S. Mondal, D. Sarma, *Coord. Chem. Rev.* **2022**, *470*, 214707; d) N. Stock, S. Biswas, *Chem. Rev.* **2012**, *112*, 933–969; e) R. Patra, S. Mondal, D. Sarma, *Dalton Trans.* **2023**, *52*, 17623–17655; f) M. Ding, R. W. Flaig, H.-L. Jiang, O. M. Yaghi, *Chem. Soc. Rev.* **2019**, *48*, 2783–2828.
- [29] a) P. R. Chivers, D. K. Smith, *Nat. Rev. Mater.* **2019**, *4*, 463–478; b) F. Xu, H. Wang, J. Zhao, X. Liu, D. Li, C. Chen, J. Ji, *Macromolecules* **2013**, *46*, 4235–4246; c) Y. Feng, Z.-X. Liu, H. Chen, Q.-H. Fan, *Chem. Commun.* **2022**, *58*, 8736–8753.
- [30] A. Lipowitz, *Ann. Chem.* **1841**, *38*, 348–355.
- [31] a) P. Sutar, T. K. Maji, *Chem. Commun.* **2016**, *52*, 8055–8074; b) A. Sharma, N. Kaur, N. Singh, *Chem. Asian J.* **2024**, *19*, e202400258.
- [32] a) J.-S. Shen, Y.-L. Chen, J.-L. Huang, J.-D. Chen, C. Zhao, Y.-Q. Zheng, T. Yu, Y. Yang, H.-W. Zhang, *Soft Matter* **2013**, *9*, 2017–2023; b) S. Mondal, N. Alam, D. Sarma, *ACS Appl. Eng. Mater.* **2024**, *2*, 1467–1482; c) J. Zhang, Y. Hu, Y. Li, J. Zhang, Y. Hu, Y. Li, in *Gel Chemistry*, Springer Singapore, Singapore **2018**, pp. 61–118.
- [33] A. M. Patel, V. Bhardwaj, A. Ballabh, *Curr. Org. Chem.* **2024**, *28*, 1046–1058.
- [34] J. Liu, J. Yan, X. Yuan, K. Liu, J. Peng, Y. Fang, *J. Colloid Interface Sci.* **2008**, *318*, 397–404.
- [35] W. Fang, Z. Sun, T. Tu, *J. Phys. Chem. C* **2013**, *117*, 25185–25194.
- [36] a) T. Kishida, N. Fujita, K. Sada, S. Shinkai, *Langmuir* **2005**, *21*, 9432–9439; b) S. S. Babu, V. K. Praveen, A. Ajayaghosh, *Chem. Rev.* **2014**, *114*, 1973–2129.
- [37] S. Mondal, D. Sarma, *Soft Matter* **2023**, *19*, 4926–4938.
- [38] A. Bochkarev, R. A. Pfuetzner, A. M. Edwards, L. Frappier, *Nature* **1997**, *385*, 176–181.
- [39] a) J. C. Ma, D. A. Dougherty, *Chem. Rev.* **1997**, *97*, 1303–1324; b) M. Staffilani, K. S. Hancock, J. W. Steed, K. T. Holman, J. L. Atwood, R. K. Juneja, R. S. Burkhalter, *J. Am. Chem. Soc.* **1997**, *119*, 6324–6335.
- [40] a) S. Kitagawa, R. Kitaura, S. i. Noro, *Angew. Chem., Int. Ed.* **2004**, *43*, 2334–2375; b) J. L. Obeso, M. T. Huxley, C. Leyva, J. Gabriel Flores, N. Martín-Guaregua, M. Viniegra, J. Aguilar-Pliego, J. Antonio De Los Reyes, I. A. Ibarra, R. A. Peralta, *Coord. Chem. Rev.* **2023**, *496*, 215403; c) S. Sahoo, S. Mondal, D. Sarma, *Eur. J. Inorg. Chem.* **2023**, *26*, e202300067.
- [41] a) V. Agarwal, N. Varshney, S. Singh, N. Kumar, A. Chakraborty, B. Sharma, H. C. Jha, T. K. Sarma, *ACS Appl. Bio Mater.* **2023**, *6*, 5018–5029; b) L. Berti, G. A. Burley, *Nat. Nanotechnol.* **2008**, *3*, 81–87.
- [42] K. Loo, N. Degtyareva, J. Park, B. Sengupta, M. Reddish, C. C. Rogers, A. Bryant, J. T. Petty, *J. Phys. Chem. B* **2010**, *114*, 4320–4326.
- [43] D. Datta, *Inorg. Chem.* **1992**, *31*, 2797–2800.
- [44] S. Saha, E.-M. Schön, C. Cativiela, D. Díaz Díaz, R. Banerjee, *Chem. - Eur. J.* **2013**, *19*, 9562–9568.

- [45] a) P. Sutar, V. M. Suresh, T. K. Maji, *Chem. Commun.* **2015**, 51, 9876–9879; b) P. Sutar, T. K. Maji, *Inorg. Chem.* **2017**, 56, 9417–9425.
- [46] A. Butler, R. M. Theisen, *Coord. Chem. Rev.* **2010**, 254, 288–296.
- [47] R. Munjal, R. Kyarikwal, S. Sarkar, P. Nag, S. R. Vennapusa, S. Mukhopadhyay, *Inorg. Chem.* **2024**, 63, 7089–7103.
- [48] K. Kuroiwa, T. Shibata, A. Takada, N. Nemoto, N. Kimizuka, *J. Am. Chem. Soc.* **2004**, 126, 2016–2021.
- [49] H. Schmidbaur, *Chem. Soc. Rev.* **1995**, 24, 391–400.
- [50] a) M. H.-Y. Chan, M. Ng, S. Y.-L. Leung, W. H. Lam, V. W.-W. Yam, *J. Am. Chem. Soc.* **2017**, 139, 8639–8645; b) J. Park, J. H. Lee, J. Jaworski, S. Shinkai, J. H. Jung, *Inorg. Chem. Front.* **2014**, 53, 7181–7187; c) M.-O. M. Piepenbrock, G. O. Lloyd, N. Clarke, J. W. Steed, *Chem. Rev.* **2010**, 110, 1960–2004.
- [51] A. Kishimura, T. Yamashita, T. Aida, *J. Am. Chem. Soc.* **2005**, 127, 179–183.
- [52] K. M.-C. Wong, L.-L. Hung, W. H. Lam, N. Zhu, V. W.-W. Yam, *J. Am. Chem. Soc.* **2007**, 129, 4350–4365.
- [53] I. Eryazici, C. N. Moorefield, G. R. Newkome, *Chem. Rev.* **2008**, 108, 1834–1895.
- [54] M. Shirakawa, N. Fujita, T. Tani, K. Kaneko, S. Shinkai, *Chem. Commun.* **2005**, 33, 4149–4151.
- [55] O. Roubeau, A. Colin, V. Schmitt, R. Clérac, *Angew. Chem.* **2004**, 116, 3345–3348.
- [56] T. Tu, W. Assenmacher, H. Peterlik, R. Weisbarth, M. Nieger, K. H. Dötz, *Angew. Chem. Int. Ed.* **2007**, 46, 6368–6371.
- [57] J. Hou, A. F. Sapnik, T. D. Bennett, *Chem. Sci.* **2020**, 11, 310–323.
- [58] J. Fu, Z. He, E. Schott, H. Fei, M. Tu, Y.-n. Wu, *Small* **2023**, 19, 2206718.
- [59] A. Mahmood, W. Xia, N. Mahmood, Q. Wang, R. Zou, *Sci. Rep.* **2015**, 5, 10556.
- [60] L. Li, S. Xiang, S. Cao, J. Zhang, G. Ouyang, L. Chen, C.-Y. Su, *Nat. Commun.* **2013**, 4, 1774.
- [61] K. Jayaramulu, F. Geyer, M. Petr, R. Zboril, D. Vollmer, R. A. Fischer, *Adv. Mater.* **2017**, 29, 1605307.
- [62] A. Chakraborty, P. Sutar, P. Yadav, M. Eswaramoorthy, T. K. Maji, *Inorg. Chem.* **2018**, 57, 14480–14483.
- [63] B. Bueken, N. Van Velthoven, T. Willhammar, T. Stassin, I. Stassen, D. A. Keen, G. V. Baron, J. F. M. Denayer, R. Ameloot, S. Bals, D. De Vos, T. D. Bennett, *Chem. Sci.* **2017**, 8, 3939–3948.
- [64] C.-W. Zhao, Y.-A. Li, X.-R. Wang, G.-J. Chen, Q.-K. Liu, J.-P. Ma, Y.-B. Dong, *Chem. Commun.* **2015**, 51, 15906–15909.
- [65] P. Liao, H. Fang, J. Zhang, Y. Hu, L. Chen, C. Y. Su, *Eur. J. Inorg. Chem.* **2017**, 2017, 2580–2584.
- [66] K. Preet, R. Kumar, L. Kaur, S. Roy, S. C. Sahoo, D. B. Salunke, *J. Mol. Struct.* **2024**, 1310, 138316.
- [67] G. Nandi, H. M. Titi, R. Thakuria, I. Goldberg, *Cryst. Growth Des.* **2014**, 14, 2714–2719.
- [68] W. Fang, Y. Zhang, J. Wu, C. Liu, H. Zhu, T. Tu, *Chem. Asian J.* **2018**, 13, 712–729.
- [69] M. Qiu, H. Wu, L. Cao, B. Shi, X. He, H. Geng, X. Mao, P. Yang, Z. Jiang, *ACS Appl. Mater. Interfaces* **2020**, 12, 19788–19796.
- [70] a) K. T. Mahmudov, A. V. Gurbanov, F. I. Guseinov, M. F. C. Guedes Da Silva, *Coord. Chem. Rev.* **2019**, 387, 32–46; b) N. Elgrishi, M. B. Chambers, X. Wang, M. Fontecave, *Chem. Soc. Rev.* **2017**, 46, 761–796.
- [71] a) A. Bavykina, N. Kolobov, I. S. Khan, J. A. Bau, A. Ramirez, J. Gascon, *Chem. Rev.* **2020**, 120, 8468–8535; b) A. H. Chughtai, N. Ahmad, H. A. Younus, A. Laypkov, F. Verpoort, *Chem. Soc. Rev.* **2015**, 44, 6804–6849; c) S. Natarajan, K. Manna, *ACS Org. Inorg. Au* **2023**, 4, 59–90.
- [72] a) C. Song, *Catal. Today* **2006**, 115, 2–32; b) U. Habib, F. Ahmad, M. Awais, N. Naz, M. Aslam, M. Urooj, A. Moqem, H. Tahseen, A. Waqar, M. Sajid, M. J. Shabbir, *J. Chem. Environ.* **2023**, 2, 14–53.
- [73] M. Fujita, Y. J. Kwon, S. Washizu, K. Ogura, *J. Am. Chem. Soc.* **1994**, 116, 1151–1152.
- [74] a) Y.-B. Huang, J. Liang, X.-S. Wang, R. Cao, *Chem. Soc. Rev.* **2017**, 46, 126–157; b) Z. Y. Gu, J. Park, A. Raiff, Z. Wei, H. C. Zhou, *ChemCatChem* **2014**, 6, 67–75; c) A. Dhakshinamoorthy, A. M. Asiri, H. Garcia, *ChemCatChem* **2020**, 12, 4732–4753.
- [75] B. Xing, M. F. Choi, B. Xu, *Chem. - Eur. J.* **2002**, 8, 5028–5032.
- [76] S. Mondal, R. Patra, J. Ray, D. Sarma, *ACS Appl. Nano Mater.* **2024**, 7, 26765–26776.
- [77] D. Markad, S. K. Mandal, *ACS Catal.* **2019**, 9, 3165–3173.
- [78] T. Sawano, N. C. Thacker, Z. Lin, A. R. McIsaac, W. Lin, *J. Am. Chem. Soc.* **2015**, 137, 12241–12248.
- [79] J. Rayadurgam, S. Sana, M. Sasikumar, Q. Gu, *Org. Chem. Front.* **2021**, 8, 384–414.
- [80] R. Martin, S. L. Buchwald, *Acc. Chem. Res.* **2008**, 41, 1461–1473.
- [81] C. C. Johansson Seechurn, M. O. Kitching, T. J. Colacot, V. Snieckus, *Angew. Chem., Int. Ed.* **2012**, 51, 5062–5085.
- [82] Y.-R. Liu, L. He, J. Zhang, X. Wang, C.-Y. Su, *Chem. Mater.* **2009**, 21, 557–563.
- [83] J. Zhang, X. Wang, L. He, L. Chen, C.-Y. Su, S. L. James, *New J. Chem.* **2009**, 33, 1070–1075.
- [84] J. Huang, L. He, J. Zhang, L. Chen, C.-Y. Su, *J. Mol. Catal. A: Chem.* **2010**, 317, 97–103.
- [85] H. Li, X. Tan, J. Zhang, *Chin. J. Chem.* **2015**, 33, 141–146.
- [86] Y.-X. Ye, W.-L. Liu, B.-H. Ye, *Catal. Commun.* **2017**, 89, 100–105.
- [87] L.-F. Niu, Y. Cai, C. Liang, X.-P. Hui, P.-F. Xu, *Tetrahedron* **2011**, 67, 2878–2881.
- [88] S. Dhibar, A. Dey, D. Ghosh, S. Majumdar, A. Dey, P. P. Ray, B. Dey, *ACS Omega* **2020**, 5, 2680–2689.
- [89] A. Dömling, W. Wang, K. Wang, *Chem. Rev.* **2012**, 112, 3083–3135.
- [90] I. Jesin, G. C. Nandi, *Eur. J. Org. Chem.* **2019**, 2019, 2704–2720.
- [91] E. Saha, A. Rahaman, S. Bhadra, J. Mitra, *Dalton Trans.* **2023**, 52, 15530–15538.
- [92] M. Breugst, H. U. Reissig, *Angew. Chem., Int. Ed.* **2020**, 59, 12293–12307.
- [93] N. K. Devaraj, M. G. Finn, *Chem. Rev.* **2021**, 121, 6697–6698.
- [94] P.-Z. Li, X.-J. Wang, Y. Zhao, *Coord. Chem. Rev.* **2019**, 380, 484–518.
- [95] Y. He, Z. Bian, C. Kang, Y. Cheng, L. Gao, *Chem. Commun.* **2010**, 46, 3532–3534.
- [96] C. K. Karan, M. C. Sau, M. Bhattacharjee, *Chem. Commun.* **2017**, 53, 1526–1529.
- [97] T. Zhao, S. Chen, K. Kang, J. Ren, X. Yu, *Langmuir* **2022**, 38, 1398–1405.
- [98] J. Bietsch, A. Chen, D. Wang, G. Wang, *Molecules* **2023**, 28, 6056.
- [99] a) K. Appiah, J. Du, J. Poku, *Environ. Sci. & Pollut.* **2018**, 25, 24764–24777; b) D. Jenkinson, D. Adams, A. Wild, *Nature* **1991**, 351, 304–306.
- [100] a) Q.-W. Song, Z.-H. Zhou, L.-N. He, *Green Chem.* **2017**, 19, 3707–3728; b) G. A. Olah, G. S. Prakash, A. Goepfert, *J. Am. Chem. Soc.* **2011**, 133, 12881–12898.
- [101] A. Taheri Najafabadi, *Int. J. Energy Res.* **2013**, 37, 485–499.
- [102] a) P. Rani, R. Das, C. Nagaraja, *Inorg. Chem. Front.* **2025**, 12, 430–478; b) I. Hazra Chowdhury, A. Hazra Chowdhury, P. Sarkar, S. M. Islam, *ChemNanoMat* **2021**, 7, 580–591; c) P. Bhanja, A. Modak, A. Bhaumik, *ChemCatChem* **2019**, 11, 244–257.
- [103] B. Zhu, G. Liu, L. Chen, L. Qiu, L. Chen, J. Zhang, L. Zhang, M. Barboiu, R. Si, C.-Y. Su, *Inorg. Chem. Front.* **2016**, 3, 702–710.
- [104] L. Liu, J. Zhang, H. Fang, L. Chen, C.-Y. Su, *Chem. Asian J.* **2016**, 11, 2278–2283.
- [105] C. K. Karan, M. Bhattacharjee, *Eur. J. Inorg. Chem.* **2019**, 2019, 3605–3611.
- [106] E. Saha, H. Jungi, S. Dabas, A. Mathew, R. Kuniyil, S. Subramanian, J. Mitra, *Inorg. Chem.* **2023**, 62, 14959–14970.
- [107] N. Alam, S. Mondal, N. Ojha, S. Sahoo, M. T. Zeyad, S. Kumar, D. Sarma, *Nanoscale* **2025**, 17, 428–439.
- [108] S. Ghosh, P. Laha, N. U. D. Mir, P. Das, P.-R. Cha, S. Biswas, *Inorg. Chem. Front.* **2024**, 63, 21450–21461.
- [109] T. Zhao, Y. Li, Y. Zhang, Y. Wu, X. Hu, *ACS Sustainable Chem. Eng.* **2018**, 6, 10886–10895.
- [110] a) M. Orlandi, D. Brenna, R. Harms, S. Jost, M. Benaglia, *Org. Process Res. Dev.* **2016**, 22, 430–445; b) P. Niyirora, P. Cyganowski, *Chem. - Eur. J.* **2025**, 31, e202500281.
- [111] J. H. Lee, S. Kang, J. Y. Lee, J. H. Jung, *Soft Matter* **2012**, 8, 6557–6563.
- [112] S. Sengupta, A. Goswami, R. Mondal, *New J. Chem.* **2014**, 38, 2470–2479.
- [113] S. Bala, R. Mondal, *ChemistrySelect* **2017**, 2, 389–398.
- [114] M. Paul, K. Sarkar, P. Dastidar, *Chem. - Eur. J.* **2015**, 21, 255–268.
- [115] D. R. Pye, N. P. Mankad, *Chem. Sci.* **2017**, 8, 1705–1718.
- [116] M. Sharma, P. J. Sarma, M. J. Goswami, K. K. Bania, *J. Colloid Interface Sci.* **2017**, 490, 529–541.
- [117] R. Kyarikwal, N. Malviya, A. Chakraborty, S. Mukhopadhyay, *ACS Appl. Mater. Interfaces* **2021**, 13, 59567–59579.
- [118] P. Nautiyal, R. Kyarikwal, R. Munjal, P. Nag, S. R. Vennapusa, S. Mukhopadhyay, *ACS Appl. Eng. Mater.* **2024**, 2, 1503–1514.
- [119] D. P. Kumar, *RSC Adv.* **2014**, 4, 45449–45457.
- [120] W.-T. Deng, X. Zhong, Y. Li, X.-J. Jia, H.-Q. Luo, X.-Z. Luo, *Inorg. Chem. Front.* **2024**, 11, 5692–5699.

- [121] H. Hosseini-Monfared, C. Näther, H. Winkler, C. Janiak, *Inorganica Chim. Acta* **2012**, *391*, 75–82.
- [122] G. Liu, Y. Wang, B. Zhu, L. Zhang, C.-Y. Su, *New J. Chem.* **2018**, *42*, 11358–11363.
- [123] W. Zhang, J. J. Dynes, Y. Hu, P. Jiang, S. Ma, *Nat. Commun.* **2019**, *10*, 1913.
- [124] a) L. Jing, P. Li, Z. Li, D. Ma, J. Hu, *Chem. Soc. Rev.* **2025**, *54*, 2054–2090; b) H. Liu, Y. Wang, X. Xue, Y. Liu, P. Chen, P. Wang, S.-F. Yin, *J. Colloid Interface Sci.* **2024**, *669*, 393–401.
- [125] P. Verma, A. Singh, F. A. Rahimi, T. K. Maji, *J. Mater. Chem. A* **2021**, *9*, 13608–13614.
- [126] H.-N. Wang, H. Chen, L.-L. Chen, W.-H. Zhang, Z.-Y. Zhou, X. Meng, *Res. Chem. Intermed.* **2018**, *44*, 1261–1274.
- [127] B. Sharma, A. Mahata, S. Mandani, N. Thakur, B. Pathak, T. K. Sarma, *New J. Chem.* **2018**, *42*, 17983–17990.
- [128] W. Song, Y. Li, L. Geng, G. Feng, J. Ren, X. Yu, *Mater. Des.* **2021**, *205*, 109744.
- [129] T. Hisatomi, K. Domen, *Nat. Catal.* **2019**, *2*, 387–399.
- [130] a) Y. Qi, Y. Zhao, Y. Gao, D. Li, Z. Li, F. Zhang, C. Li, *Joule* **2018**, *2*, 2393–2402; b) C. Descorme, P. Gallezot, C. Geantet, C. George, *ChemCatChem* **2012**, *4*, 1897–1906.
- [131] K. C. Christoforidis, P. Fornasiero, *ChemCatChem* **2019**, *11*, 368–382.
- [132] a) D. Kim, V. Q. Dang, T. S. Teets, *Chem. Sci.* **2024**, *15*, 77–94; b) B. Maiti, A. Abramov, R. Pérez-Ruiz, D. Díaz Díaz, *Acc. Chem. Res.* **2019**, *52*, 1865–1876.
- [133] P. Liao, Y. Hu, Z. Liang, J. Zhang, H. Yang, L.-Q. He, Y.-X. Tong, J.-M. Liu, L. Chen, C.-Y. Su, *J. Mater. Chem. A* **2018**, *6*, 3195–3201.
- [134] P. Verma, A. Singh, F. A. Rahimi, P. Sarkar, S. Nath, S. K. Pati, T. K. Maji, *Nat. Commun.* **2021**, *12*, 7313.
- [135] P. Verma, F. A. Rahimi, D. Samanta, A. Kundu, J. Dasgupta, T. K. Maji, *Angew. Chem., Int. Ed.* **2022**, *61*, e202116094.
- [136] G. Yang, S. Li, N. Li, P. Zhang, C. Su, L. Gong, B. Chen, C. Qu, D. Qi, T. Wang, J. Jiang, *Angew. Chem., Int. Ed.* **2022**, *61*, e202205585.
- [137] N. Alam, N. Ojha, S. Kumar, D. Sarma, *ACS Sustainable Chem. Eng.* **2023**, *11*, 2658–2669.
- [138] Y. Gao, Y. Li, D. Zou, *Chem. Eng. J.* **2024**, *480*, 148049.
- [139] S. Mondal, F. A. Rahimi, T. N. Das, S. Nath, T. K. Maji, *Chem. Sci.* **2025**, *16*, 3646–3654.
- [140] a) C. Freire, D. M. Fernandes, M. Nunes, V. K. Abdelkader, *ChemCatChem* **2018**, *10*, 1703–1730; b) Y. Liang, Y. Li, H. Wang, H. Dai, *J. Am. Chem. Soc.* **2013**, *135*, 2013–2036.
- [141] Y. Li, Q. Liu, S. Zhang, G. Li, *ChemCatChem* **2019**, *11*, 861–867.
- [142] J. Lai, A. Nsabimana, R. Luque, G. Xu, *Joule* **2018**, *2*, 76–93.
- [143] T. He, Z. Li, Z. Sun, S. Chen, R. Shen, L. Yi, L. Deng, M. Yang, H. Liu, Y. Zhang, *RSC Adv.* **2015**, *5*, 77296–77302.
- [144] B. Dhara, S. Sappati, S. K. Singh, S. Kurungot, P. Ghosh, N. Ballav, *Dalton Trans.* **2016**, *45*, 6901–6908.
- [145] H. Jiang, C. Li, H. Shen, Y. Liu, W. Li, J. Li, *Electrochim. Acta* **2017**, *231*, 344–353.
- [146] H. Wang, X. Cheng, F. Yin, B. Chen, T. Fan, X. He, *Electrochim. Acta* **2017**, *232*, 114–122.
- [147] E. Saha, K. Karthick, S. Kundu, J. Mitra, *ACS Sustainable Chem. Eng.* **2019**, *7*, 16094–16102.
- [148] E. Saha, K. Karthick, S. Kundu, J. Mitra, *J. Mater. Chem. A* **2021**, *9*, 26800–26809.
- [149] N. Shang, S. Li, X. Zhou, S. Gao, Y. Gao, C. Wang, Q. Wu, Z. Wang, *Appl. Surf. Sci.* **2021**, *537*, 147818.
- [150] E. Saha, G. R. Bhadu, J. Mitra, *Int. J. Hydrog. Energy* **2023**, *48*, 8115–8126.
- [151] L. Wagh, D. Singh, V. Kumar, S. N. Upadhyay, S. Pakhira, A. K. Das, *ACS Appl. Mater. Interfaces* **2024**, *16*, 28307–28318.
- [152] T. Mondal, S. Patra, B. Mondal, P. Ghosh, I. W. Hamley, A. Banerjee, *ACS Appl. Polym. Mater.* **2024**, *6*, 11383–11391.
- [153] H. Kim, T. Y. Yoo, M. S. Bootharaju, J. H. Kim, D. Y. Chung, T. Hyeon, *Adv. Sci.* **2022**, *9*, 2104054.
- [154] K. Shijina, R. Illathvalappil, N. S. Sumitha, G. S. Sailaja, S. Kurungot, B. N. Nair, A. Peer Mohamed, G. M. Anilkumar, T. Yamaguchi, U. S. Hareesh, *New J. Chem.* **2018**, *42*, 18690–18701.
- [155] Z. Cao, Z. Jiang, Y. Li, C. Huang, Y. Li, *ChemSusChem* **2019**, *12*, 2480–2486.
- [156] H. Guo, Q. Feng, K. Xu, J. Xu, J. Zhu, C. Zhang, T. Liu, *Adv. Funct. Mater.* **2019**, *29*, 1903660.
- [157] T. Zhu, Q. Feng, S. Liu, C. Zhang, *Compos. Commun.* **2020**, *20*, 100376.
- [158] H. Wang, W. Zhu, Q. Xue, C. Wang, K. Liu, *Chem. Commun.* **2020**, *56*, 7781–7784.
- [159] Y. Xiao, Q. Wang, X. Feng, J. Wu, P. Liao, Y. Tong, J. Zhang, *J. Mater. Chem. A* **2021**, *9*, 17451–17458.
- [160] X. Zhang, H. Zhao, C. Li, S. Li, K. Liu, L. Wang, *Appl. Catal. B: Environ.* **2021**, *299*, 120641.
- [161] X. Feng, Y. Xiao, H. H. Huang, Q. Wang, J. Wu, Z. Ke, Y. Tong, J. Zhang, *Chem. Asian J.* **2021**, *16*, 3213–3220.
- [162] L. Song, T. Xue, Z. Shen, S. Yang, D. T. Sun, J. Yang, Y. Hong, Y. Su, H. Wang, L. Peng, J. Li, *J. Colloid Interface Sci.* **2022**, *621*, 398–405.
- [163] X. Zhang, C. Li, H. Lan, Y. Liu, H. Zhao, M. Yuan, Y. Song, S. Li, L. Wang, K. Liu, *J. Colloid Interface Sci.* **2022**, *624*, 100–107.
- [164] Y. Tong, X. Yan, J. Liang, S. X. Dou, *Small* **2021**, *17*, 1904126.
- [165] W. Huang, H. Wang, J. Zhou, J. Wang, P. N. Duchesne, D. Muir, P. Zhang, N. Han, F. Zhao, M. Zeng, J. Zhong, C. Jin, Y. Li, S.-T. Lee, H. Dai, *Nat. Commun.* **2015**, *6*, 10035.
- [166] M. Mansor, S. N. Timmiati, K. L. Lim, W. Y. Wong, S. K. Kamarudin, N. H. Nazirah Kamarudin, *Int. J. Hydrogen Energy* **2019**, *44*, 14744–14769.
- [167] Y.-J. Wang, J.-H. Wei, S. Li, J.-Y. Luo, X.-W. Chang, Y.-Y. Sun, Q. Pi, Y.-P. Wu, D.-S. Li, *Inorg. Chem. Front.* **2021**, *8*, 927–933.
- [168] Z. Liang, H.-Y. Wang, H. Zheng, W. Zhang, R. Cao, *Chem. Soc. Rev.* **2021**, *50*, 2540–2581.
- [169] L. Xie, Y. Wang, Q. Kong, R. Cao, *ChemCatChem* **2024**, *16*, e202400956.
- [170] J. Choi, J. Kim, P. Wagner, S. Gambhir, R. Jalili, S. Byun, S. Sayyar, Y. M. Lee, D. R. MacFarlane, G. G. Wallace, D. L. Officer, *Energy Environ. Sci.* **2019**, *12*, 747–755.
- [171] G. Cai, L. Zeng, L. He, S. Sun, Y. Tong, J. Zhang, *Chem. Asian J.* **2020**, *15*, 1963–1969.
- [172] C. Wei, Y. He, X. Shi, Z. Song, *Coord. Chem. Rev.* **2019**, *385*, 1–19.
- [173] Q. Liu, Q. Wang, J. Wang, Z. Li, J. Liu, X. Sun, J. Li, Y. Lei, L. Dai, P. Wang, *Adv. Funct. Mater.* **2020**, *30*, 2000593.
- [174] Q. Liu, Q. Wang, Y. Tan, L. Zhu, Z. Jiang, M. Chen, J. Wang, Y. Li, Y. Lei, Y. Zhang, L. Dai, P. Wang, *J. Mater. Chem. A* **2022**, *10*, 13305–13314.
- [175] X. Hou, J. Sun, M. Lian, Y. Peng, D. Jiang, M. Xu, B. Li, Q. Xu, *Macromol. Mater. Eng.* **2023**, *308*, 2200469.
- [176] S. Sun, P. Liao, L. Zeng, L. He, J. Zhang, *RSC Adv.* **2020**, *10*, 14778–14784.
- [177] C. Gu, J. Li, J.-P. Liu, H. Wang, Y. Peng, C.-S. Liu, *Appl. Catal. B: Environ.* **2021**, *286*, 119888.
- [178] S.-i. Shoda, H. Uyama, J.-i. Kadokawa, S. Kimura, S. Kobayashi, *Chem. Rev.* **2016**, *116*, 2307–2413.
- [179] C. A. Ballesteros, L. A. Mercante, A. D. Alvarenga, M. H. Facure, R. Schneider, D. S. Correa, *Mater. Chem. Front.* **2021**, *5*, 7419–7451.
- [180] X. Wang, C. Wei, J. H. Su, B. He, G. B. Wen, Y. W. Lin, Y. Zhang, *Angew. Chem.* **2018**, *130*, 3562–3566.
- [181] N. Malviya, C. Sonkar, B. K. Kundu, S. Mukhopadhyay, *Langmuir* **2018**, *34*, 11575–11585.
- [182] S. Dominic Kurbah, N. Simisi Clovis, *Inorg. Chim. Acta* **2024**, *565*, 122000.
- [183] L. He, Y. Li, Q. Wu, D. M. Wang, C. M. Li, C. Z. Huang, Y. F. Li, *ACS Appl. Mater. Interfaces* **2019**, *11*, 29158–29166.
- [184] S. D. Kurbah, R. A. Lal, *New J. Chem.* **2020**, *44*, 5410–5418.
- [185] S. Sarkar, P. K. Maji, Y. Negishi, S. Dutta, T. N. Das, R. Pan, S. Sarkar, *ACS Appl. Nano Mater.* **2021**, *4*, 1455–1466.
- [186] T. Ishiwata, K. Kokado, K. Sada, *Angew. Chem., Int. Ed.* **2017**, *56*, 2608–2612.
- [187] Z. Zhuang, Z. Mai, T. Wang, D. Liu, *Coord. Chem. Rev.* **2020**, *421*, 213461.
- [188] X. F. Lu, Y. Fang, D. Luan, X. W. D. Lou, *Nano Lett.* **2021**, *21*, 1555–1565.
- [189] W. Xia, B. Qiu, D. Xia, R. Zou, *Sci. Rep.* **2013**, *3*, 1935.

Manuscript received: April 8, 2025

Revised manuscript received: June 24, 2025

Accepted manuscript online: June 24, 2025

Version of record online: ■ ■ ■